

Presentation on Texas Seismicity for the Texas House of Representatives Energy Resources Committee

May 4th, 2015

John H. Reagan Building, Room 140

Testimony Provided by:

Matthew J. Hornbach, Ph.D.
Associate Professor of Geophysics
Southern Methodist University
Dallas, Texas

Brian Stump, Ph.D.
Albritton Professor of Earth Sciences
Southern Methodist University
Dallas, Texas

Jon E. Olson, PhD, PE
Chairman and Professor
Petroleum and Geosystems Engineering
The University of Texas at Austin
Austin, Texas

Report Provided By:

Heather R. DeShon, Ph.D.
Associate Professor of Geophysics
Southern Methodist University

Matthew J. Hornbach, Ph.D.
Associate Professor of Geophysics
Southern Methodist University

Brian Stump, Ph.D.
Albritton Professor of Earth Sciences
Southern Methodist University

Chris Hayward, , Ph.D.
Director of the Geophysics Research Program
Southern Methodist University

Jon E. Olson, PhD, PE
Chairman and Professor
Petroleum and Geosystems Engineering
The University of Texas at Austin
Austin, Texas

Cliff Frohlich
Associate Director
Institute for Geophysics
University of Texas at Austin
Austin, Texas

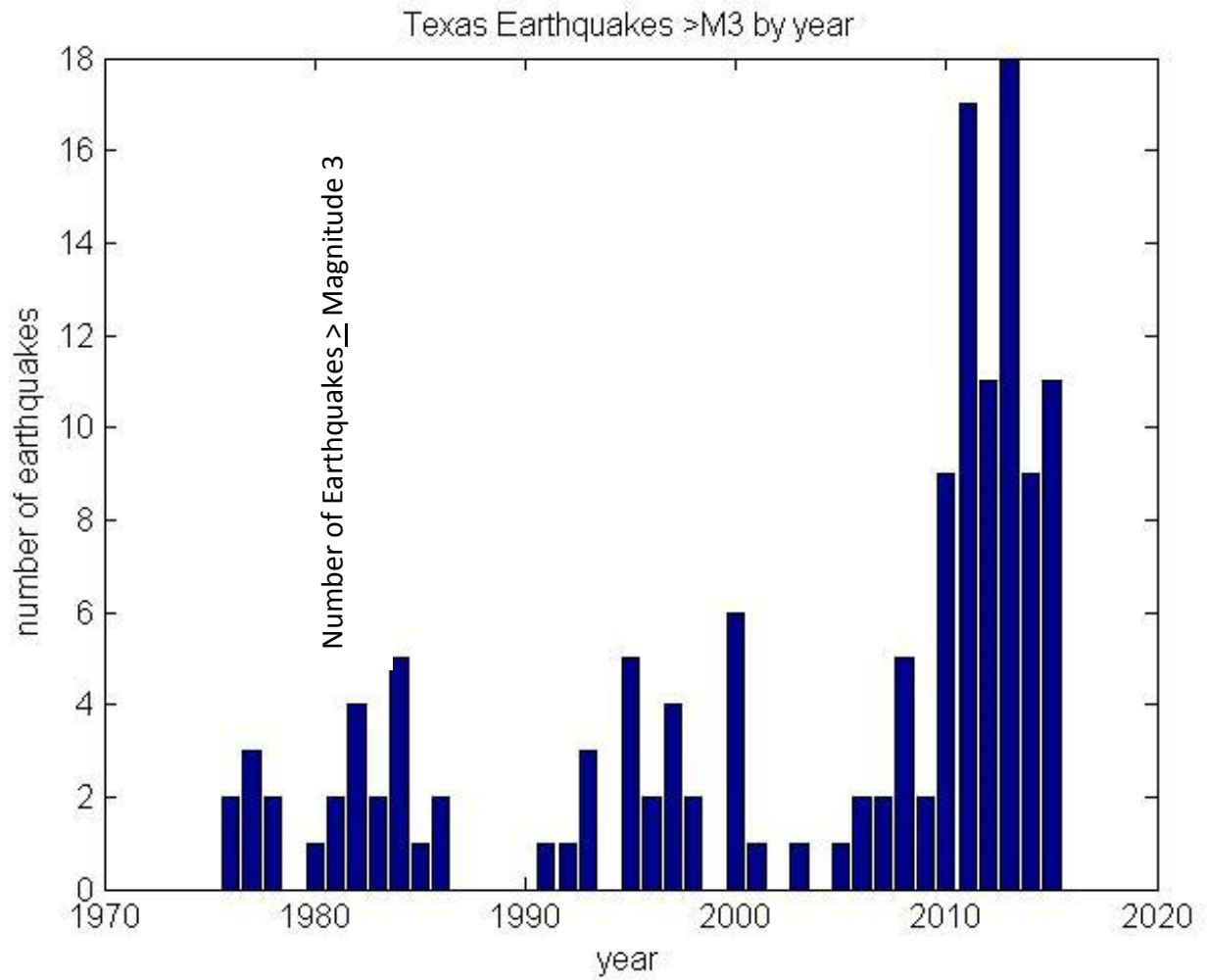
Maria Beatrice Magnani, Ph.D.
Associate Professor of Geophysics
Southern Methodist University

The findings and conclusions in this testimony are those of the authors and do not necessarily represent the views of their respective funding agencies or employers.

Table of Contents

Recent increased seismicity in Texas.....	2
Increased seismicity in central US.....	4
Examples of Injection Induced Earthquakes.....	5
Causal Factors for Seismicity near Azle and Beyond.....	6
Azle-Based Observation, Results.Recommendations.....	21
Induced Seismicity Hazard Implications.....	22
Past, Present, and Recommended Future Seismic studies.....	25
Appendix A: Rate changes for Seismicity in Texas.....	29
Appendix B: RANGE OF EQUIPMENT, PERMANENT AND TEMPORARY, RECORDING DATA FROM NORTH TEXAS EARTHQUAKES.....	30
Appendix C: Dallas/Irving Earthquakes Prelim. Rept.....	35
Appendix D: Researcher Biographies.....	41
Appendix E: Complete 2015 Azle Nature Communications Publication with Supplementary Material.....	45

Texas Earthquakes \geq Magnitude 3, 1975 - April, 2015



USGS Felt Reports in North Texas Since 2008

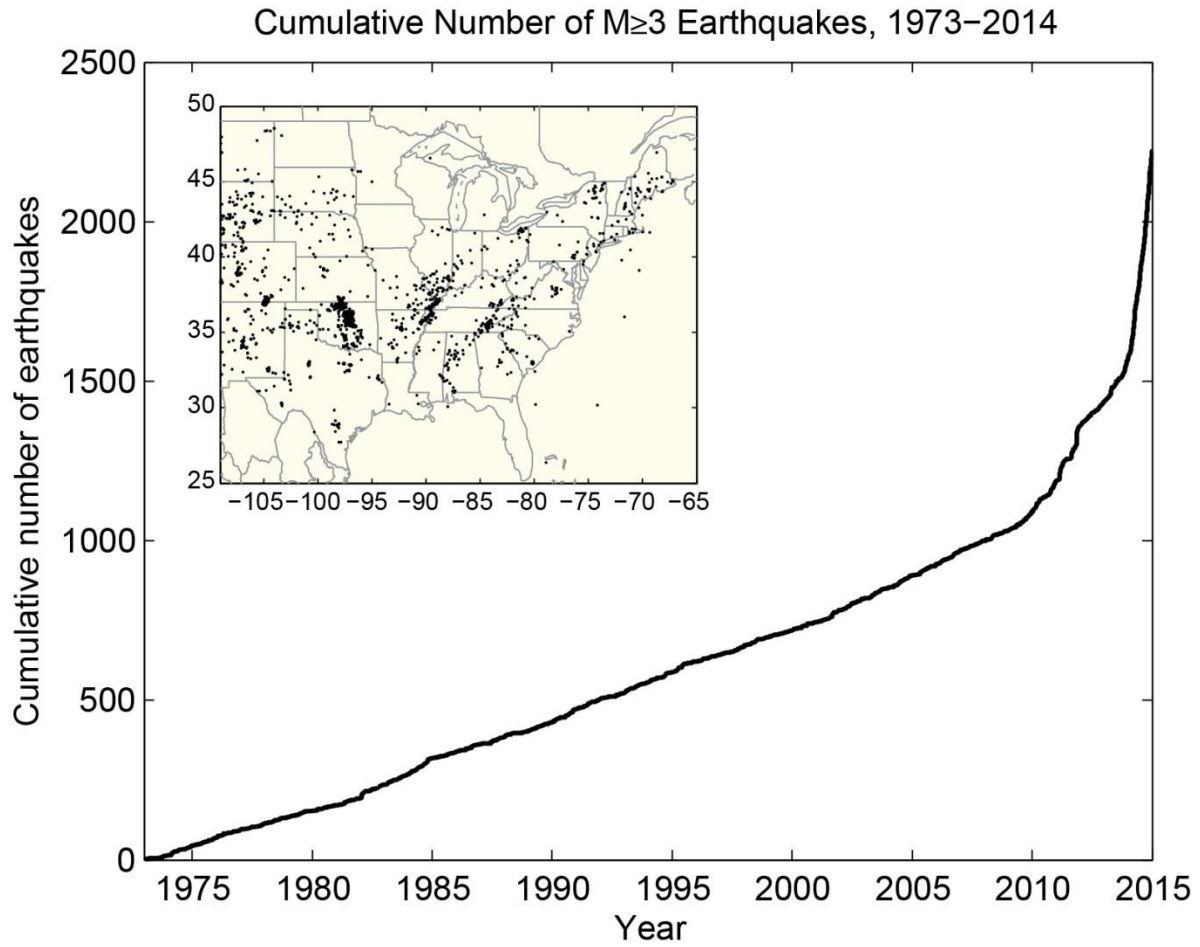
Showing 1 to 50 of 135 results for "[Northern Texas](#)"

View Page: 1 | [2](#) | [3](#) [Next»](#)

<u>MMI</u>	<u>Mag</u>	<u>Location</u>	<u>Event Time</u>	<u>Event ID</u>	<u>Response</u>
V	3.6	NORTHERN TEXAS 32.85°N -96.89°W 5Km Deep	2015-01-07 00:52:09 UTC 2015-01-06 18:52:09 LOCAL	USC000TCA7	1870
IV	3.5	NORTHERN TEXAS 32.84°N -96.90°W 5Km Deep	2015-01-06 21:10:31 UTC 2015-01-06 15:10:31 LOCAL	USC000TC7Z	2775
V	3.4	NORTHERN TEXAS 32.50°N -97.13°W 5Km Deep	2014-11-30 05:52:24 UTC 2014-11-29 23:52:24 LOCAL	USB000T1C3	199
V	3.3	NORTHERN TEXAS 32.85°N -96.94°W 6Km Deep	2015-04-02 22:36:21 UTC 2015-04-02 17:36:21 LOCAL	US10001TG3	697
V	3.3	NORTHERN TEXAS 32.84°N -96.89°W 3Km Deep	2014-11-23 03:15:47 UTC 2014-11-22 21:15:47 LOCAL	USB000SZ6Q	1224
IV	3.1	NORTHERN TEXAS 32.83°N -96.89°W 5Km Deep	2015-02-27 12:18:21 UTC 2015-02-27 06:18:21 LOCAL	USC000TTJU	220
V	3.1	NORTHERN TEXAS 32.84°N -96.91°W 5Km Deep	2015-01-07 06:59:03 UTC 2015-01-07 00:59:03 LOCAL	USC000TCC6	465
V	3.0	NORTHERN TEXAS 32.83°N -96.90°W 8Km Deep	2015-01-20 20:25:49 UTC 2015-01-20 14:25:49 LOCAL	USC000THKY	644
V	2.9	NORTHERN TEXAS 32.81°N -96.90°W 8Km Deep	2015-01-07 02:11:17 UTC 2015-01-06 20:11:17 LOCAL	USC000TCAG	383
IV	2.7	NORTHERN TEXAS 32.87°N -96.91°W 5Km Deep	2015-04-02 10:38:06 UTC 2015-04-02 05:38:06 LOCAL	US10001T33	138
IV	2.7	NORTHERN TEXAS 32.86°N -96.92°W 5Km Deep	2015-03-14 07:31:16 UTC 2015-03-14 02:31:16 LOCAL	US10001MC1	57
V	2.7	NORTHERN TEXAS 32.85°N -96.92°W 7Km Deep	2015-01-07 15:57:30 UTC 2015-01-07 09:57:30 LOCAL	USC000TCE9	185

From USGS-NEIC web reporting site

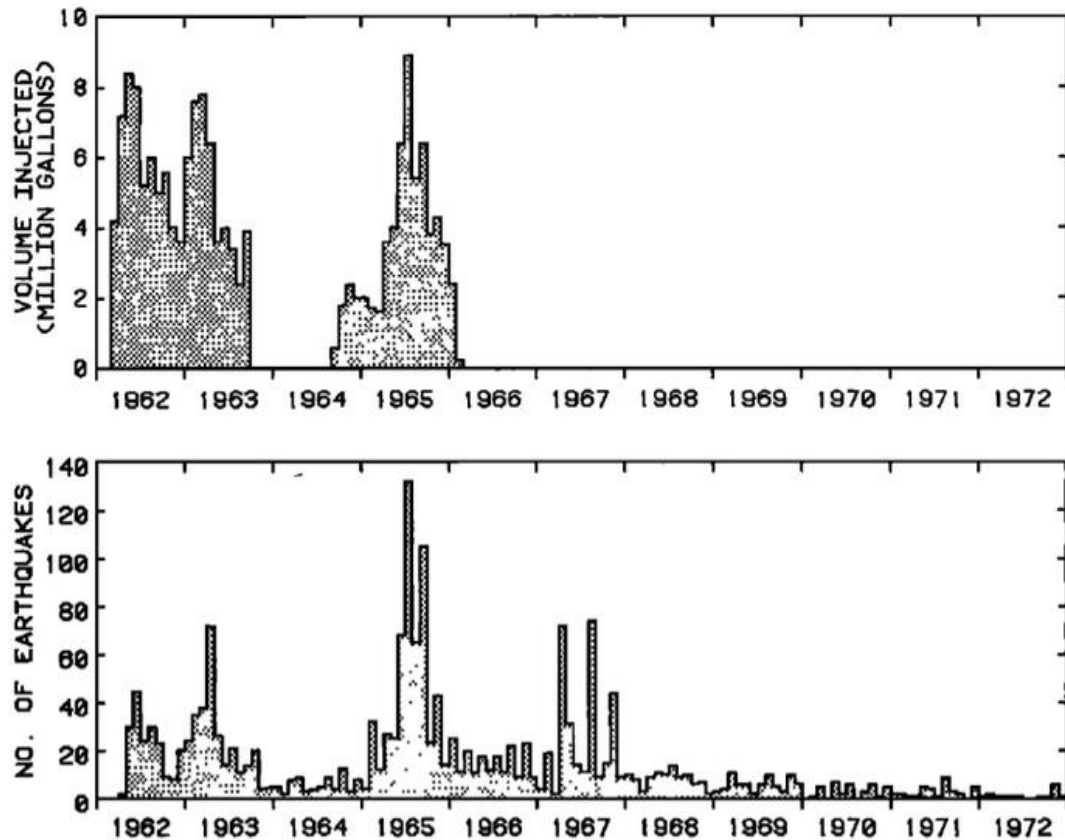
Increased Seismicity in the Central US and Texas is Attributed to Industrial Activity



From Petersen et al., 2015 (For Earthquake counts in Texas, see Appendix A)

The Concept of Injection/Removal of Fluids as a Cause of Earthquakes is not New

Results From Rocky Mountain Arsenal (northeast of Denver Colorado)



Hsieh and Bredehoeft, *Journal of Geophysical Research*, 1981

From 1961-1966, the US Army injected water down an well as a means of testing whether they could store chemical weapons waste in the earth.

The Injection Well was shut down in 1966 because fluid injection triggered a series of earthquakes in the area.

Key things to Note:

- 1.) Prior to the injector wells use, the area was not recognized as a seismically active region.
- 2.) The seismicity generally follows the injection volume pattern, but not perfectly.
- 3.) Greatest seismicity often, but not always, matches the greatest injection rates.
- 4.) Aftershocks in the region continued for several years following injection, despite attempts to depressurize the reservoir.

Paradox Valley, Colorado: An Example of Using the Data to Constrain/Manage Risk

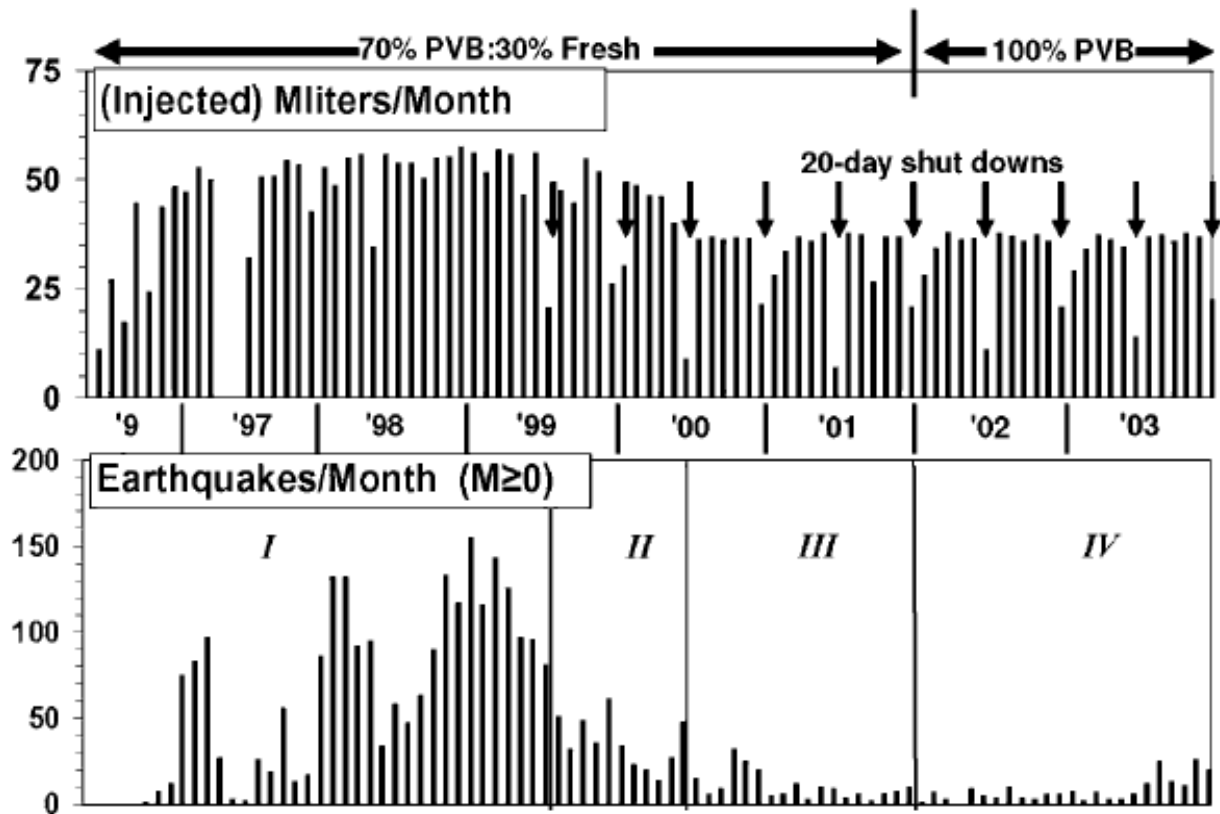


Figure 6. Four phases of continuous pumping (1996–2003) superimposed on monthly injected volumes and induced seismic events per month versus time. PVB designates Paradox Valley Brine, the extract fluid from the local aquifer.

(Aki et al., 2005)

--After a series of Felt Earthquakes occurred in Paradox Valley due to brine injection, scientists began collecting more data and changed their injection strategy in hopes of reducing seismic risk.

--The changes to the injection strategy substantially reduced the seismic risk, with seismicity dropping from 1100 events/year to as low as 60 events per year (see Aki et al, 2005).

Causal Factors for Seismicity Near Azle, Texas (or anywhere on Earth)

Natural and Human-Made Stress Changes that Cause Earthquakes

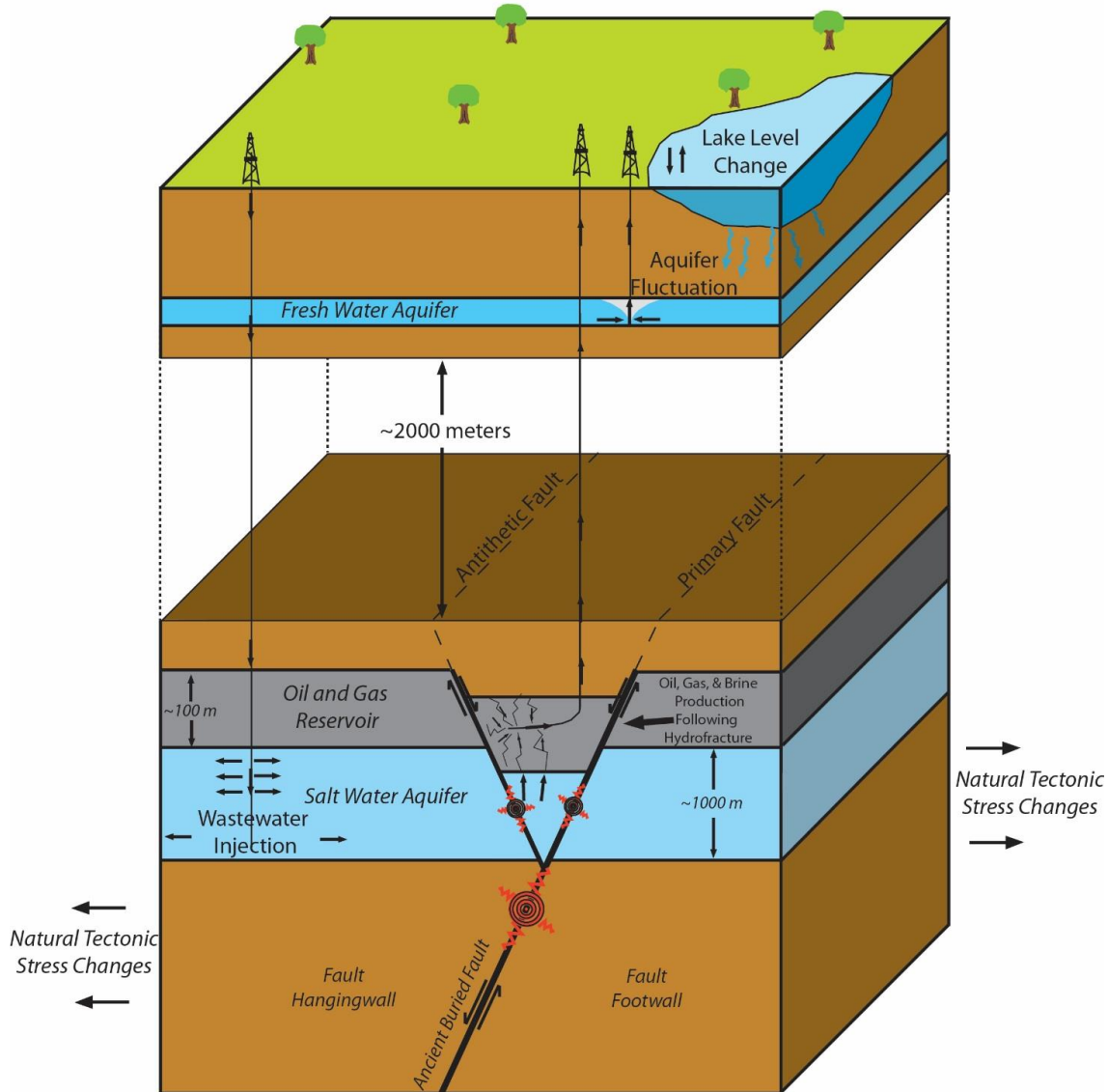
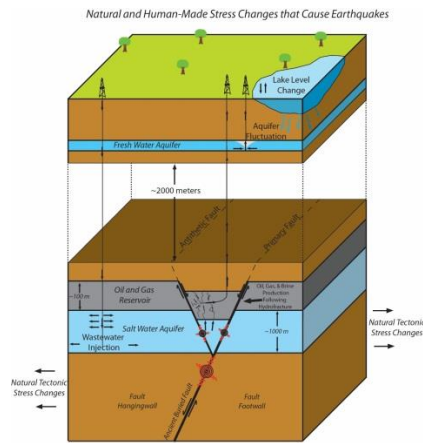


Figure not to scale

(Figure 1 from Hornbach, DeShon et al., 2015) Several natural and anthropogenic (man-made) factors can influence the subsurface stress regime resulting in earthquakes. Natural stress changes that promote earthquakes include intraplate stress changes related to plate tectonics^{9, 10} and natural water table or lake levels variations caused by changing weather patterns or water drainage patterns with time, and in some instances (not pictured) the advance or retreat of glaciers. Anthropogenic stress changes that promote earthquakes include human-generated changes to the water table (including dam construction^{2,3}) and

Stress Changes Required to Cause Earthquakes are small



This is because many of the faults in Earth's crust are *near-critically stressed*.

Helpful references providing further insight:

- Barton, Colleen A., Mark D. Zoback, and Daniel Moos. "Fluid flow along potentially active faults in crystalline rock." *Geology* 23.8 (1995): 683-686.
- Davies, Richard, et al. "Induced seismicity and hydraulic fracturing for the recovery of hydrocarbons." *Marine and Petroleum Geology* 45 (2013): 171-185.
- Gomberg, J., et al. "Earthquake nucleation by transient deformations caused by the M=7.9 Denali, Alaska, earthquake." *Nature* 427.6975 (2004): 621-624.
- Grasso, J-R. "Mechanics of seismic instabilities induced by the recovery of hydrocarbons." *Pure and Applied Geophysics* 139.3-4 (1992): 507-534.
- Grasso, J-R. "Mechanics of seismic instabilities induced by the recovery of hydrocarbons." *Pure and Applied Geophysics* 139.3-4 (1992): 507-534.
- Gupta, Harsh K. *Reservoir induced earthquakes*. Elsevier, 1992.
- Moeck, Inga, Grzegorz Kwiatek, and Günter Zimmermann. "Slip tendency analysis, fault reactivation potential and induced seismicity in a deep geothermal reservoir." *Journal of Structural Geology* 31.10 (2009): 1174-1182.
- Rutqvist, J., Rinaldi, A. P., Cappa, F., & Moridis, G. J. (2013). Modeling of fault reactivation and induced seismicity during hydraulic fracturing of shale-gas reservoirs. *Journal of Petroleum Science and Engineering*, 107, 31-44.
- Scholz, Christopher H. *The mechanics of earthquakes and faulting*. Cambridge university press, 2002.
- Simpson, D. W., W. S. Leith, and C. H. Scholz. "Two types of reservoir-induced seismicity." *Bulletin of the Seismological Society of America* 78.6 (1988): 2025-2040.
- Stein, Ross S. "The role of stress transfer in earthquake occurrence." *Nature* 402.6762 (1999): 605-609.
- Talwani, Pradeep, and Steve Acree. "Pore pressure diffusion and the mechanism of reservoir-induced seismicity." *Pure and Applied Geophysics* 122.6 (1984): 947-965.
- Townend, John, and Mark D. Zoback. "How faulting keeps the crust strong." *Geology* 28.5 (2000): 399-402.
- Zoback, Mark D., and Hans-Peter Harjes. "Injection-induced earthquakes and crustal stress at 9 km depth at the KTB deep drilling site, Germany." *Journal of Geophysical Research: Solid Earth (1978-2012)* 102.B8 (1997): 18477-18491.
- Zoback, Mark D., and John Townend. "Implications of hydrostatic pore pressures and high crustal strength for the deformation of intraplate lithosphere." *Tectonophysics* 336.1 (2001): 19-30.

Examples of Peer-Reviewed Measured Stress Changes that cause Earthquakes

Location	EQ Induced Stress (psi)	Suspected Cause	Source(s)
Lacq Field, Fr.	~14.5	Oil and Gas Activity	Segal et al., 1994
Imogene Field, Tx	<59	Oil and Gas Activity	Grasso, 1992; Grasso and Sornette, 1998
Global	0 - 7	Large ocean tides	Cochran et al., 2004
Gasli Field, Uzb.	5.8 - 7.3	Oil and Gas Activity	Adushkin et al., 2000
Kettleman Field, Ca	~1.5	Oil and Gas Activity	Segal 1985; McGarr, 1991
Loma Prieta, Ca.	5.8 - 7.3	Distant Earthquakes	Reasenberg and Simpson, 1992

Note: Pressures required to cause earthquakes are generally much lower than pressures required for hydrofracture.

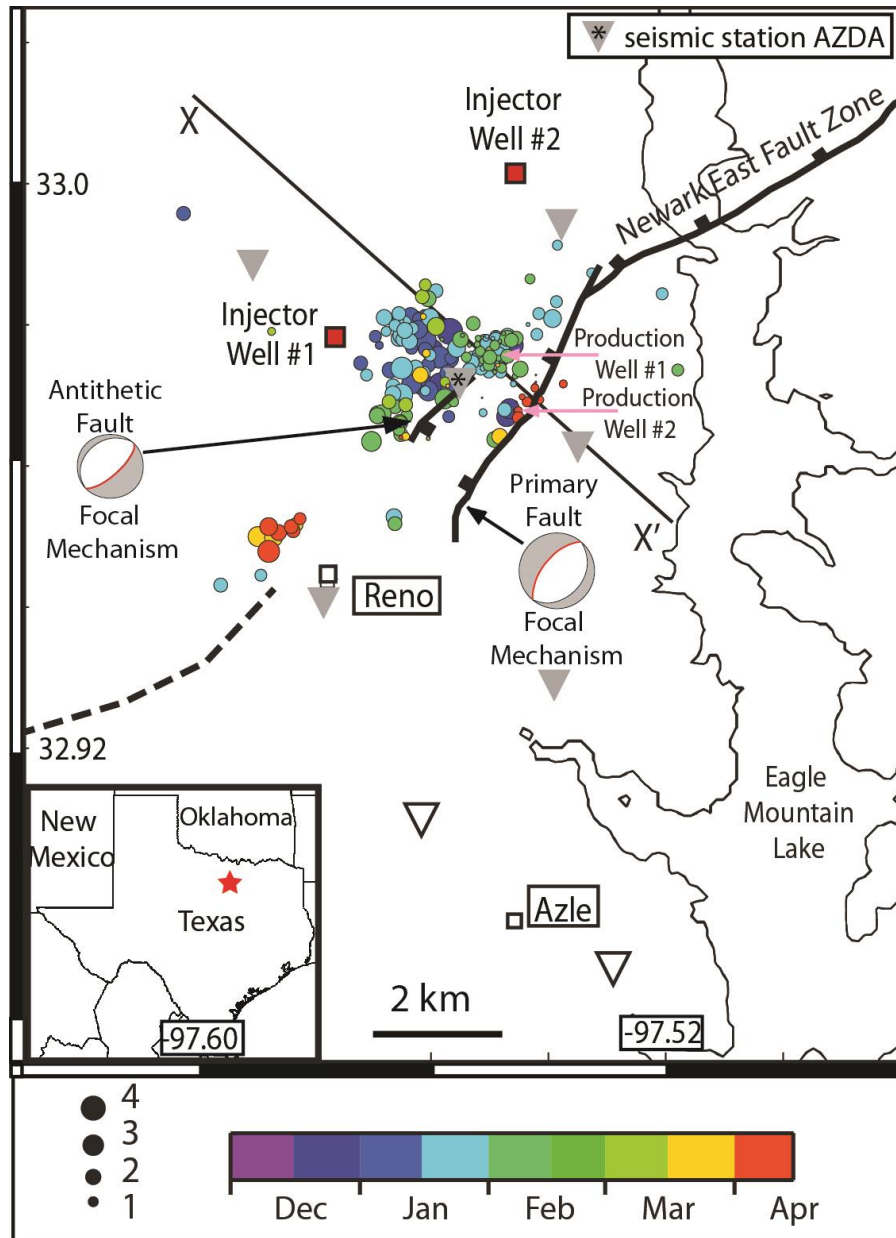
--Hydrofracture generally requires the breaking of rock.

--With earthquakes, the rocks are often already fractured and failure occurs along pre-existing, often lubricated (over-pressured or low sliding friction) faults.

Although Pressures Necessary for Failure are Small, Total Force on the Fault can be Large

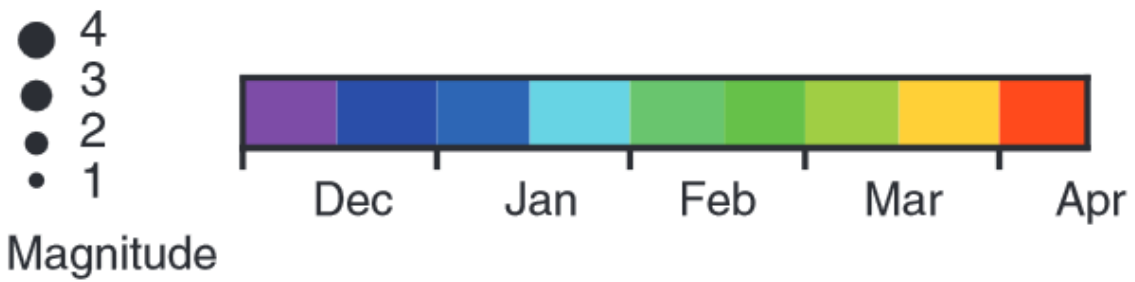
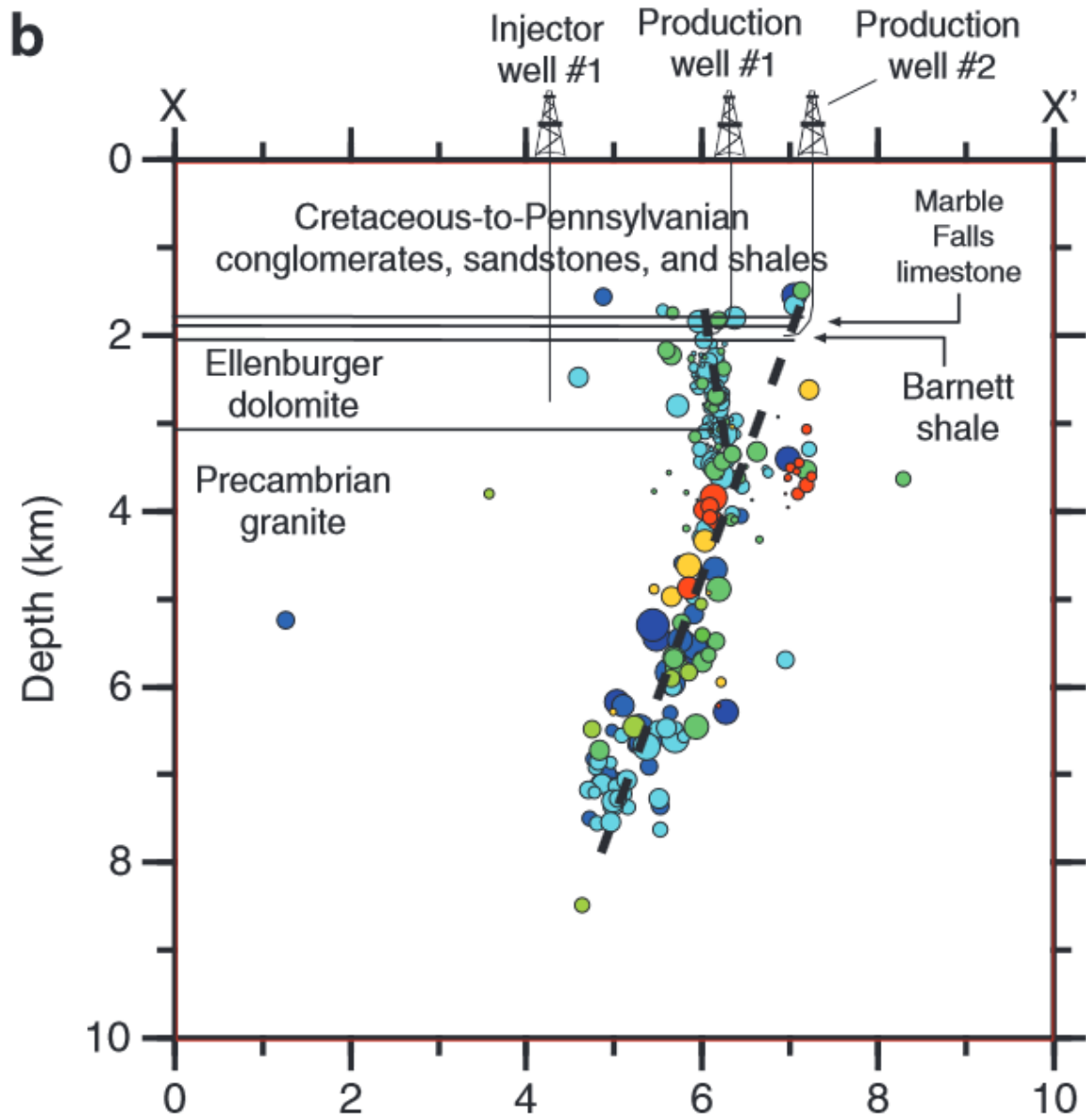
- 1.) 5 psi is a small force over an area of just 1 square inch.**
- 2.) 5 psi on the surface of a typical door is a force > 17,000 lbs.**
- 3.) A pressure change of 5-10 psi causes severe building damage (e.g. The Murrah Building in Oklahoma City was designed to with stand no more than 2-3 psi before failing) (Ngo et al., 2007).**
- 4.) If a fault like those below Azle/Reno is at least 1 mile long and at least half a mile tall and has a mean increase in pressure of only 5 psi applied to it, the fault experiences an excess force of at least 10 billion pounds.**

A Detailed Look at Azle Earthquakes, Nov. 2013-April 2014



From Hornbach, DeShon et al., 2015, Figure 2: Azle Earthquake Locations and Regional Geologic Structure. Map showing the location of NEFZ (black) at the top of the Ellenburger formation, inferred faults (dashed) at the top of the Ellenburger formation, injection wells (red squares), two production wells (API 36734045 and 36734139) with significant brine production near the faults (pink arrows) and earthquake epicenters (colored circles) recorded by the temporary seismic network (triangles) (a). The red star in the inset of a shows the map location. Grey (white) triangles indicate the locations of active (inactive) seismic stations.

Improved Earthquake Locations Based on SMU Seismic Network

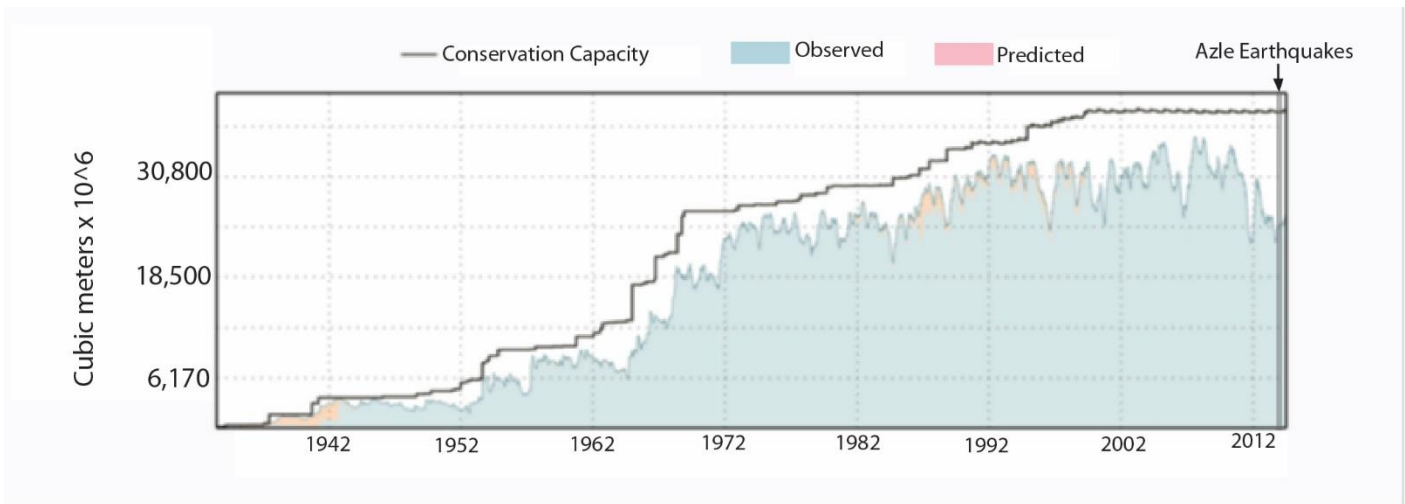


It is Possible, but Improbable That the Azle Earthquakes are Natural

1. During the past 150 years of settlement, there had been no felt earthquakes in the Azle/Reno area prior to November, 2013.
2. There is no clear evidence for fault surface expressions indicative of large-scale active faulting in the region.
3. Publicly available regional seismic data, though limited, show no significant fault offsets in sediment deposited more than ~300 million years ago.
4. The seismicity pattern in Azle is not consistent with the typical foreshock-main-shock-aftershock sequence observed in classic (tectonic) earthquake sequences, but is consistent with earthquake swarm patterns often associated with induced seismicity.

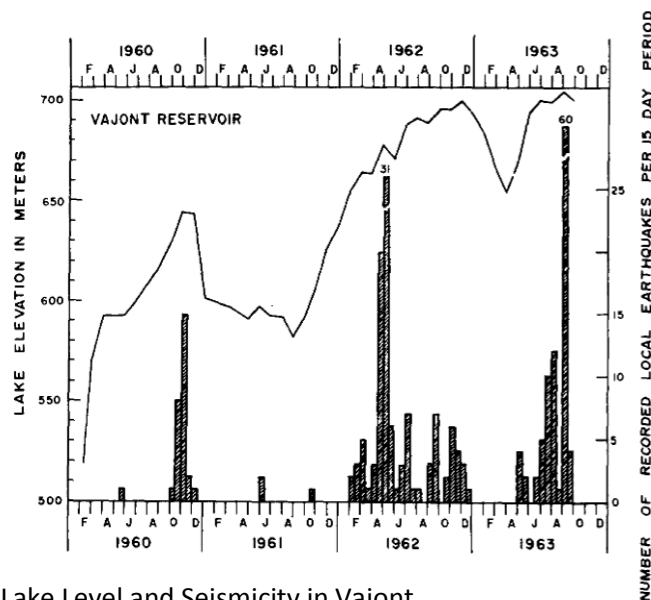
Greatest Stresses from Lake Level Variations Occurred ~50 year ago

The greatest stress/lake level changes in this region occurred ~50 years ago with the rapid filling of Eagle Mountain Lake. Based on other peer-reviewed studies (e.g. Simpson, 1976), the largest reservoir-induced earthquakes typically occur within 5 years of impoundment. None were reported near Eagle Mountain Lake during the first 70 year of impoundment.



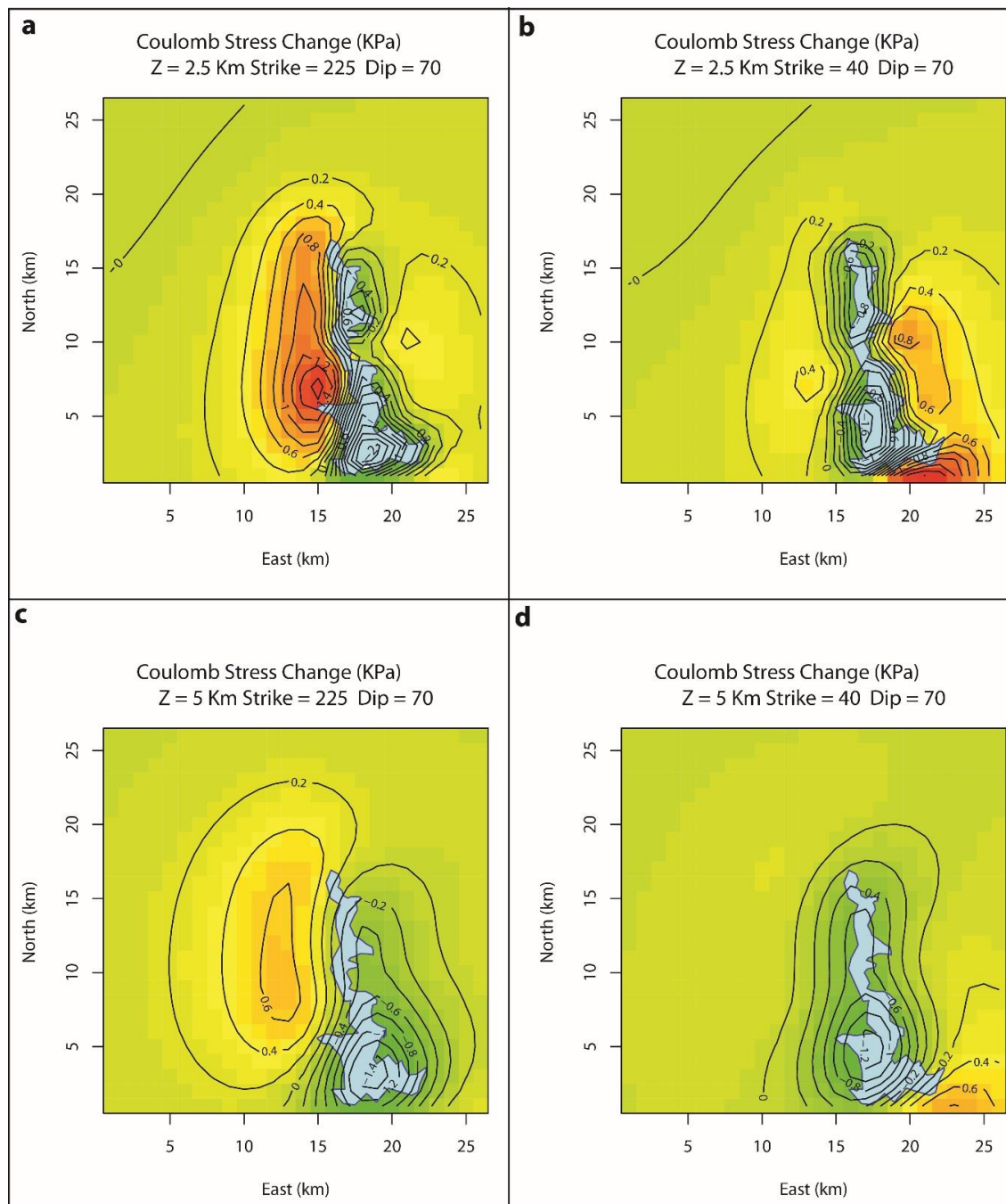
Water volume stored in Eagle Mountain Lake since dam construction in 1932

(<http://www.waterdatafortexas.org/reservoirs/statewide>). During the period of earthquake activity, lake volumes have not been at record high or record low values.



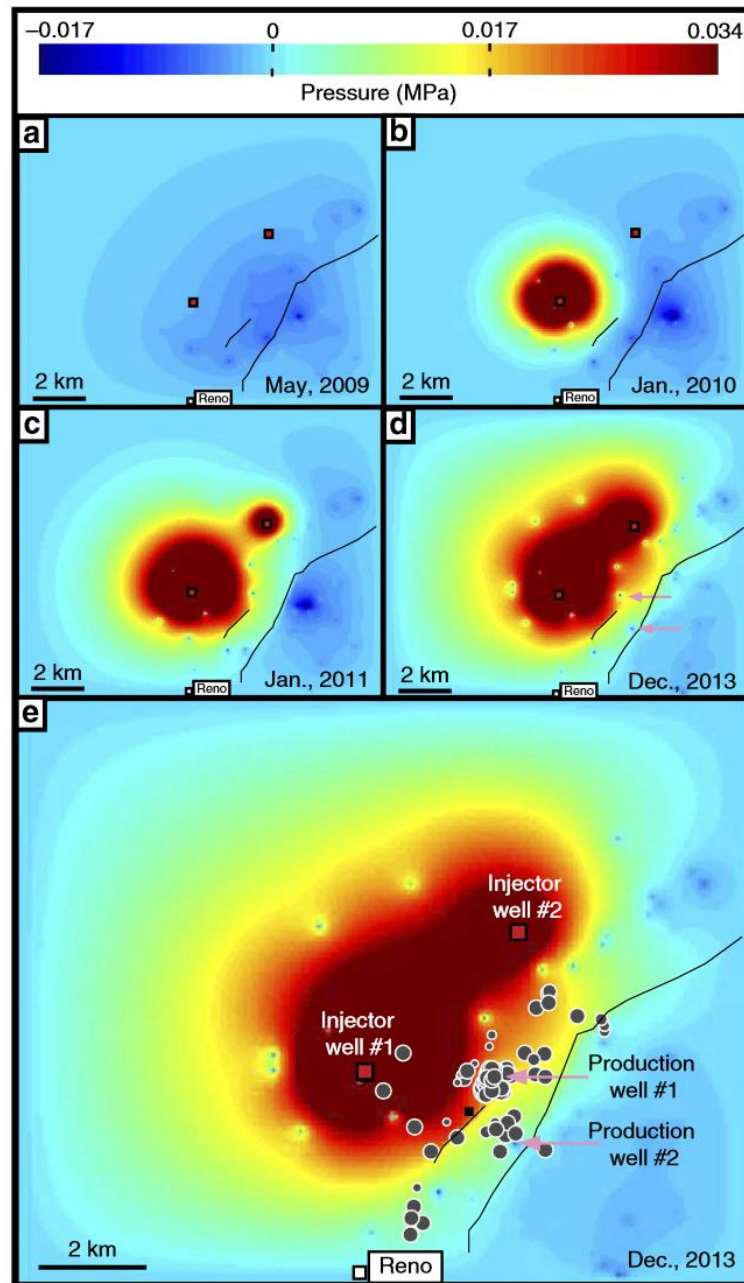
Variations in Lake Level and Seismicity in Vajont Reservoir, Greece (See Galanopoulos, 1967; Gupta et al., 1972)

Estimated stress changes caused by recent lake-level and ground water change in the Azle/Reno are tiny (comparable to tidal stresses)



From Hornbach, DeShon, et al., 2015, Supplementary Figure 2: Change in Coulomb stress at 2.5 km (a, b) and 5 km (c, d) depth for normal faulting caused by the 2.1 m drop in water level in Eagle Mountain Lake between April 2012 and November 2013, computed using the Boussinesq solution for a change in surface load on an elastic half-space³⁷. Warm colours indicate increased failure potential; cool colours indicate decreased failure potential. **a** and **c** correspond to orientation of the main fault defined by earthquake hypocentres. **b** and **d** correspond to antithetic normal fault orientation.

Estimated Stress Changes due to Industry Activity



From Hornbach, DeShon et al., 2015, Fig. 5. Modelled Pressure Changes in the Ellenburger Caused by Injection and Production. Map view of modelled excess pressures at a depth of ~2500 m for May 2009 (a), January 2010 (b), January 2011 (c), and December 2013 (d, e). The model uses average monthly reported water injection rates and the Dupuit-Theim equation to estimate bottom hole pressure values. Pressure above hydrostatic averages 0.58 MPa for injector well #1 and 0.28 MPa for injector well #2 during injection. Ellenburger permeability is assumed constant at $5 \times 10^{-14} \text{ m}^2$; boundary conditions are open along the side and closed at the top and bottom. We apply an average rate of brine production based directly on reported TRC G-10 water production values for the 70 largest water producing production wells in the region. The images show the system prior to injection (a) through the onset of seismicity (e). Black lines: the NEFZ location at the top of the Ellenburger formation. Red squares: injector locations. Pink arrows: approximate location of two large brine production wells that are located both near the faults and near reported earthquakes swarms within the Ellenburger (grey circles with white outlines).. Note that the most significant amount of brine removal occurs along the fault trend (a).

We used Conservative Numbers and a Broad Range of Model Parameters Based on the Best Data Available

Table 1: Examples of Model Parameters and Associated Results

Well #1 mean excess bottom hole pressure in (MPa)	Well #2 mean excess bottom hole pressure in (MPa)	mean effective permeability (m ²)	Thickness of high perm. zone (m)	Producers included?	Boundary Conditions	Specific Storage (m ⁻¹)	Excess pressure on fault at AZDA, Jan. 1st, 2014 (MPa)
0.53	0.17	3x10 ⁻¹⁴	1000	yes	closed	5 x 10 ⁻⁶	0.008
0.53	0.17	3x10 ⁻¹⁴	1000	yes	closed	13x10 ⁻⁶	0.02
0.53	0.17	3x10 ⁻¹⁴	1000	no	closed	7.3x10 ⁻⁶	0.011
4.4	2.96	3x10 ⁻¹⁴	300	no	closed	7.3x10 ⁻⁶	0.14
2.42	1.63	3x10 ⁻¹⁴	300	no	closed	7.3x10 ⁻⁶	0.08
2.42	1.63	3x10 ⁻¹⁴	300	no	open	7.3x10 ⁻⁶	0.015
2.42	1.63	3x10 ⁻¹⁴	1000	yes	closed	13x10 ⁻⁶	0.03
2.42	1.63	3x10 ⁻¹⁴	1000	no	closed	5 x 10 ⁻⁶	0.05
2.42	1.63	3x10 ⁻¹⁴	1000	no	open	5x10 ⁻⁶	0.01
2.42	1.63	1x10 ⁻¹⁴	1000	yes	closed	1x10 ⁻⁶	0.11
2.42	1.63	1x10 ⁻¹⁴	1000	yes	closed	13x10 ⁻⁶	0.1
2.42	1.63	1x10 ⁻¹⁴	1000	yes	closed	7.3x10 ⁻⁶	0.11
0.58	0.28	5x10 ⁻¹⁴	1000	yes	open	7.3x10 ⁻⁶	0.02
2.42	1.63	5x10 ⁻¹⁴	1000	yes	closed	7.3 x 10 ⁻⁶	0.1
2.42	1.63	10x10 ⁻¹⁴	1000	yes	open	7.3 x 10 ⁻⁶	0.017

--Pressures on the fault are consistently higher than those predicted by recent drought or lake level variations.

--Even when we completely remove the fault (no permeability change) the pressures in the area of seismicity are larger than pressures caused by drought (Hornbach 2015, supplementary figure 9).

--Nonetheless, we welcome and encourage more data, and more scientific discussion to improve/refine these results.

Basic Observations, Results, Implications and Recommendation for the Azle Study and Beyond (to Date)

Observations:

1. No earthquakes were known in Azle before late 2013.
2. No seismicity was felt or reported during or immediately following the filling of Eagle Lake Dam, when reservoir seismicity typically occurs.
3. Many earthquakes have been felt in Azle since Dec. 2013.
4. A state-of-the-art network was in place within two months after the first events felt.
5. This allowed determining quakes' map locations and depths to within a km or less.
6. These locations define a fault or faults, at depths of 2-8 km, an extension of a known mapped fault system.
7. There was a very high-volume injector injecting at depths of 3 km, only 2 km from these earthquakes.

Results:

1. Pressure modeling confirms it is plausible injection/production caused pressure changes sufficient to trigger earthquakes.
2. Pressure modeling indicates pressure changes associated with the drought were orders of magnitude lower than those associated with injection/production.

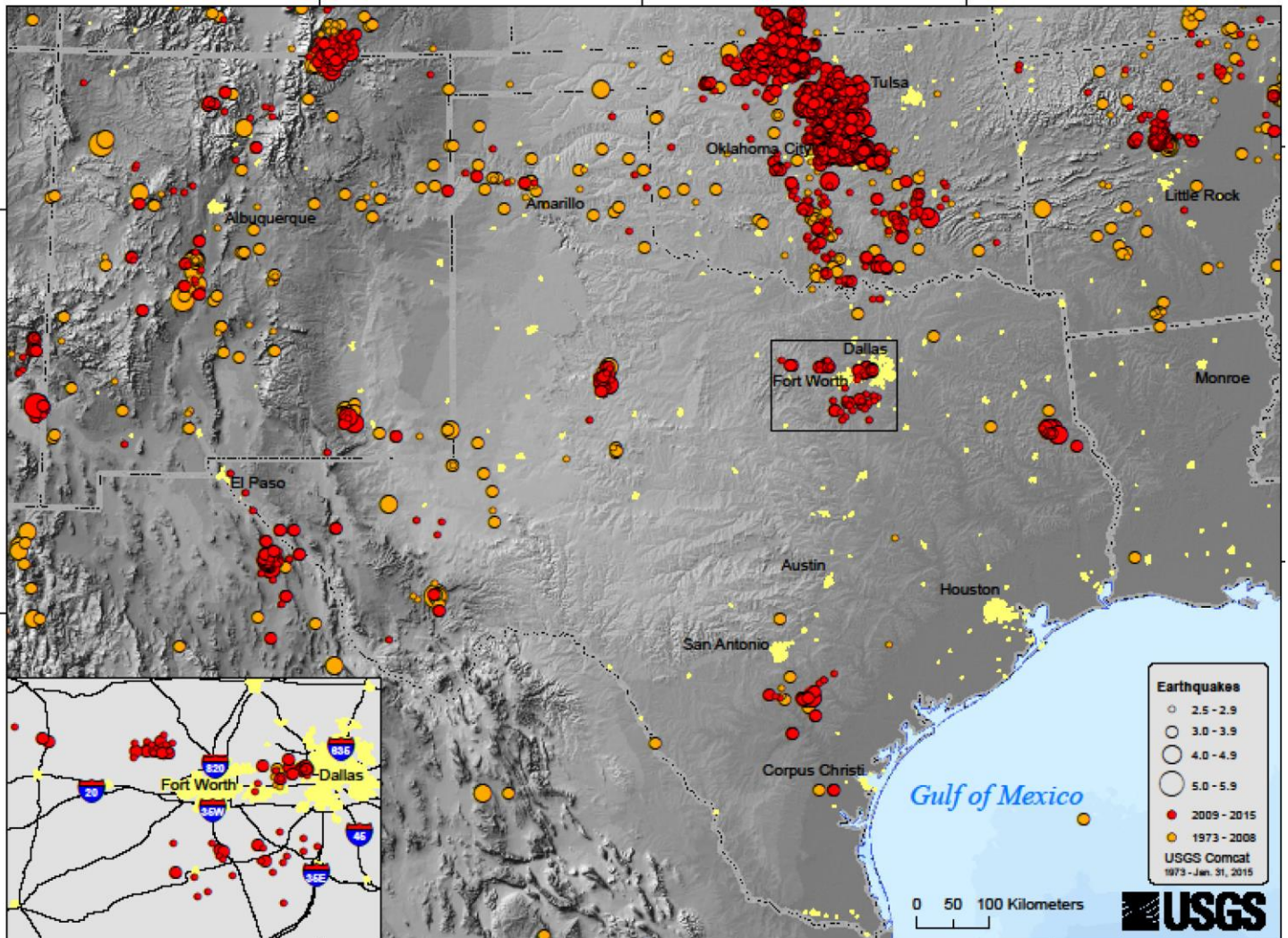
Implications:

1. Faults near the Azle/Reno area, though historically inactive, appear near-critically stressed.
2. Currently, Industry activities appear to represent the largest quantifiable stress driver on the fault system.

Recommendations/Needs for Future Study:

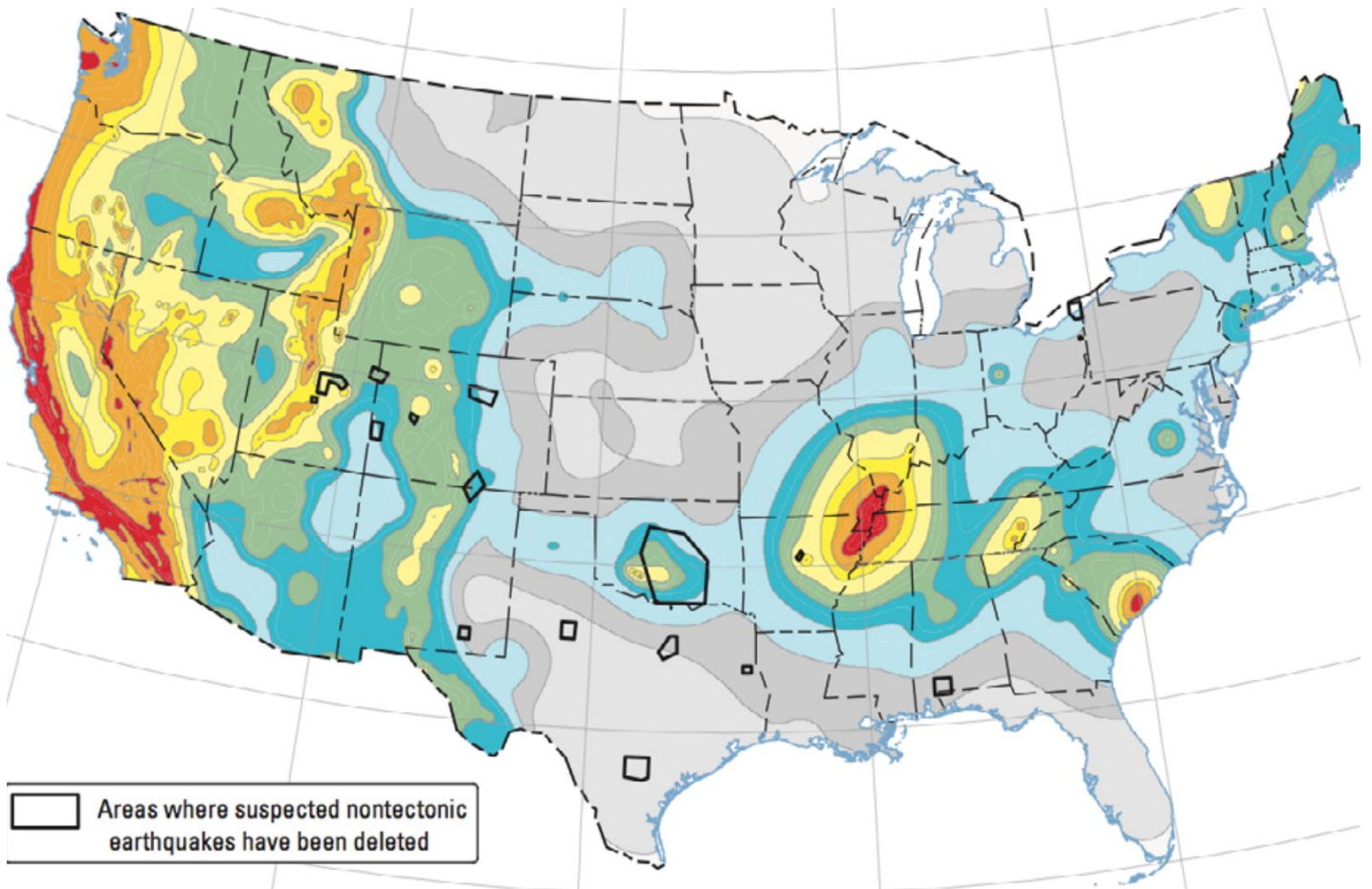
1. To mitigate risk, it would be valuable to recognize what areas in Texas have faults at or very near failure, ideally, before extraction/injection occurs.
2. To mitigate risk, it would be valuable to monitor what areas are experiencing the most significant subsurface stress changes due to extraction/injection.
3. It would be valuable to know with greater accuracy the permeability and reservoir characteristics of injection reservoirs at the basin scale.
4. It would be valuable to know the location and orientation of faults in the subsurface across the state of Texas.

US Geological Survey – Recent Seismicity



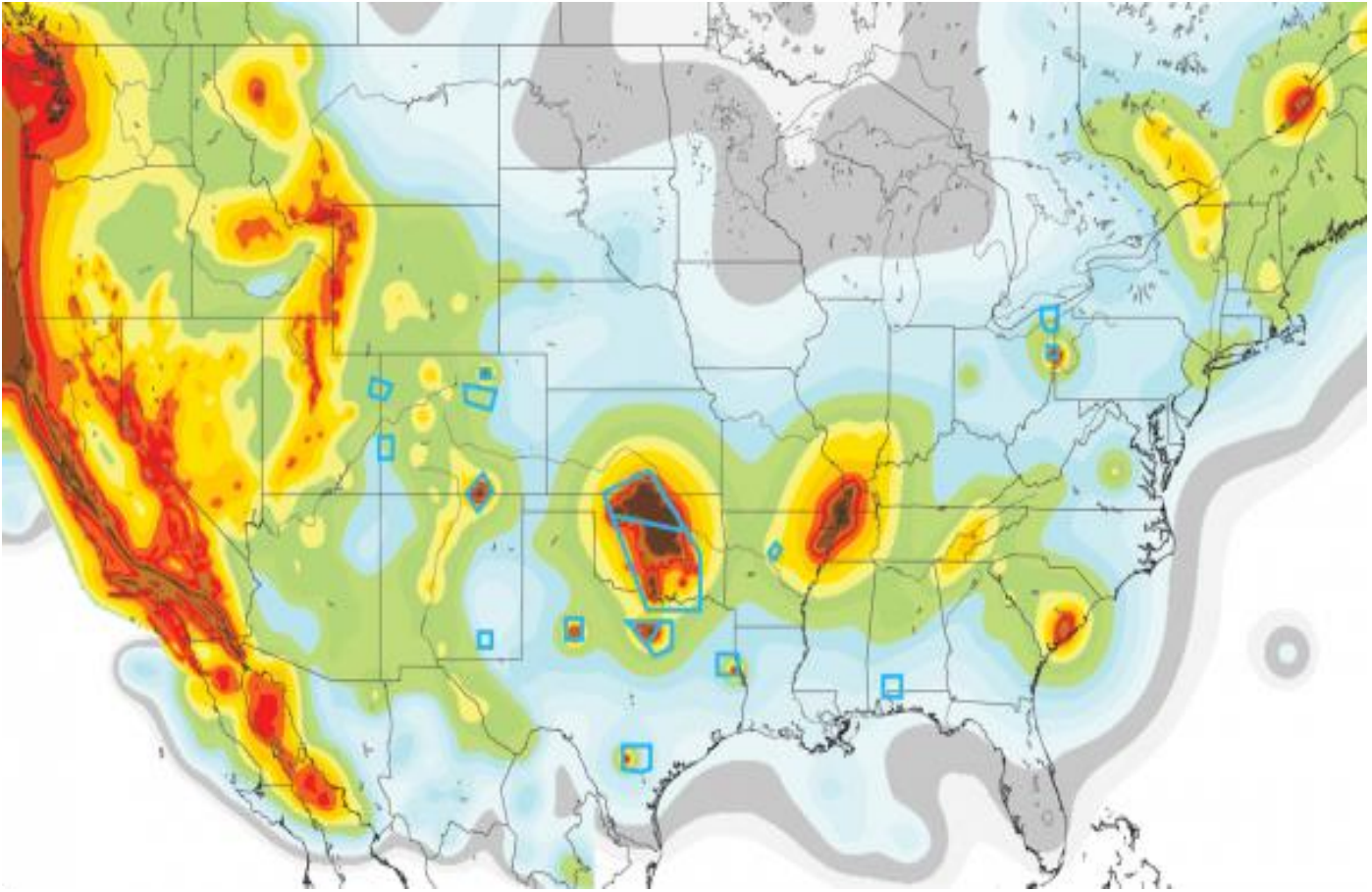
earthquake.usgs.gov/earthquakes/states/texas/seismicity.php

2014 USGS Earthquake Hazard Assessment from Natural Earthquakes



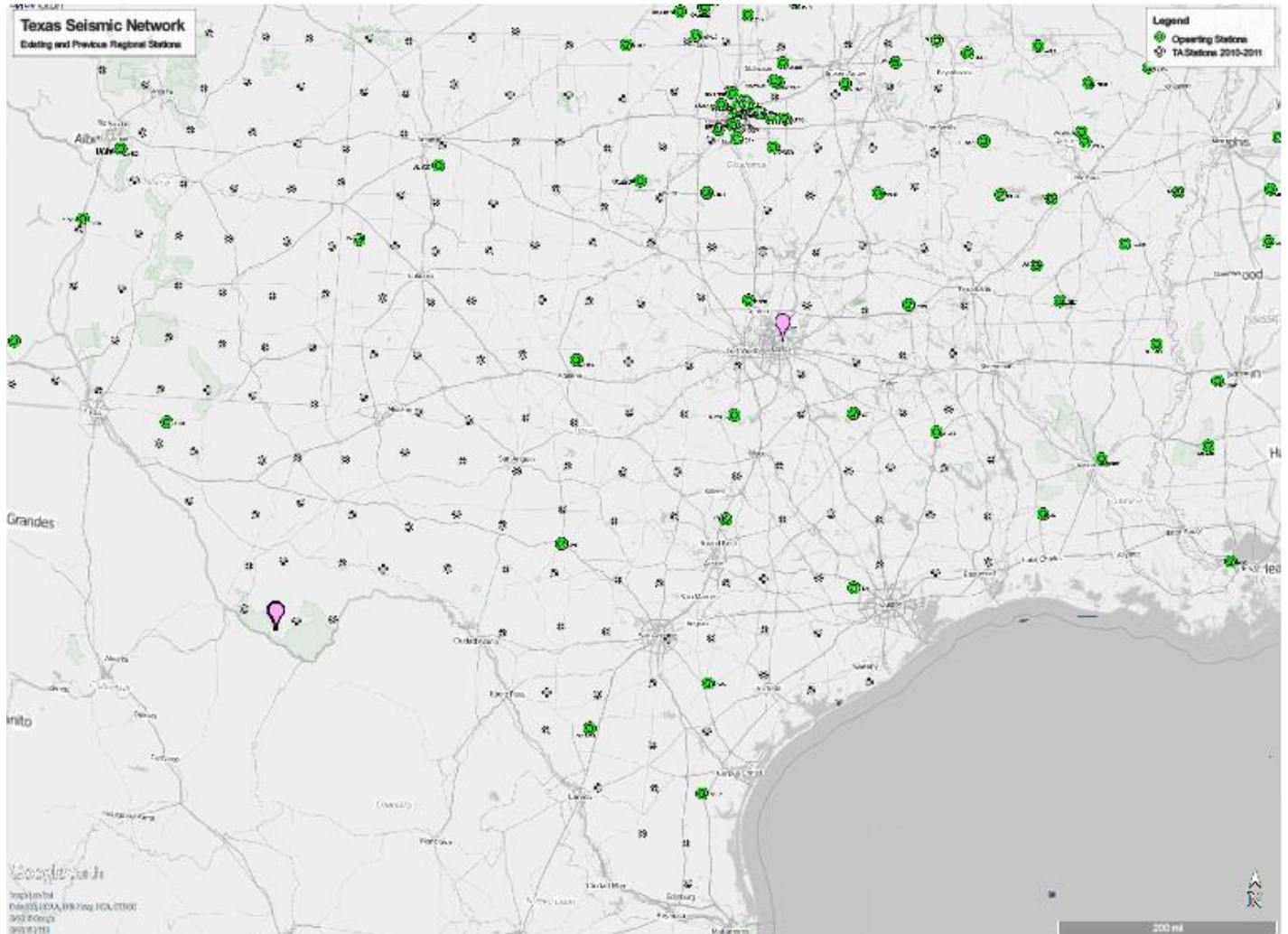
From Petersen et al. 2015, USGS Open File Report 2015-1070. Black boxes indicate areas of likely induced seismicity.

2014 USGS Earthquake Hazard Assessment from All Earthquakes

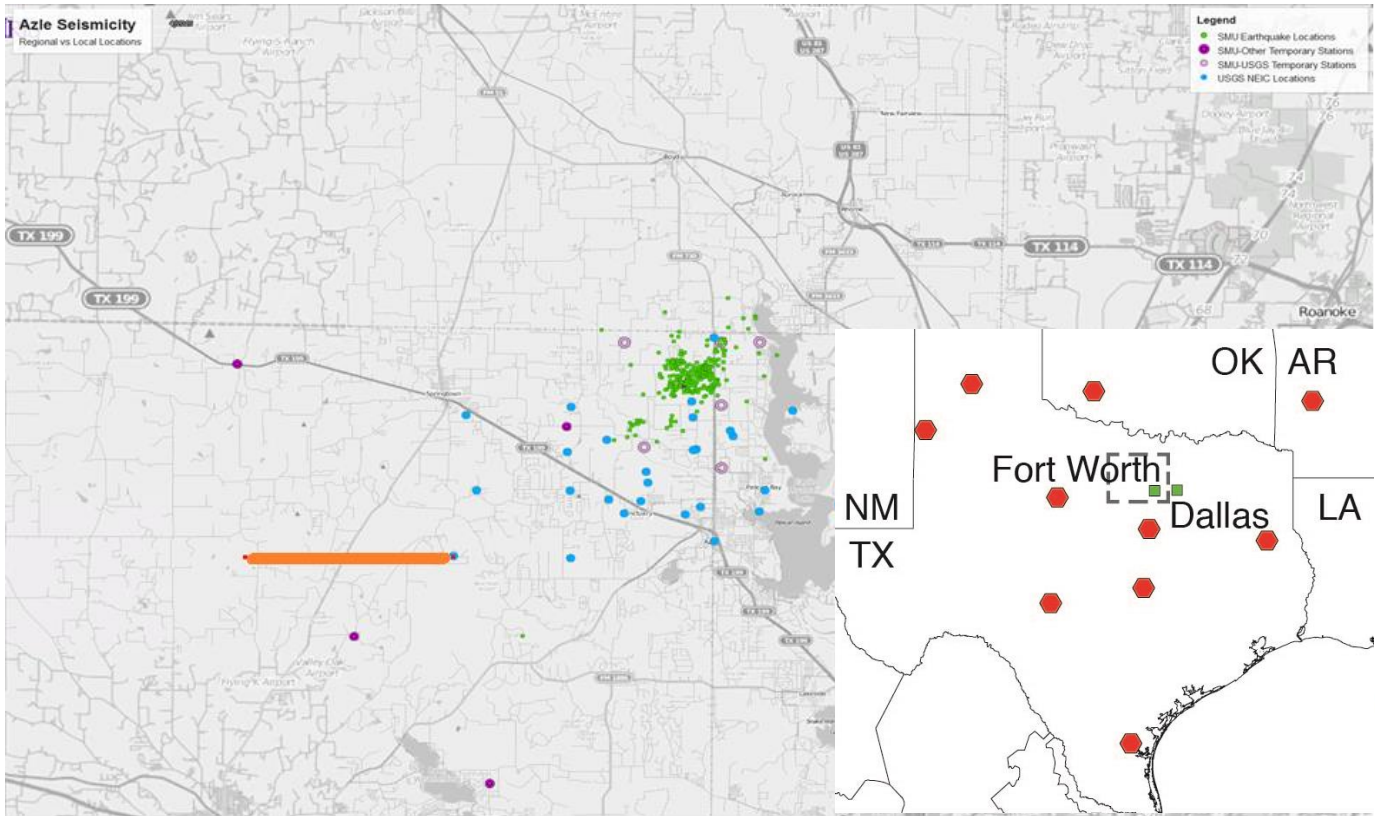


From Petersen et al. 2015, USGS Open File Report 2015-1070. Blue boxes indicate areas of likely induced seismicity. The 2015 Dallas/Irving earthquakes are not incorporated into this study.

Operating and Past Seismic Stations

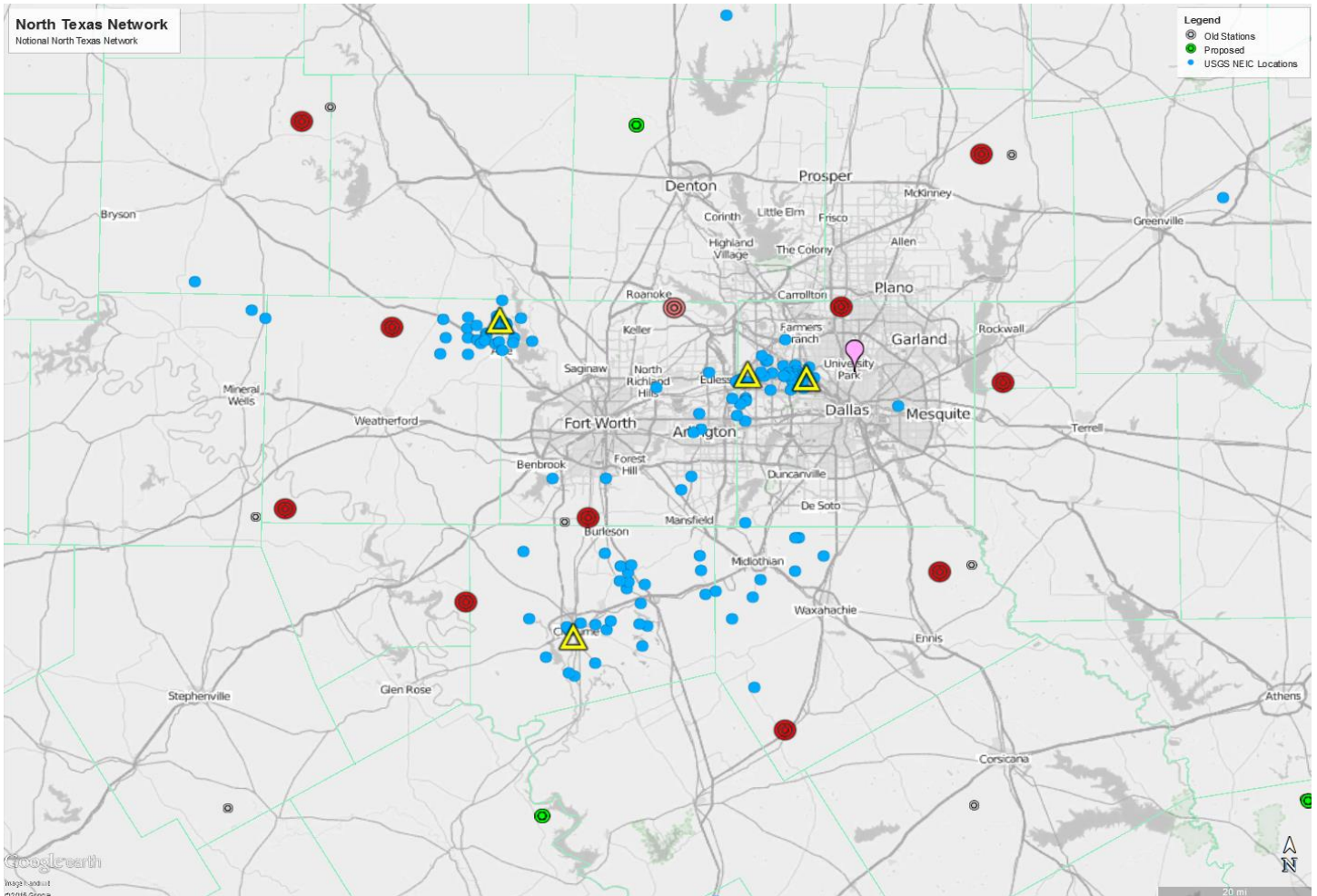


Azle Earthquake Locations: NEIC Regional vs Local Network



Orange line is 10km long, the approximate error in the regional seismic locations

Notional Long Term Monitoring Network for North Texas



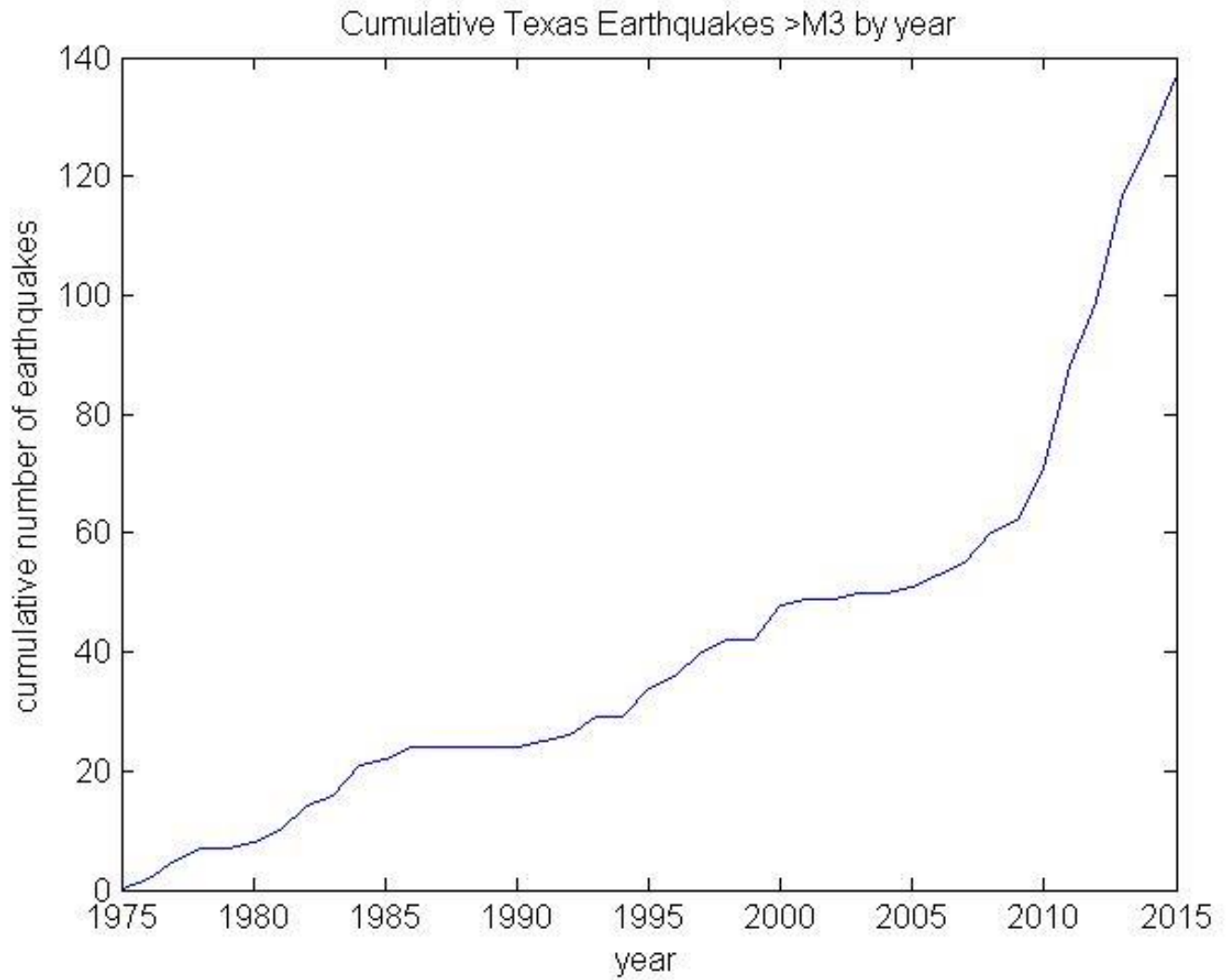
Notional Network: Yellow triangles represent urban seismic monitoring networks consisting of multiple stations with a possible mix of instruments suitable for seismic detection and location in urban environments. Red circles are the North Texas regional network designed to detect and provide the first locations for new centers of seismicity

Comments on North Texas Monitoring¹

1. North Texas network is a notional plan to develop scoping for North Texas.
2. There is a need for closely spaced regional stations in order to provide better initial locations when new seismic activity begins. Better locations provide better hazard estimates in order to prioritize further study and avoid false alerts or alerts in the wrong area.
3. Seismic network designs for urban areas need a known minimum magnitude for detection. This design usually requires careful research.
4. There is a need to respond rapidly (a day or two) with a local drop-in network upon the first detection of new seismicity.
5. Results from local networks need to rapidly incorporated into the USGS ANSS program
6. There is a need for long term (>5 years) monitoring near high risk areas that have had active seismicity (based upon sequence beginning 2008 at DFW).
7. Seismic systems for urban environments may be different than those used for regional stations, and installation costs may be higher.

¹ Comments are based upon SMU's experience with 4 studies in urban areas as well as ongoing experience in installing, maintaining, operating, and analyzing data from the CTBTO seismic arrays and other seismic stations used in SMU's seismology research program.

Appendix A: Rate of Seismicity in Texas from 1975 to April 2015 complete to Magnitude 3 or greater.



Appendix B: RANGE OF EQUIPMENT, PERMANENT AND TEMPORARY, IS RECORDING DATA FROM NORTH TEXAS EARTHQUAKES

SMU seismologists are frequently asked about the equipment they use to monitor the increased seismic activity occurring in the Fort Worth Basin since 2008.

How many permanent seismic stations do we have in North Texas? How many are operated/owned by USGS and how many belong to SMU or other parties?

An interesting look at this question is provided by the table below showing partial information from the stations contributing to the National Earthquake Information Center (NEIC) locations for the April 2, 2015 magnitude 3.3 earthquake in Dallas/Irving. On each line, the channel names start with a two-letter network code that in general indicates the owner of the station and something about the planned duration for the station operation. The phase arrival table lists the times that the seismic waves arrive at each station sorted in order of distance from the earthquake. Distance between the station and the estimated earthquake epicenter is given in degrees. One degree is about 69 miles. The table lists the contributing networks:

Phase Arrival Times

Channel	Distance	Azimuth	Phase	Arrival Time	Status
NQ UDFB HNZ 01	0.01°	114.41°	Pg	22:36:22.30	manual
ZW IFS3 EHZ 00	0.03°	149.48°	Pg	22:36:22.50	manual
NQ NLKCP HNZ 01	0.03°	303.79°	Pg	22:36:22.58	manual
ZW IFBF EHZ 00	0.07°	15.49°	Pg	22:36:22.69	manual
ZW ITL1 EHZ 00	0.07°	15.49°	Pg	22:36:22.30	manual
ZW ITSC EHZ 00	0.08°	63.24°	Pg	22:36:22.67	automatic
ZW AZDA EHZ 01	0.53°	283.06°	Pg	22:36:31.39	manual
N4 Z35B BHZ --	0.55°	330.94°	Pg	22:36:31.07	manual
TA WHTX BHZ --	0.97°	207.21°	Pg	22:36:39.20	manual
N4 237B BHZ --	1.28°	131.38°	Pn	22:36:44.59	manual
N4 Z38B BHZ --	1.69°	75.57°	Pn	22:36:49.58	manual
TA 435B BHZ --	2.14°	195.14°	Pn	22:36:59.37	automatic
OK X37A BHZ --	2.17°	36.57°	Pn	22:36:58.00	automatic
US NATX BHZ 00	2.21°	118.89°	Pn	22:36:57.50	automatic
TA ABTX BHZ --	2.29°	265.00°	Pn	22:36:59.57	automatic
US WMOK BHZ 10	2.43°	321.26°	Pn	22:37:01.90	automatic
OK FNO HHZ 01	2.43°	350.99°	Pn	22:37:03.23	automatic
OK OKCSW EHZ --	2.58°	350.86°	Pn	22:37:05.82	automatic
OK OKCFA HHZ --	2.59°	350.66°	Pn	22:37:06.07	automatic
GS OK025 HHZ 00	2.74°	353.14°	Pn	22:37:08.02	automatic

Channel	Distance	Azimuth	Phase	Arrival Time	Status
OK BCOK HHZ --	2.85°	348.92°	Pn	22:37:10.06	automatic
GS OK029 HHZ 00	2.97°	351.83°	Pn	22:37:11.64	automatic
US MIAR BHZ 00	3.27°	58.01°	Pn	22:37:11.67	automatic
AG WLAR HHZ 00	3.31°	74.39°	Pn	22:37:12.75	automatic
AG WLAR HHZ 00	3.31°	74.39°	Pg	22:37:20.35	automatic
US JCT BHZ 00	3.40°	226.67°	Pn	22:37:14.90	automatic

NQ - Netquakes stations. These are portable stations deployed to catch aftershocks or new events when an earthquake sequence starts. They are temporary and not as sensitive as the more useful permanent stations, but because they are close to the events, they help tremendously with locations. They are typically deployed by local volunteers at sites where the site owner can contribute a network connection. SMU has installed and maintains seven of these in the North Texas area. They are on loan from the USGS.

ZW - SMU's temporary network. These are instruments on loan to SMU, and the bulk of the 18 currently operating stations come from Incorporated Research Institutes for Seismology (IRIS). SMU is currently operating these.

N4 - Central and Eastern US network (CEUSN). These are high quality redeployed stations from the temporary TA network. They are funded through 2017.

TA - Transportable Array stations. This is the National Science Foundation-funded IRIS operated transportable array. The stations listed here are the U.S. Reference stations and are expected to operate through the end of the EarthScope experiment.

OK - Oklahoma Geological Survey Network.

US - USGS Network

GS – USGS-funded stations, usually temporary.

AG - Arkansas Network

SS – Single, miscellaneous stations. SMU's DAL station falls into this category. SMU operates this station on the SMU campus.

IM - International Monitoring System (this is only the site in far West Texas). SMU operates and maintains this array (a set of 9 stations)

In the April 2, 2015 M3.3 earthquake, the NEIC used stations out to about 240 miles away in solving

for the location. This included stations in Texas, Oklahoma, and Arkansas. The closest station was one of the temporary SMU stations, about six miles from the epicenter. The closest long-term station was N4.Z35B, at about 40 miles. The closest miscellaneous station was SMU's basement seismometer in Heroy Hall, an instrument graciously on loan to SMU from Geotech Instruments here in Dallas. The closest permanent government-funded station was OK.X37A at about 150 miles. The closest "permanent" station owned by the USGS was US.NATX just beyond 150 miles. N4 and TA stations are National Science Foundation research stations currently operated as part of an experiment, but will likely evolve into permanent stations once the experiment is complete.

At the end of this text you will find an image of the regional stations in Texas operating after 12/15/2013.

How many permanent stations are needed in North Texas?

The role of permanent stations in an integrated network is to first detect earthquakes where no portable network exists, provide accurate enough locations and magnitudes to make an initial assessment of the hazard that the earthquakes might represent, and to provide a long-term monitoring network for any active faults. Networks with more stations generally mean better detection of small magnitude earthquakes, better estimates of magnitudes and locations, and better estimates of time constants for developing earthquake sequences.

To answer the question with some scientific basis, seismologists typically look at network simulations or calculations that take into account the detection capability of stations in various locations. The network is designed to solve a particular problem, for example to have a 90% probability of detection of any earthquake larger than magnitude 2.0, and to be able to locate the hypocenter to an accuracy of +/- 1 mile for earthquakes within 150 miles of DFW. In addition it might be designed to reliably detect earthquakes down to magnitude 1 for any fault showing recent activity. (These are arbitrary figures - so far no one has published a set of criteria for Texas). Alternatively, in seismically active areas seismologists evolve a network, starting with roughly evenly spaced seismic stations and then infilling where the network does not meet the defined capability criteria.

As a rough illustration, the magnitude 1.1 Irving/Dallas earthquake occurring at 16:01 UTC Jan. 23, 2014, was barely visible on only one existing regional station about 40 miles from the station. To reliably detect an earthquake, seismologists like to see the earthquake at three or more stations. In urban areas, where traffic can often "blind" a station for a moment, additional stations are used.

The magnitude 2.0 Venus, Texas earthquake occurring at 5:45 UTC Nov. 2, 2013 in an area with recent activity not monitored by portable stations, was recorded by nine regional stations BUT only one of the stations was within 100 miles of the earthquake, producing a location uncertainty so large that it would be impossible to attribute the earthquake to any specific fault in the area. In these

situations, locations may be in error by 10 miles or more. Initial deployment of portable stations requires a large number of stations to be certain of getting enough stations near the true epicenter.

In 2008 to 2012 the EarthScope experiment covered Texas with stations spaced roughly every 45 miles (except in the urbanized DFW areas where there were none). This network, with each station operating for two years, provided significantly better seismic coverage than the permanent stations of today, but was insufficient to reliably and accurately locate small earthquakes. As an evolutionary improvement in the 45-mile spacing, and without developing a network criterion, SMU suggested reducing the spacing used during the experiment in North Texas to roughly half, 22.5 miles. Combined with the few existing permanent stations, this would cover the currently active part of the North Texas area with 16-20 permanent stations.

How many portable stations do we have in North Texas? Who owns/operates them?

Currently in North Texas, SMU is the only station operator that has portable stations deployed and is producing publicly available data that may be used by the USGS or other interested parties for earthquake analysis. SMU currently has deployed a total of 26 stations, with most borrowed from IRIS and the USGS. Only two of the stations use SMU owned equipment, the rest have all been borrowed. Currently 9 of the stations are scheduled to be returned at the end of 2015 with most others on indefinite, but on-call loans. Most portable networks operate only for a year or two.

How many portable stations do we need in addition to those?

Because some of the earthquake sequences seem to continue over a number of years, some of the portable stations might need to stay in a location for 5 or more years. In our current situation, none of the portable stations is likely to be available for that period of time. For each earthquake sequence, SMU has found that having a set of 10 instruments provides enough initial coverage. While it is possible to cover an area with as little as five instruments, provided there is a good permanent network with the personnel to operate and do routine analysis, the coverage is not as reliable and it takes substantially more time to establish the optimum placement for the stations in the network. We experienced this in the cases of Azle and Cleburne where the initial work was done with just 5 instruments.

To keep the current temporary network running, we'd like to see 15-20 portable instruments in the North Texas area. The number of additional instruments beyond the initial 20 that could be useful is probably more limited by the funding for investigators and technicians than places to put seismometers. An investigation in Johnson County where there has been recent activity could use 10 additional instruments. There are areas to the north and west that are potential areas of study as well. To some extent this also depends on the type of installation.

Is the number of stations proposed under TexNet enough?

The network design for TexNet (station locations, equipment capability, emplacement depth, etc.) has not been finalized and it is therefore not possible to comment on the capabilities of the network for earthquakes in North Texas. However, if the total number of stations is spread evenly over the state, the network capability in heavily urbanized regions may not be adequate for induced earthquake hazard assessments. It may be that an uneven network could improve the capability.

However, it isn't just the number of stations that is needed, but also an analysis and alert capability. As additional stations are added to the network, additional manpower is needed to conduct data analysis in a timely enough manner to support the more intensive portable deployments.

Additional stations, coupled with a local analysis center, provide two advantages: First, the overall detection threshold (or catalog completeness) magnitude is reduced. Thus, if we currently reliably detect all M3.0 earthquakes in Texas, the additional stations may allow us to capture data from more earthquakes - such as those at M2.5 or lower. While smaller earthquakes are not generally considered damaging, they do provide insight into the probability and location of possible larger earthquakes, and if induced, may give an indication of areas where some form of mediation or changes in practices are needed. It is also an open research question as to whether the characteristics of small earthquakes may give an indication as to whether a particular sequence is likely induced or natural. Knowing this may refine hazard estimates.

Appendix C: Dallas/Irving Earthquake Preliminary Report



Preliminary Report – Irving, Texas, earthquake sequence

6 February, 2015

The Honorable Beth Van Duyne
Mayor of Irving
825 W. Irving Blvd
Irving, TX 75060

The Honorable Mike
Rawlings
Mayor of Dallas
1500 Marilla Street
Dallas, TX 75201

Dear Ms. Van Duyne and Mr. Rawlings:

In response to the recent earthquakes felt in Irving and Dallas, seismologists at Southern Methodist University (SMU) and the U.S. Geological Survey (USGS) have been collaborating to produce more accurate locations for felt and smaller events and to identify the source region of the ongoing activity. The purpose of this letter is to report on the initial earthquake relocations using the local seismic network, which provides a more accurate understanding of the true geographical extent of the epicenters. At this time, we cannot identify a causative fault nor provide any conclusions as to cause.

Since 2008, the USGS National Earthquake Information Center (NEIC) in Golden, CO, began reporting felt and locatable earthquakes in the DFW area, a region with no prior earthquake activity going back to at least 1970. We identify the beginning of the ongoing earthquake sequence in Irving as April 17, 2014 based on the first felt earthquake (magnitude 2.4) reported for eastern Irving and Dallas. Since then, the rate of earthquakes has varied but increased significantly in early January 2015 including the occurrence of two magnitude 3.5 and 3.6 events on January 6. For this sequence, the NEIC reports that the largest earthquake to date has been a magnitude of 3.6, that there have been five earthquakes over magnitude 3, and that there have been 46 total reported earthquakes with the smallest reported magnitude being 1.1. The NEIC locations are scattered over a roughly circular area with a 2 mile radius, approximately centered on the TX Highway 114-183 exchange, locally referred to as the old Texas stadium site in the City of Irving (Figure 1). The rate of felt earthquakes in the sequence slowed in late January and early February, and the last reported felt earthquake reported by the NEIC was a magnitude 2.2 on January 23, 2015. SMU continues to record smaller earthquakes that are not locally felt.

SMU, assisted by the City of Irving, has deployed seismic recorders within 10 miles of the NEIC epicenters. Two days after the widely felt November 23, 2014 magnitude 3.3 earthquake, SMU reinstalled a seismograph south of the DFW International Airport that was used to record the 2008-2009 DFW earthquake sequence. On January 5, 2015, as soon as instruments became available, SMU worked with the City of Irving to install a station in north Irving. Following the widely felt earthquakes on January 6, the USGS provided two “NetQuakes” seismographs, and SMU deployed these and an additional 12 temporary seismographs designed to stay in the field for 10 days. Over the following weeks, SMU has continued to deploy longer-term, higher-quality seismographs made available through the Incorporated Research Institutions for Seismology (IRIS) to record the ongoing seismicity and has recovered the 12 temporary stations with associated data. We deeply appreciate the help in siting stations we have

received from the staffs and local residents of Irving, Dallas, Farmers Branch and Coppell, and the telemetry equipment provided by Irving that allows the data from almost all stations to be relayed directly to the USGS and publicly archived. The instrument locations are shown in Figure 2.

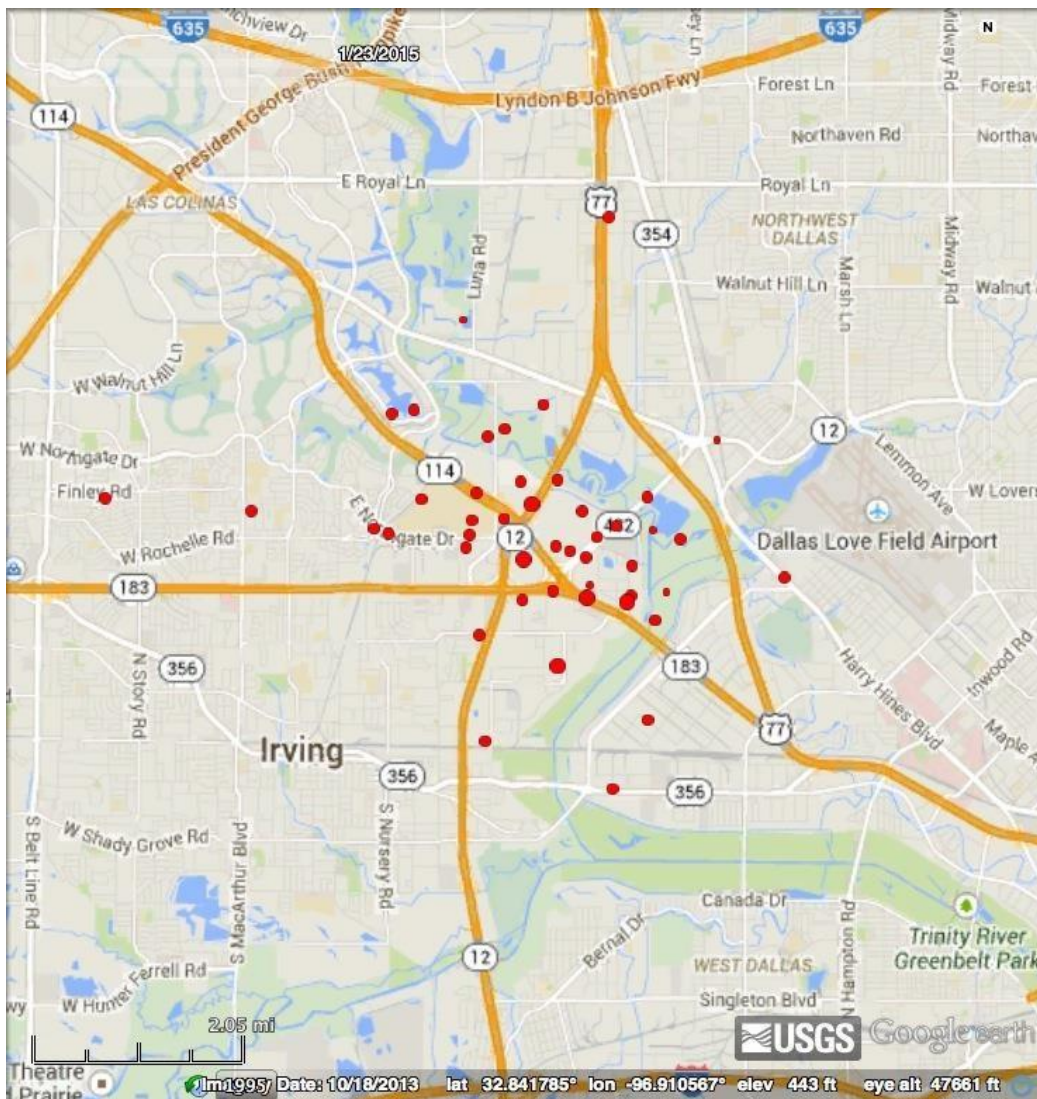


Figure 1. Earthquake epicenters determined by USGS-NEIC, April 17, 2014 through January 23, 2015. Circle size is scaled by magnitude, which ranges from 1.1 – 3.6. Because the NEIC must rely on a regional seismic network in this area where station spacing is over 100 miles, the reported locations near Dallas may be in error by as much as 5 miles, especially for earthquakes smaller than about magnitude 2.5. Scale at lower left is 2.05 miles.

SMU scientists have now relocated 26 felt earthquakes reported by the NEIC in January 2015, using the data recorded by the SMU/USGS temporary local seismic network combined with a geologically based model for the velocity of seismic waves beneath the urban region. The improved epicenters are confined to a limited area extending north from TX Highway 114 to Walnut Hill Rd. along the Trinity River (Figure 3). Note that the new earthquake locations extend the source area through parts of Irving and west Dallas. This source area includes the epicenters of the magnitude 3.5 and 3.6 earthquakes of January 6, 2015. Figure 4 shows the same earthquakes and instrumentation in a series of time-slices so you can better see how the instrumentation and earthquake locations have changed over the month of January.

As with previous North Texas earthquake sequences (DFW, Cleburne, Azle), the local stations provide more precise locations and reduce the earlier scattered NEIC locations shown in Figure 1 to linear feature(s) potentially consistent with a fault(s) trend. As they did in our analysis of the Azle sequence, the epicenters shift to the north relative to the NEIC initial locations. The earthquakes are shallow, between 4.5 and 7 km deep. It is not unusual to have a range of depths like this, as the earthquakes may be occurring on different parts of the fault(s). The depths are uncertain, however, because critical details of the subsurface geology and seismic velocity remain poorly known. The current locations and depths were determined with a slightly modified geologic model that was used in the study of the DFW earthquakes just to the west. We tested a various subsurface geologic assumptions to determine the range of probable earthquake depths (focal depths). Based upon this analysis, we conclude that most of the earthquakes are located in the shallow crystalline basement (granites) below the sedimentary rocks (sandstones, shales, limestones, etc.) that comprise the Fort Worth Basin. We expect that the depth uncertainty in our current locations will be reduced as we integrate additional geologic information.

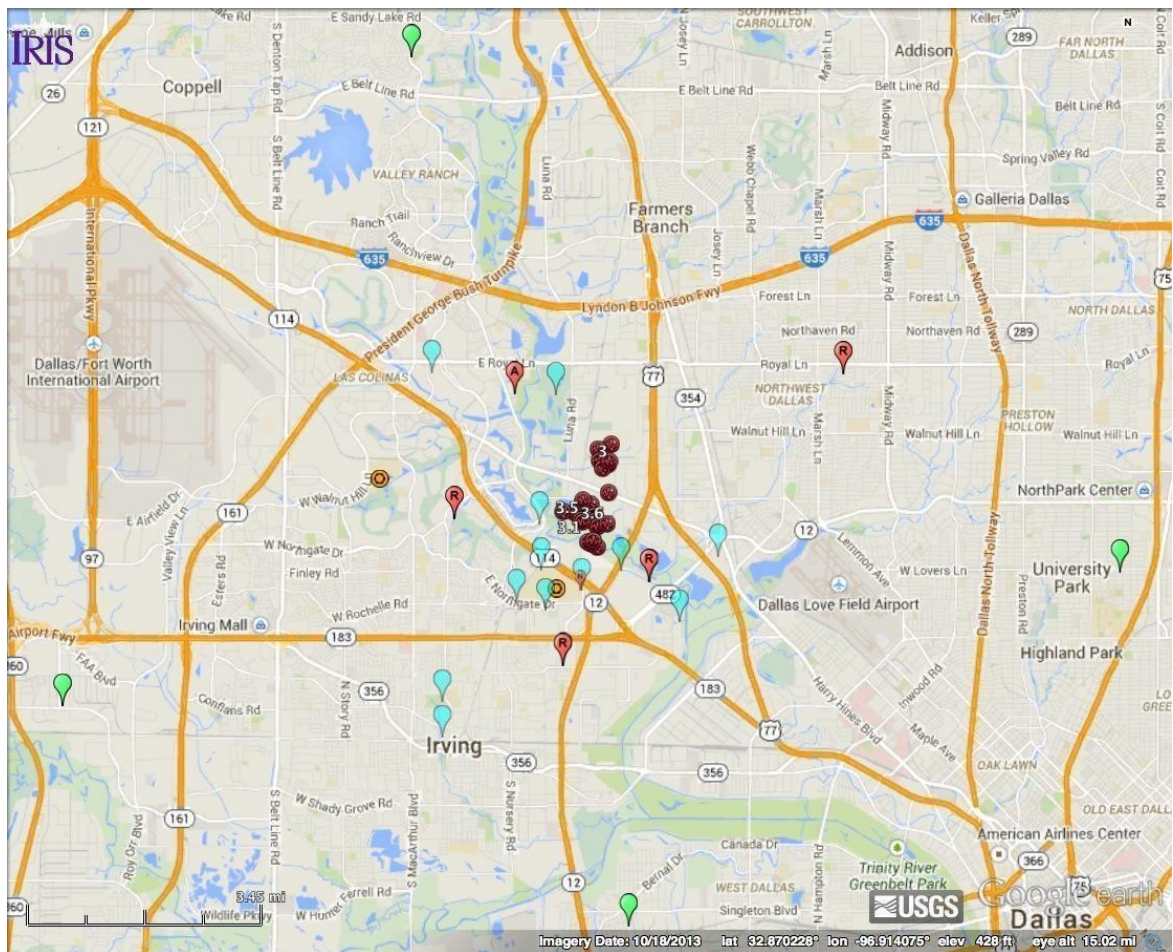


Figure 2. Locations of seismographic instruments as of January 30, 2015 together with revised earthquake locations (dark red). The network became fully operational for the purpose of locating earthquakes well on January 5th, but significant real-time location improvement did not occur until mid-January. Short-term stations deployed from Jan 7-17th are shown in cyan. USGS “Netquakes” stations are shown in orange circles. SMU/IRIS stations are shown in green (broadband sensors) and red (shortperiod sensors). Earthquake relocations are described further in Figure 3. Scale at lower left is 3.45 miles.

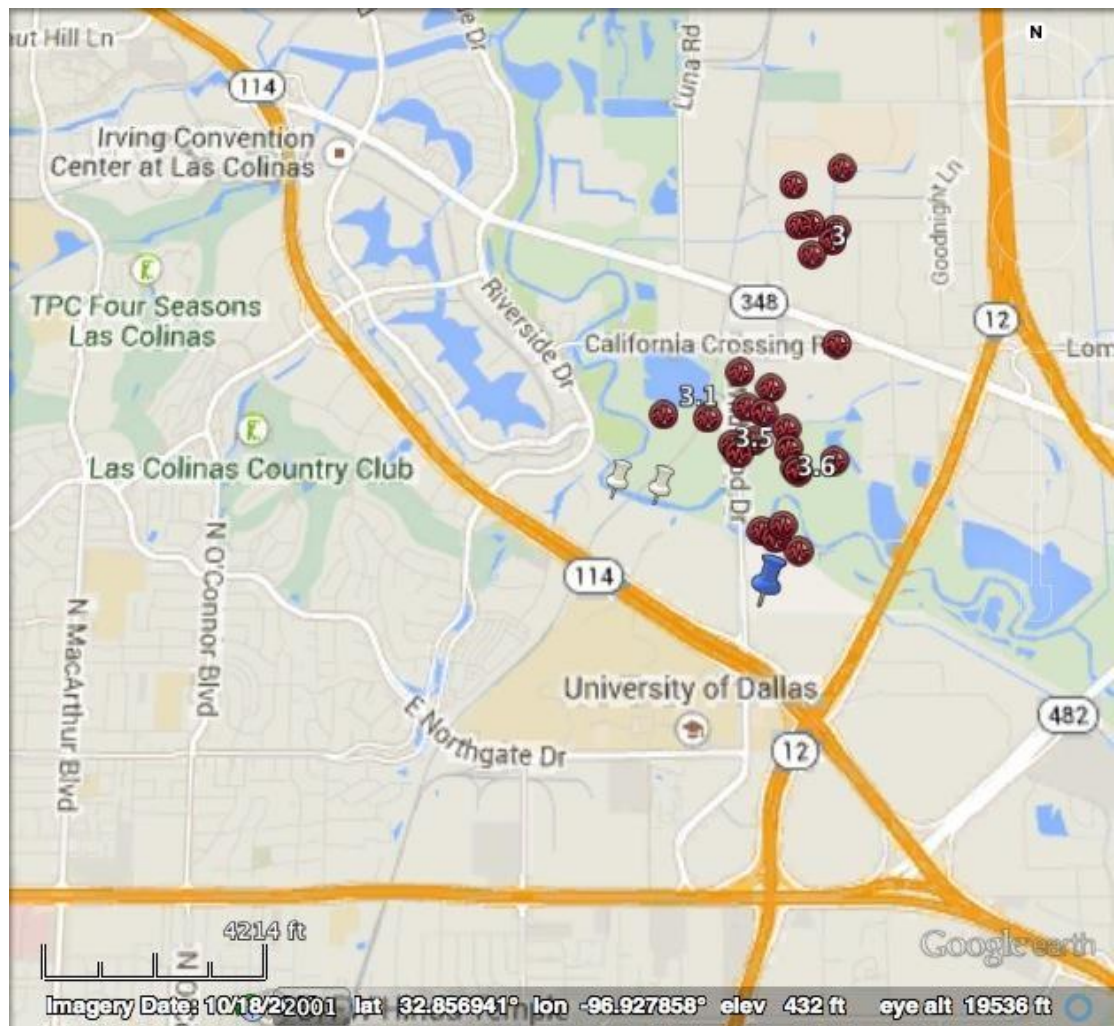


Figure 3. Detail showing epicenters of earthquakes (red symbols) located using the local seismographs from January 6-23, 2014. Magnitude 3+ earthquakes reported by the NEIC have been marked. The only production wells in the region [API 42-113-30147 and API 42-113-30189] (pad site: blue pushpin; well bottoms: white pushpins) was developed in 2009 and ceased production in 2012. The scale at the bottom left is ~0.80 miles.

Scientific questions about the nature of events in North Texas have heightened local and national concerns about the impact of activities related to shale gas production on geological infrastructure and subsurface structures. SMU scientists continue to explore all possible natural and anthropogenic causes for the Irving earthquakes and do not have conclusions at this time. Due to the public interest in these questions, however, we note here that there is one set of inactive shale gas production wells [API 42-11330147 and API 42-113-30189] near the Irving earthquake epicenters (Figure 3). The wells ceased production in 2012 and are the only known production wells in the region mapped in Figure 3. A more detailed history on the wells can be found through the Texas Railroad Commission public archive. The nearest wastewater injection well is located ~8 miles to the northwest. Production and disposal activities in this region are generally confined to the sedimentary units overlying the basement rocks discussed in the preceding paragraph. As part of our studies of North Texas earthquakes in general, we continue efforts to gather more detailed information on the history of production and wastewater disposal activities throughout the region.

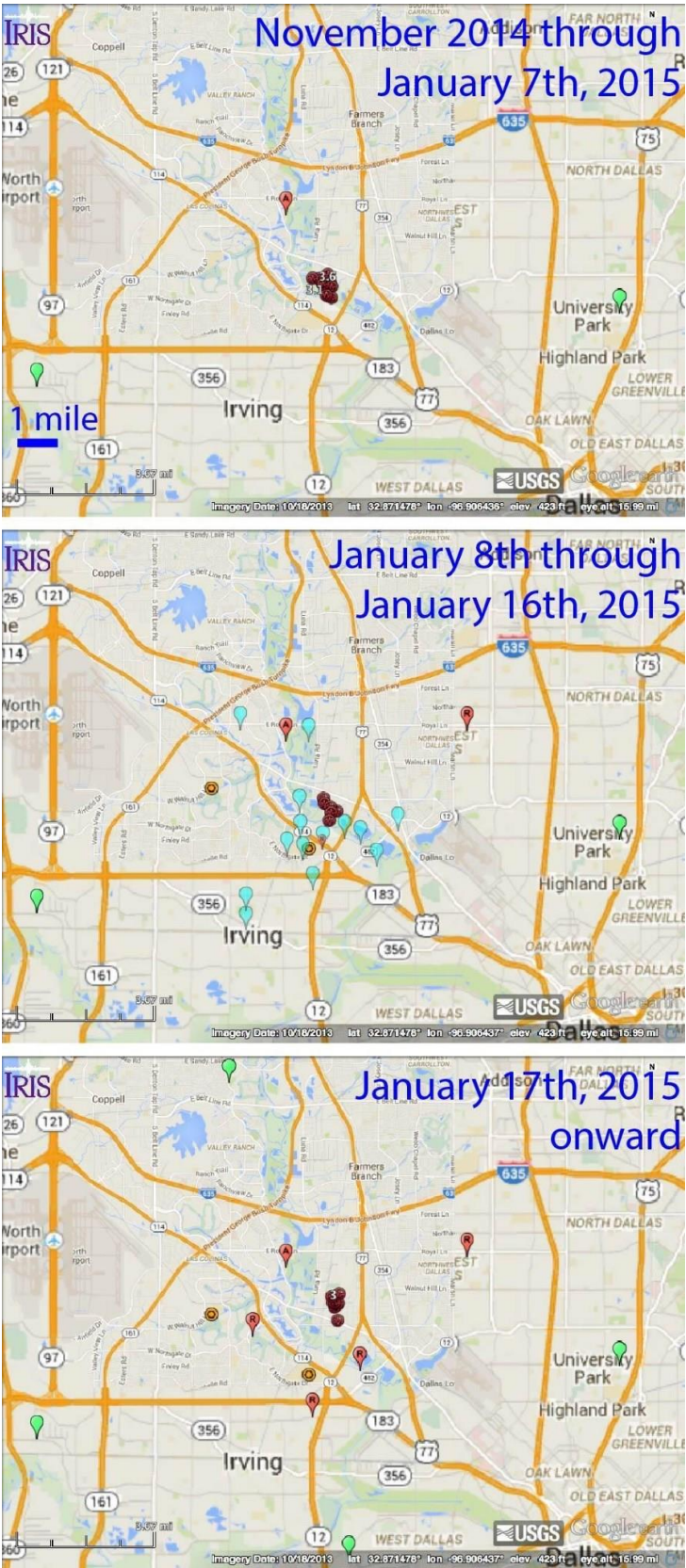
Figure 4. Time history of epicenters and station distribution.

Top) Epicenters and station distribution from late November 2014 through January 7th, 2015. During this time period, we had up to three local stations in place (red and green placemarks). Earthquakes reported by the NEIC and relocated using the local stations are shown (red earthquake symbols). These stations captured the high level of activity on Jan. 6-7th, 2015.

Middle) Epicenters and station distribution from January 8-16, 2015. In response to the increase in activity, shortterm seismographs (blue placemarks), USGS “Netquakes” seismographs (orange circles), and one additional local station (red placemarks) were deployed during this time period. Seismicity reported by the NEIC and relocated over this time period are shown (red earthquake symbols).

Bottom) Epicenters and station distribution from January 17, 2015 and moving forward. Five additional local stations (red and green placemarks) have been or will be placed to provide sufficient distance and azimuthal coverage to monitor the ongoing seismic activity. There will be 11 seismographs run as part of the temporary Irving network moving forward. Seismicity reported by the NEIC and relocated since January 17th is shown (red earthquake symbols). Earthquake activity shifts about 0.5 miles north during this time interval.

The next steps of the Irving earthquake study are already underway. The USGS will continue to report 24/7 felt earthquakes in near real-time and post this information (event pages, Did You Feel It? reports, ShakeMaps) of use to the general public on their website (earthquakes.usgs.gov). Due to differences in how the NEIC and SMU handle local and distant locations may continue to fall outside of the epicenter



station data, it should be expected that the USGS catalog

trend shown in this report. SMU will continue to maintain the seismic network and locate both felt and smaller earthquakes in the area, including repeating our relocation analysis to improve upon the initial NEIC locations of any future felt earthquakes in the sequence. This will help refine the geometry of the fault(s) at depth and aid in hazard assessment. We will also continue to work on more advanced location methods, determine the direction of fault motion, and investigate causal factors leading to this swarm. As we refine the geologic models and re-analyze the earthquake data, it would not be surprising for the refined epicenters to be as much as a half-mile different than what we now estimate. In other words, our estimated error in location is currently at most about a half-mile. Even so, we think that it is unlikely that the overall picture will significantly change; therefore, we are providing this current information to help guide the cities moving forward.

Questions regarding data and analysis presented in this document should be directed to Heather DeShon (hdeshon@smu.edu), Brian Stump (bstump@smu.edu), Robert Williams (rawilliams@usgs.gov) and Michael Blanpied (mblanpied@usgs.gov).

Sincerely,

Heather DeShon
Southern Methodist University



Brian Stump
Southern Methodist University

Robert Williams
USGS Geologic Hazards Science Center



Michael Blanpied
USGS Earthquake Hazards Program
Reston, VA



Golden, CO

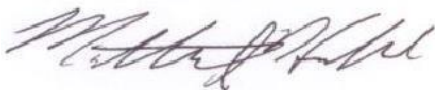
Chris Hayward
Southern Methodist University



M. Beatrice Magnani
Southern Methodist University



Matthew Hornbach
Southern Methodist University



cc: Rocky Vaz, Director of Emergency Management, City of Dallas
Jason Carriere, Emergency Manager Coordinator, City of Irving
Craig Pearson, Texas Railroad Commission Seismologist

APPENDIX D: Researcher Biographies

MATTHEW J. HORNBACH

Associate Professor of Geophysics
Roy M. Huffington Dept. of Earth Sciences
Southern Methodist University
PO Box 750395
Dallas, Texas, 75275-0395

Cell:512-636-5030
mhornbach@smu.edu

EDUCATION

Ph.D., Geophysics, University of Wyoming, Dec. 2004
A.B., Magma cum Laude in Physics, Hamilton College, 1998

SUMMARY

Dr. Matthew Hornbach's research includes the numerical modeling of heat flow, fluid flow and pore pressure in earth systems; high resolution 2D/3D/4D seismic imaging and analysis of marine sedimentary basins; detecting, quantifying, and modeling methane hydrate systems; and geohazards. Recent presentations include "Tsunami potential of the Enriquillo Plantain Garden Fault: Past, Present, Future" before a UNESCO meeting in Port-au-Prince, Haiti in July 2013. Before completing his Ph.D. in 2004, Hornbach was invited to speak by ExxonMobil in Houston on 3D seismic imaging of gas hydrates in 2003; by ConocoPhillips in Houston on hydrates imaging and pressure modeling also in 2003; and by Conoco in Houston on 3Dpoststack inversion for oil and gas discovery in 2002.

- Published >39 peer-reviewed manuscripts
- Grants of more than \$3.3 million since completing Ph.D.
- Invited by U.S. Sec. of Energy to serve on Methane Hydrates Advisory Committee
- Member, U.S. Advisory Panel for International Ocean Discovery Program
- Associate Editor, Journal of Geophysical Research-Solid Earth, 2013-Present
- National Academy of Science review panel member, NRC Associateship Program

CURRENTLY FUNDED PROJECTS

DOE-NETL, "Gas Hydrate Dynamics on the Alaskan Beaufort Continental Slope: Modeling and Field Characterization" Lead-PI: M. Hornbach. Oct. 2012-March. 2017.

NSF-GeoPrisms, "*Collaborative Research: A community seismic experiment targeting the pre-, syn-, and post-rift evolution of the Mid Atlantic US margin.*" Lead PI: B. Magnani (SMU). Co-PI: M. Hornbach, September 2013-July, 2016

DOE-NETL: "Geothermal Play Fairway Analysis," Co-PI: M. Hornbach. October 2014-September, 2015

Anadarko Petroleum Corporation, "*3D heat flow analysis of shale plays in the Denver Basin,*" Lead PI: Hornbach, December 2014-December 2016.

BRIAN W. STUMP

Albritton Professor of Earth Sciences
 Roy M. Huffington Dept. of Earth Sciences
 Southern Methodist University
 P.O. Box 750395
 Dallas, TX 75275-0395

Office: 214-768-1223
 bstump@smu.edu

EDUCATION

Ph.D., geophysics, University of California, Berkeley, 1979
 Master of Arts, University of California, Berkeley, 1975
 B.A., summa cum laude in physics, Linfield College, 1974

SUMMARY

Brian Stump was named an American Association for the Advancement of Science (AAAS) Fellow in 2015 for distinguished contributions to his field, particularly in the area of seismic monitoring in support of the Comprehensive Nuclear-Test-Ban Treaty. His expertise includes seismic wave propagation, inverse theory, earthquake and explosion source theory, mining related phenomenology and low frequency acoustics.

Stump is well known regionally for his continued work researching the increase of small earthquakes that have been occurring in North Texas since 2008. But his work in detecting ground motion from explosions has for more than 20 years proved invaluable to the United States government in ensuring that the world's nuclear powers abide by their agreements related to underground nuclear testing. He served as scientific adviser to the U.S. delegation to the Conference on Disarmament from 1994 through 1996 and continues to be called upon frequently to assist the U.S. government in the interpretation of seismic and acoustic data.

Stump recently completed a term as board chair for Incorporated Research Institutions for Seismology (IRIS), a consortium of more than 100 universities funded by the National Science Foundation that in conjunction with the United States Geological Survey operates the Global Seismic Network and has implemented USArray, a set of closely spaced seismic systems deployed across the US.

- Chair of Air Force Technical Applications Seismic Review Panel
- Published >65 peer-reviewed manuscripts
- Continuous funding from U.S. Dept. of Energy and Dept. of Defense since 1983 for research in nuclear explosion monitoring using seismic and acoustic data.
- Committee member, National Academy of Sciences Committee on Seismology and Continental Dynamics, 2007-2012
- Associate Editor, Journal of Geophysical Research, 2007-2009
- Member, American Association for the Advancement of Science, American Geophysical Union, Society of Exploration Geophysicists, International Society of Explosives Engineers and Seismological Society of America
- Fellow, Royal Astronomical Society

HEATHER RENE DeSHON

Associate Professor of Geophysics
Roy M. Huffington Dept. of Earth Sciences
Southern Methodist University
PO Box 750395
Dallas, TX 75275-0395

Office: (214) 768-2916
Fax: (214) 768-2701
hdeshon@smu.edu
faculty.smu.edu/hdeshon

EDUCATION

Ph.D., Earth Science (Geophysics), University of California, Santa Cruz, June 2004.
B.S., magna cum laude with honors in the liberal arts, Geophysics and Mathematics, Southern Methodist University, May 1999.

SUMMARY

Dr. Heather DeShon is a seismologist whose research focuses on understanding earthquake rupture complexity along active faults in order to better estimate seismic, tsunami, and volcanic hazard. She is an expert in high-resolution earthquake relocation and subsurface imaging using seismic tomography techniques. Her experience encompasses studies of small to large magnitude earthquakes in subduction zones (examples: Sumatra, Middle America, Kuriles, etc.), along intraplate faults (examples: New Madrid, North Texas), and in volcanic environments (examples: Aleutians, Costa Rica). She was a Distinguished Lecturer for the National Science Foundation GeoPRISMS program from 2012-2014, which highlighted her work on subduction zone processes, and she currently serves on the U.S. Ocean Bottom Seismometer Instrument Pool Oversight Committee.

- Published >40 peer-reviewed manuscripts
- Received grants totaling >\$750k
- Served as Associate Editor, *Bulletin of the Seismological Society of America*, 2009-2014
- Organized or convened professional workshops, field trips and scientific sessions at national meetings
- Overseen and/or participated in seven land or marine deployments of local seismic networks

RELEVANT CURRENT RESEARCH & FUNDING

Principal Investigator: North Texas Earthquake Project,
<http://www.smu.edu/News/NewsIssues/EarthquakeStudy>

Hornbach, M., H.R. DeShon, W.L. Ellsworth, B.W. Stump, C. Hayward, C. Frolich, H.R. Oldham, J.E. Olson, M.B. Magnani, C. Brokaw, J.H. Luetgert (2015), Causal factors for seismicity near Azle, Texas, *Nature Communications*, **6**, 6728, doi:10.1038/ncomms7728.

SMU University Research Council grant, Understanding recent North Texas Seismicity: A scientific investigation of the Azle and Mineral Wells earthquake sequences

Pending United States Geological Survey grant, North Texas Earthquake Study and Network Operations – Irving & Azle, PI: H.R. DeShon and M.B. Magnani

Jon Olson

George H. Fancher Professorship in Petroleum Engineering,
The Lois K. and Richard D. Folger Leadership Chair in Petroleum and Geosystems Engineering
The University of Texas at Austin
Cockrell School of Engineering

Email: jolson@austin.utexas.edu

Phone: (512) 471-7375, (512) 471-3161

Office: CPE 5.168B, CPE 2.502

Research Areas: Reservoir Geomechanics, Hydraulic Fracturing, Induced Seismicity, Naturally Fractured Reservoir Characterization, Unconventional Resources

Educational Qualifications:

B.S., Civil Engineering, B.S., Earth Sciences, University of Notre Dame, 1984, magna cum laude

Ph.D., Applied Earth Sciences, Stanford University, 1991.

Research: Dr. Olson's research currently focuses on production optimization and environmental impact issues related to hydraulic fracturing and unconventional oil and gas development. His students and I work on problems of induced seismicity, physical and numerical modelling of hydraulic fracture propagation from horizontal wells, the interaction of hydraulic fractures with natural fractures, shear-enhanced permeability due to deformation in heavy oil reservoirs stimulated by steam injection, modelling production from unconventional gas and oil reservoirs, wellbore stability and reservoir compaction and subsidence. I also continue to do work in quantitative structural geology related to natural fracture characterization.

Awards & Honors:

SPE Distinguished Lecturer, 2014-2015 tour.

AAPG Distinguished Lecturer, 2007-2008 tour.

Michel T. Halbouty '30 Visiting Chair in Geology and Geophysics, Texas A&M University, Fall 2005.

Anadarko Fellowship #2 in Petroleum Engineering.

APPENDIX E: COMPLETE 2015 PAPER IN NATURE COMMUNICATIONS WITH SUPPLEMENTARY MATERIAL.

ARTICLE

Received 18 Aug 2014 | Accepted 24 Feb 2015 | Published xx xxx 2015

DOI: 10.1038/ncomms7728

OPEN

Causal factors for seismicity near Azle, Texas

Matthew J. Hornbach¹, Heather R. DeShon¹, William L. Ellsworth², Brian W. Stump¹, Chris Hayward¹, Cliff Frohlich³, Harrison R. Oldham¹, Jon E. Olson⁴, M. Beatrice Magnani¹, Casey Brokaw¹ & James H. Luetgert²

In November 2013, a series of earthquakes began along a mapped ancient fault system near Azle, Texas. Here we assess whether it is plausible that human activity caused these earthquakes. Analysis of both lake and groundwater variations near Azle shows that no significant stress changes were associated with the shallow water table before or during the earthquake sequence. In contrast, pore-pressure models demonstrate that a combination of brine production and wastewater injection near the fault generated subsurface pressures sufficient to induce earthquakes on near-critically stressed faults. On the basis of modelling results and the absence of historical earthquakes near Azle, brine production combined with wastewater disposal represent the most likely cause of recent seismicity near Azle. For assessing the earthquake cause, our research underscores the necessity of monitoring subsurface wastewater formation pressures and monitoring earthquakes having magnitudes of $\sim M2$ and greater. Currently, monitoring at these levels is not standard across Texas or the United States.

¹Huffington Department of Earth Sciences, Southern Methodist University, Dallas, Texas 75275, USA. ²USA Geological Survey, 345 Middlefield Road, MS977, Menlo Park, California 94025, USA. ³Institute for Geophysics, The University of Texas at Austin, Austin, Texas 78758-4445, USA. ⁴Department of Petroleum and Geosystems Engineering, The University of Texas at Austin, Austin, Texas 78712-2100, USA. Correspondence and requests for materials should be addressed to M.J.H. (email: mhornbach@smu.edu) or to H.R.D. (email: hdeshon@smu.edu).

Several factors, both natural and anthropogenic, can reactivate faults and cause earthquakes^{1–4}. These factors include, but are not limited to, stress changes caused by the natural shift of Earth's plates, stress changes induced by water table fluctuations^{2,3} and stress changes induced by the removal and the injection of fluids in the deep subsurface⁴ (Fig. 1). We use the term 'induced' to include earthquakes triggered by anthropogenic causes that release tectonic stress as well as earthquakes that release stresses created by industrial activity¹. Determining which factor is the primary driver of seismicity is often difficult without a detailed understanding of the subsurface stress regime and geology.

Surveys of crustal stress and observations from deep boreholes at locations worldwide indicate that stress in continental interiors maintains consistent orientation within the regional provinces having dimensions of hundreds to thousands of km⁵; the brittle crust is often in a state of near-failure equilibrium⁶; although aseismic deformation can occur, stress levels are often limited by the frictional strength of pervasive naturally occurring faults governed by Coulomb frictional failure theory⁷; and increased fluid pressure along faults promotes failure by reducing effective stress⁸. In areas where the Earth's crust is critically stressed,

surprisingly small changes in stress (typically 0.01–0.1 MPa) can trigger fault reactivation and cause earthquakes^{9,10}.

Both nationally^{1,11–15} and in Texas^{16–19}, studies examining the recent seismicity in oil- and gas-producing areas often attribute earthquakes to high-volume wastewater injection based on the proximity of injection wells to hypocenters and because the onset of seismic activity follows the emplacement and use of injection wells. Most of these studies, however, do not evaluate other possible anthropogenic causes of seismicity or do not utilize physical models to quantify stress change. Critics of these studies note, correctly, that tens of thousands of currently active injection wells apparently do not induce earthquakes or at least not earthquakes large enough to be felt or recorded by seismic networks⁴. Why some injection wells induce seismicity while others do not is unclear. Here we consider several regional factors that might cause seismicity near Azle, Texas.

This analysis demonstrates that brine production combined with wastewater injection generates more significant subsurface stress changes at earthquake depths than regional groundwater or lake level changes. Regional geologic interpretations and historical accounts of regional seismicity independently suggest that natural tectonic stress changes represent an unlikely cause of

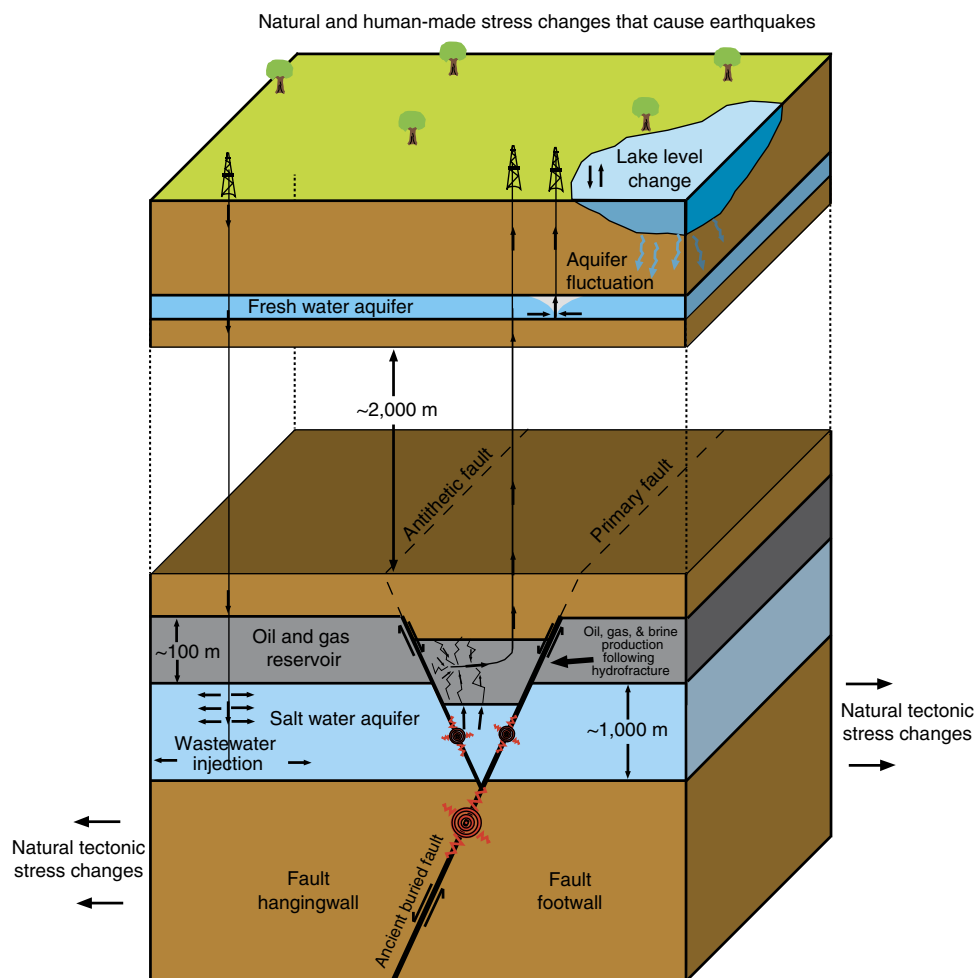


Figure 1 | Natural and anthropogenic stress changes that may trigger earthquakes in the Azle area. Several natural and anthropogenic (man-made) factors can influence the subsurface stress regime resulting in earthquakes. Natural stress changes that promote earthquakes include intraplate stress changes related to plate tectonics^{9,10} and natural water table or lake levels variations caused by changing weather patterns or water drainage patterns with time, and in some instances (not pictured) the advance or retreat of glaciers. Anthropogenic stress changes that promote earthquakes include human-generated changes to the water table (including dam construction^{2,3}) and industrial activities involving the injection or removal of fluids from the subsurface⁴. The figure is not to scale.

the Azle earthquakes. The analysis therefore indicates subsurface stress changes associated with brine production and wastewater injection represents the most probable cause of recent earthquakes in the Azle area. The study highlights the need for better subsurface pore pressure and seismic monitoring to address future potential-induced seismicity hazards.

Results

Linking seismicity with regional geology. From early November 2013 through January 2014, the United States Geological Survey's National Earthquake Information Center (NEIC) reported 27 earthquakes near the cities of Azle and Reno, Texas, including two widely felt M3.6 events (Fig. 2 and Supplementary Fig. 1). To improve locations, refine magnitudes and characterize the fault geometry associated with the events, a temporary local seismic network was deployed in mid-December 2013 (see Supplementary Fig. 1; Supplementary Table 1). We report high-accuracy earthquake locations and magnitudes based on these data for earthquakes occurring up through 30 April 2014 (Figs 2b and 3). Seismicity occurs on two steeply dipping, conjugate faults consistent with the general strike of the Newark East fault zone (NEFZ)²⁰ (Fig. 2a,b). First motion composite focal mechanism solutions are consistent with a primary normal fault extending down-dip through the crystalline basement (strike 225°, dip ~60–70°) and a more steeply dipping (~70–80°) shallow conjugate normal fault (Fig. 2b). Earthquake locations using regional velocity models (Supplementary Table 2) suggest that both faults extend into the overlying Ellenburger sedimentary unit, and formation depths based on well logs indicate perhaps 100 m of offset exists along the primary fault²⁰, with the fault dipping to the northwest. Earthquake focal mechanisms and fault orientations are consistent with previous stress regime studies

suggesting that the maximum principal stress is vertical in this area^{5,6}. On the basis of the conversations with industry representatives, the location and dip of the faults defined in our three-dimensional (3D) fault model using passive source seismic data are consistent with industry regional fault interpretations using 3D seismic data.

The Newark East Gas Field (NEGF), a major gas-producing field in the Fort Worth Basin, extends north and east of Azle²⁰. Hydraulic fracturing is applied to produce gas from the low permeability ($\sim 10^{-18}$ – 10^{-19} m²) Mississippian Barnett Shale (Fig. 2b). Along with natural gas, hydraulically fractured gas wells in the Azle area of the NEGF can unintentionally produce (and remove from the subsurface) significant volumes of water, mostly brine, through fractures that extend to the underlying high-permeability (10^{-14} – 10^{-15} m²) Ellenburger formation, a flat-lying ~1,000-m thick dolomitic limestone^{20,21}. Brine and fracturing fluid produced from production wells are reinjected through disposal wells completed in the Ellenburger formation. Lower permeability (10^{-19} – 10^{-20} m²) Precambrian granite underlies the Ellenburger²⁰ (Fig. 2b).

At least one major (>50 km long) fault system, the NEFZ, extends northeast–southwest across the NEGF where recent Azle earthquakes occurred. Comparing the earthquake locations with multiple structural interpretations provided by industry representatives, it appears that the deeper earthquakes occur along part of the main NEFZ, whereas many shallow earthquakes associated with short-duration seismic swarms occur along a conjugate fault likely associated with a collapsed Ellenburger karst feature^{21,22} (Fig. 2). The location and geometry of this fault system is complex and difficult to constrain in the area of recent earthquake activity but is well defined to the northeast²⁰ (Fig. 2). On the basis of discussions with industry concerning proprietary seismic data, the fault is well imaged through the production and injection

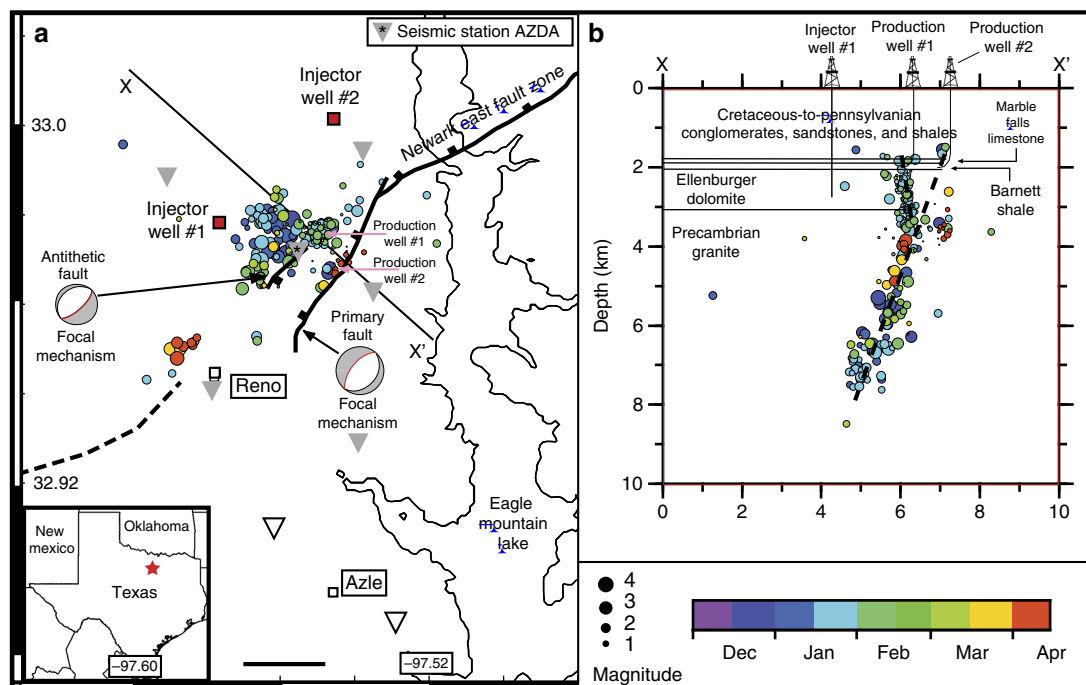


Figure 2 | Azle Earthquake locations and regional geologic structure. Map showing the location of NEFZ (black) at the top of the Ellenburger formation, inferred faults (dashed) at the top of the Ellenburger formation, injection wells (red squares), two production wells (API 36734045 and 36734139) with significant brine production near the faults (pink arrows) and earthquake epicentres (coloured circles) recorded by the temporary seismic network (triangles) (a). The red star in the inset of a shows the map location. The black scale bar in a is 2 km. Grey (white) triangles indicate the locations of active (inactive) seismic stations. Line X–X' in a shows the location of the cross-section shown in (b). We interpret two faults based on earthquake location and consistent with industry interpretations: a primary normal fault and a shallower antithetic normal fault.

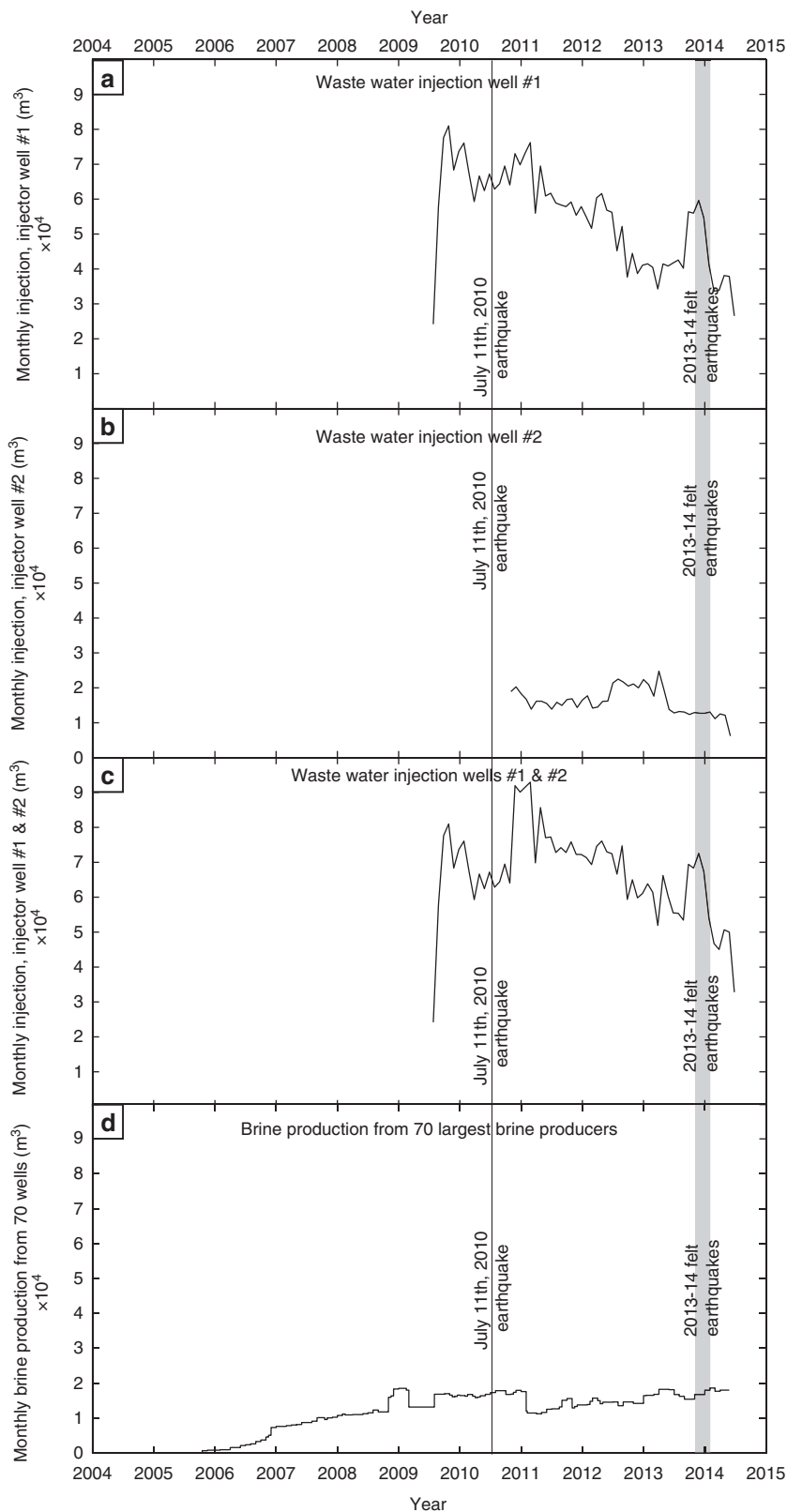


Figure 3 | Regional wastewater injection and production volumes versus time. Monthly injection volume versus time at injector well #1 (a). Monthly injection volume versus time at injector well #2 (b). Combined monthly injection volume for both injector well #1 and injector well #2 (c). Estimated monthly water production with time for the 70 largest water producing wells within 10 km of earthquake epicentres (d). Note that the scales for all of these plots are the same.

depth intervals. Above the production interval and within the Precambrian basement, the fault geometry is not well known. Historically, there has been no evidence for seismicity in this region or along this fault²³.

Assessing water table stress changes. Induced seismicity is sometimes attributed to water-level and lake-level variations^{2,3}. Eagle Mountain Lake is a large reservoir located ~5 km east of the earthquake epicentres; drought caused it to drop in elevation by 2.1 m from April 2012 to November 2013. Our calculations indicate that at Ellenburger depths, this water level drop will reduce Coulomb stress by only ~0.0006 MPa (Supplementary Fig. 2). This is one to three orders of magnitude smaller than typical stress changes associated with triggered seismicity^{9,10}, although KPa stress changes do sometimes trigger earthquakes at other locations²⁴. Eagle Mountain Lake water level changes during the past few years, however, are within historic values (Supplementary Fig. 3). It is therefore difficult to attribute recent seismicity in Azle to lake level change.

We also looked at variations in the Trinity Aquifer recorded at groundwater monitoring wells (Supplementary Fig. 4). The unconfined Trinity Aquifer exists ~100 m below the surface near Azle. Although data are limited, where data exist we observe no significant or systematic changes in the depth of the aquifer for the past 6–8 years. This implies water level changes in the aquifer are not responsible for recent seismicity.

Assessing natural tectonic stress changes. Though rare, natural intraplate tectonic stress changes have reactivated ancient fault systems far from known seismic zones, causing earthquakes^{25,26}. We acknowledge that it is possible, but unlikely, that natural tectonic stress changes are responsible for recent seismicity in Azle since the region is historically inactive. Before the occurrence of probable injection-induced earthquakes in the Dallas-Fort Worth area in 2008, the historic seismicity record includes only one felt earthquake within the 140,000 km² Fort Worth Basin^{16,17}. That felt event, however, is based on a single felt report with no associated stories in regional newspapers and suspected poor location quality. One small (<M2.5), unfelt earthquake (11 July 2010) was detected in the Azle region when the Earthscope Transportable Array moved through North Texas¹⁷. The unusual increase in north Texas seismicity since 2008 is consistent with other seismicity studies in the central United States that document significant increases in the rate of earthquakes greater than magnitude 3.0 in the past 6 years^{1,13–19}. These studies generally conclude that the recent increase in US seismicity is not a natural phenomenon but is instead caused by human practices, primarily wastewater injection.

No obvious surface expression exists for the NEFZ, implying no recent surface rupture, and although only limited publically available seismic data exist, analysis suggests that the majority of faults extending through the Ellenburger are associated with karst collapses that occurred ~300 Myr ago^{21,22}. This is consistent with the observation that until 2010, no earthquakes had been either recorded or felt in the Azle region during more than 150 years of settlement^{16,17,23}. On the basis of earthquake locations, focal mechanisms and regional seismic interpretations, most shallow Azle earthquake events occur along the antithetic fault associated with a ~300 million-year-old Ellenburger karst collapse. Although long-term stress monitoring is ultimately needed, the lack of evidence for significant faulting in the region during the last ~300 million years and the fact that no reliable historic earthquake reports exist near Azle during the past ~150 years of permanent settlement supports the premise that natural

intraplate tectonic stress changes are an unlikely cause of seismicity in this region.

Assessing stress changes associated with oil and gas activity.

Several production and injection wells drilled during the past decade in the Fort Worth Basin represent an additional potential cause of seismicity⁴. Two high-volume wastewater injection wells (Fig. 2a) and more than 70 production wells that produce gas and brine (Supplementary Fig. 5) are situated within 10 km of the Azle earthquake sequence and the NEFZ. Average monthly wastewater injection pressures and volumes are available from the Texas Railroad Commission (TRC). injector well #1 began injecting in June 2009 and has averaged ~44,000 m³ per month (Fig. 3a, Supplementary Fig. 6). Injector well #2 began injecting in October 2010 and has averaged ~13,000 m³ per month (Fig. 3b, Supplementary Fig. 6). Injection pressures are reported only at the wellhead, and the TRC collects no downhole formation pressures or subsurface shut-in pressures that would allow for formation pressure monitoring. Fluid production from oil and gas production wells in this region, including brine likely from the Ellenburger, is only reported to the TRC during the annual 48-h pump tests (G-1 and G-10 forms) and is highly variable—typically ranging from 0 to 800 m³ per month per well. Since G-10 reporting typically occurs only on an annual basis, it provides only a crude estimate of brine production across the region. We use G-10 production reports combined with gas production reports for the 70 largest brine-producing wells in the region to make first-order estimates of brine production (Fig. 3d). In general, the most significant brine production occurs along the NEFZ.

It is difficult to draw a simple correlation between the timing of fluid injection, fluid production and seismicity in Azle (Fig. 3). Although there is an increase in injection volumes in mid-2013 before the recent events (Fig. 3a), even higher volumes and pressures are reported in prior years at both injectors, when no felt earthquakes occurred (Fig. 3, Supplementary Figs 6 and 7). A key issue is how fluid pressure changes caused by the injection and removal of fluid impact subsurface stress along the fault. To estimate how fluid pressure changed over time and space in the area of earthquake activity, we developed a 3D pore pressure model for the Ellenburger formation. The model calculates variations in subsurface pressure due to two regional wastewater injection wells and the 70 largest brine production wells in the modelling domain located near NEFZ earthquake activity²⁷.

We ran the model for a 10-year period from 2004 to the end of 2013 over a range of parameters (see, for example, Table 1). Permeability in the Ellenburger is constrained using pump test data supplied by energy companies (Supplementary Fig. 8). Injection and production well pressures are varied with time based on data provided by the TRC (Supplementary Tables 3–5). We begin the model run in 2004 to account for the 70 regional brine production wells that may have removed water from the Ellenburger as early as 2004, thereby reducing the pressure. We vary brine production monthly so that it only occurs when a well is also producing gas. Owing to uncertainties in gas production and gas volumes in the Ellenburger, the model currently does not account for multiphase flow.

Model results show that a pressure differential develops along the antithetic fault as a combined result of high fluid injection rates to the west and high water removal rates to the east (Figs 4 and 5). While the absolute pressure change depends on input parameters (Table 1), in the area of recent seismicity, the differential pressure development along the faults remains a consistent feature of all model runs. Modelled pressure changes on the faults typically range between 0.01 and 0.2 MPa, depending

Table 1 | Examples of model parameters and associated results.

Well #1 mean excess bottom-hole pressure in (MPa)	Well #2 mean excess bottom-hole pressure in (MPa)	Mean effective permeability ($\times 10^{-14} \text{ m}^2$)	Thickness of high permeability zone (m)	Producers included?	Boundary conditions	Specific storage ($\times 10^{-6} \text{ m}^{-1}$)	Excess pressure on fault at AZDA, 1 January 2014 (MPa)
0.53	0.17	3	1,000	Yes	Closed	5	0.008
0.53	0.17	3	1,000	Yes	Closed	13	0.02
0.53	0.17	3	1,000	No	Closed	7.3	0.011
4.4	2.96	3	300	No	Closed	7.3	0.14
2.42	1.63	3	300	No	Closed	7.3	0.08
2.42	1.63	3	300	No	Open	7.3	0.015
2.42	1.63	3	1,000	Yes	Closed	13	0.03
2.42	1.63	3	1,000	No	Closed	5	0.05
2.42	1.63	3	1,000	No	Open	5	0.01
2.42	1.63	1	1,000	Yes	Closed	1	0.11
2.42	1.63	1	1,000	Yes	Closed	13	0.1
2.42	1.63	1	1,000	Yes	Closed	7.3	0.11
0.58	0.28	5	1,000	Yes	Open	7.3	0.02
2.42	1.63	5	1,000	Yes	Closed	7.3	0.1
2.42	1.63	10	1,000	Yes	Open	7.3	0.017

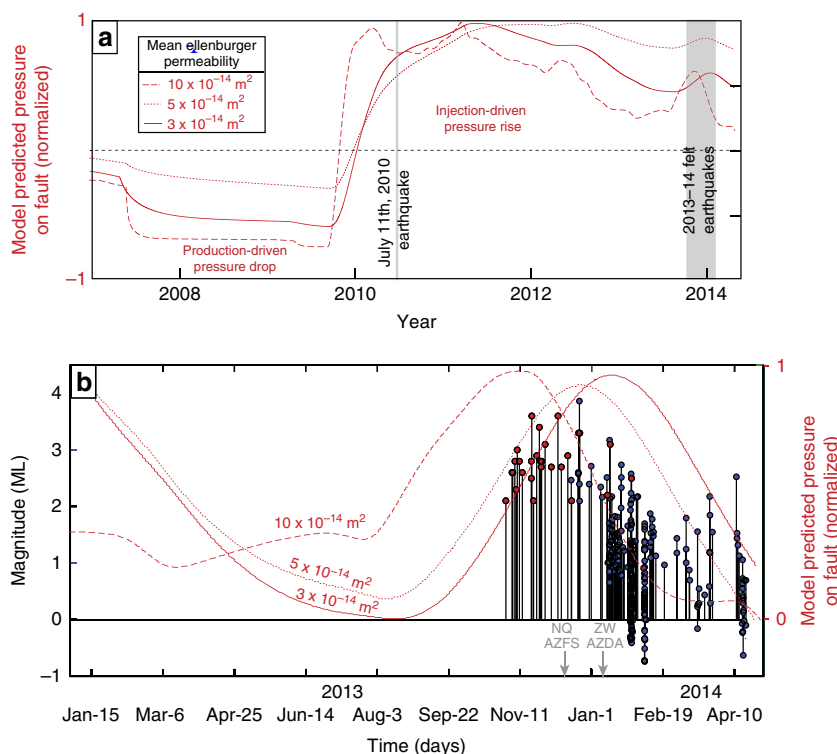


Figure 4 | Pressure at the antithetic fault versus time. Modelled pressure versus time at the antithetic fault, directly below seismometer AZDA (Fig. 2a) (a). Results include three different mean Ellenburger permeability values and demonstrate earthquake activity correlates in time with a local pressure maximum but not an absolute maximum at this site. Higher resolution time image of modelled injection pressures versus time at AZDA with earthquakes (stem and circle) coloured by network (NEIC-red; SMU-blue) (b). In 2010, one small ($M < 2.5$) earthquake was detected in the study area¹⁷. Event detection increases beginning on 15 December, the date when the first Netquakes station (NQ_AZFS) was deployed. Detection further improved when station ZW_AZDA was installed. Model results indicating pressures increase along the fault near the time of felt seismicity, with a 1–3-month delay between injection rate increase and pore pressure change at the fault based on permeability values measured at injector well #1.

on model parameters (see, for example, Table 1). Although uncertainty exists, the model-predicted pressure changes are consistent with values that are known to trigger earthquakes on critically stressed faults^{9,10} and are one to three orders of magnitude greater than stress changes associated with lake and water table changes in the region. This is true even when we use end-member bottom-hole injection pressures that are an order of

magnitude lower than reported wellhead injection pressures (see, for example, Table 1, Supplementary Fig. 9).

Discussion

It is notable that we observe earthquake swarms in the Ellenburger apparently associated with extraction, not just

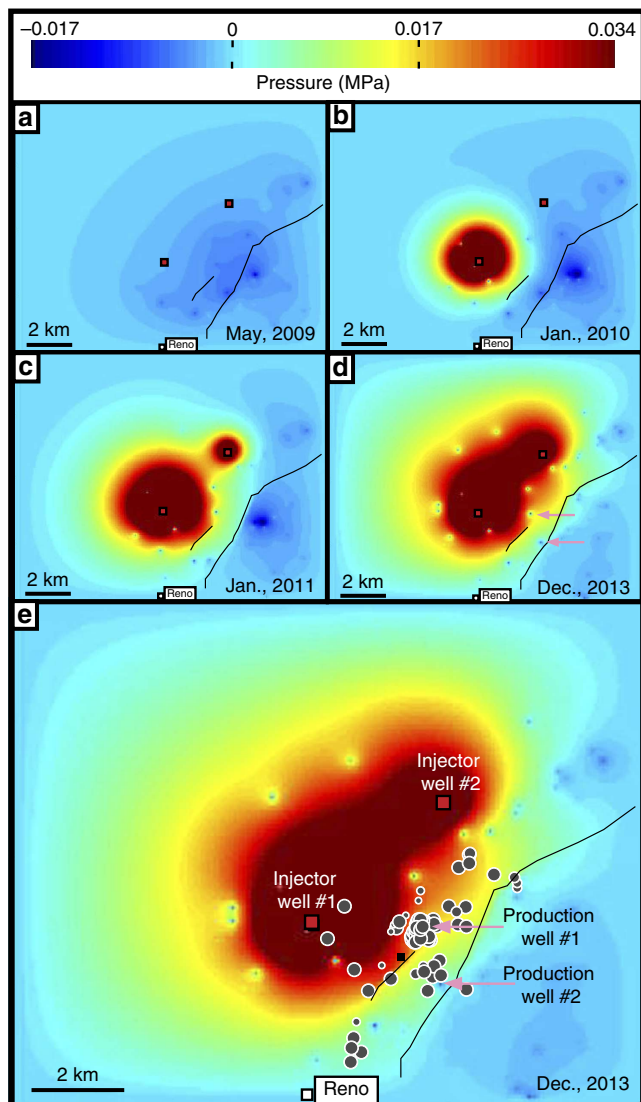


Figure 5 | Modelled pressure changes in the Ellenburger caused by injection and production. Map view of modelled excess pressures at a depth of $\sim 2,500$ m for May 2009 (a), January 2010 (b), January 2011 (c) and December 2013 (d,e). The model uses average monthly reported water injection rates and the Dupuit-Thiem equation to estimate bottom-hole pressure values. Pressure above hydrostatic averages 0.58 MPa for injector well #1 and 0.28 MPa for injector well #2 during injection. Ellenburger permeability is assumed constant at $5 \times 10^{-14} \text{ m}^2$; boundary conditions are open along the side and closed at the top and bottom. We apply an average rate of brine production based directly on reported TRC G-10 water production values for the 70 largest water producing production wells in the region. The images show the system before injection (a) through the onset of seismicity (e). Black lines, the NEFZ location at the top of the Ellenburger formation; red squares, injector locations; pink arrows, approximate location of two large brine production wells that are located both near the faults and near reported earthquake swarms within the Ellenburger (grey circles with white outlines). Note that the most significant amount of brine removal occurs along the fault trend (a).

injection, that is, they occur almost directly below the estimated subsurface location of two large brine production wells in the region, as indicated by TRC G-10 reports. On the basis of fault and well locations and the nature of permeability along faults, it is likely that these two production wells remove fluids from sediments immediately adjacent to the fault^{7,28}. Earthquakes

caused by fluid extraction near faults are not a new phenomenon in the United States or even Texas^{29–31}. Induced seismicity is often associated with subsurface pressure changes, and extensional stresses will concentrate on the boundary of the fluid draw-down region, promoting normal faulting^{29,32}. It is therefore perhaps no coincidence that we observe swarms of normal-faulting events in regions where more significant near-fault stress changes occur (Fig. 5d,e).

For simplicity, the model assesses pressure only in the Ellenburger formation where several earthquakes were recorded. The absolute focal depth of several of the initial large NEIC catalogue events remains unknown, but the larger magnitude earthquakes recorded by the temporary network occur in the underlying basement along the primary fault (Fig. 2a,b). We hypothesize that the deeper earthquakes are due to downward pressure transfer within the fault system. If the underlying basement granite has very low ($< 10^{-19} \text{ m}^2$) permeability, pressure transfer will preferentially occur along the higher permeability fracture zone and damaged zones within and parallel to the fault^{7,28}. Little is known about the permeability along the unconformity between the Ellenburger and granite basement. Currently, no publically available permeability data exist for either basement rock or the NEFZ, making it difficult to assess pore pressure change along the fault system below the Ellenburger. Industry researchers have, however, drilled through the NEFZ in the Barnett, and they suggest regional permeability is complex, with both high- and low-permeability pathways associated with the fault, consistent with detailed permeability studies of faulted formations²⁸.

Modelling results indicate that a combination of formation fluid production and wastewater injection generate the most significant stress changes at earthquake depths compared with other studied phenomena (such as groundwater or lake level fluctuations). The lack of evidence for both regional fault reactivation during the past ~ 300 million years and regional seismicity for the past ~ 150 years also supports the conclusion that brine production and wastewater injection represent the most likely cause of recent seismicity near Azle. The location, magnitude and timing of oil- and gas-generated subsurface pressure changes provide a more consistent explanation for recent seismicity than the other causal factors analysed. A complex interplay between brine production and wastewater injection likely promotes seismic activity. Nonetheless, several uncertainties remain, in part, due to the limited amount of data available that would allow more accurate calculations of *in situ* stress and possible changes in the subsurface stress regime over time (Table 1).

Nearly 50 years ago, industry researchers such as Van Everdingen³³ recognized the critical importance of baseline monitoring of subsurface pressures and fluid volumes in wastewater reservoirs to minimize hazards. Baseline pressure monitoring data, including shut-in pressure tests and pump-tests are easy to obtain, routinely collected by industry and invaluable in assessing reservoir permeability and subsurface pressure changes with time, but are currently neither required nor typically available for analysis. Similarly, improved regional seismic monitoring in areas of ongoing or potential oil and gas activity can provide invaluable insights concerning areas of potential seismic hazards. To address fully the role oil and gas activities play in promoting earthquakes, and to prepare properly for the future, induced earthquake hazard analysis ultimately requires significantly more comprehensive data sets than are currently available. These data should accurately monitor and quantify not only seismicity, volume changes and subsurface stress, but also regional subsurface structure and stress changes in space and time within a well-constrained 3D geologic framework.

Methods

Earthquake locations. Twenty-seven felt earthquakes were reported by the USGS NEIC through 28 January 2014 (Supplementary Fig. 1). Owing to the sparse distribution of seismic stations, routine NEIC earthquake location uncertainty in North Texas is roughly 10 km, and the initial locations exhibited a spread of nearly 20 km west to east. To reduce the location uncertainty and characterize the size and faulting associated with the earthquakes, we deployed five temporary seismic stations in the Reno–Azle area in mid-December 2013 and completed a 12-station deployment in January 2014 (Supplementary Table 1). Stations are a mix of USGS NetQuakes accelerometers, broadband and short-period velocity sensors, and one infrasound sensor recording at 100 or 200 Hz (Supplementary Fig. 1 and Supplementary Table 1). Waveforms from the USGS NetQuakes stations and SMU temporary stations, reported to the IRIS Data Management Center as network code NQ and ZW, respectively, for 2013/2014, are combined with other regional US seismic stations to provide consistent detection across multiple stations to a magnitude of ~ 1.0 .

All waveform data are telemetered in near real-time. P-wave onsets are identified using short-term-average/long-term average automated techniques applied to all vertical channels. Events are then manually reviewed for additional P- and S-wave onsets. Pick uncertainty is estimated to be 0.02 s for P-waves and 0.04 s for S-waves based on the sampling rates of the waveform data. Events are relocated using GENLOC, a flexible implementation of the Gauss–Newton inversion method applied to a single-event location³⁴ and a layered one-dimensional (1D) velocity model developed for the Azle area (Supplementary Table 2). The 1D P-wave model is based on sonic log information from injection well #2 and published 1D models for other earthquake sequences in the Dallas/Fort Worth area¹⁸. Constant V_p/V_s of 1.80 is applied to derive S-wave velocity¹⁸. Location uncertainty is reported as 68% confidence ellipses based on the formal covariance matrix for each earthquake³⁴. For the 283 events reported here, the mean epicentre major axes length is 570 ± 362 m, minor axes length is 310 ± 228 m, depth uncertainty is 346 ± 171 m and origin time uncertainty is 0.054 ± 0.031 s. Tests using alternative 1D constant V_p/V_s , which may affect depth estimates outside of formal uncertainty ranges, results in mean depth changes of 450 ± 820 m (deeper) for V_p/V_s 1.732 and $-650 \pm 1,400$ m (shallower) for V_p/V_s 1.90. The mean of the travel time residuals root mean square is 0.08 ± 0.12 s.

The two composite focal mechanisms discussed in the main text were calculated by hand using P-wave first motions. The composite mechanism for the main fault used larger, well-recorded events from December 2014; the antithetic composite used larger events occurring on 28 January 2014. The mechanisms confirm that first motions were consistent with the overall strike, dip and normal faulting offset expected from 3D seismic data and hypocentres. Future work will focus on calculating a more comprehensive set of focal mechanism solutions using P, S and amplitude information.

Local (Richter) magnitudes are based on the maximum S-wave amplitudes recorded on the horizontal velocity and acceleration seismograms transferred to the Wood–Anderson displacement. Magnitudes are generally consistent with NEIC magnitudes for like events (Fig. 2d). Before the installation of station AZDA, magnitude completeness is estimated to be 1.6 ml; after AZDA, completeness increases to 1.0 ml and many smaller events down to -1.0 ml are accurately recorded during periods of swarm activity. Estimates of b value using the NEIC magnitudes and using the local magnitudes are ~ 1.0 . The initial catalogue locations and magnitudes reported are not a complete record of seismicity recorded on the temporary network but provide sufficient information to constrain fault geometry for modelling. Future work will refine locations, including periods of swarm activity and provide refined magnitude estimates with more accurate b value calculations.

Modelling the effects of water level change. It has long been known that impoundment of artificial reservoirs can induce earthquakes either by the direct effect of the added surface load or the indirect effect of pore pressure diffusion to the earthquake focal region². The close proximity of Eagle Mountain Lake to the Azle area earthquakes raises the possibility that the reservoir was involved in inducing the sequence. The west fork of the Trinity River was dammed in 1932 to form the lake with a maximum depth of 14 m. No felt earthquakes were reported in the vicinity of the reservoir for 150 years before October 2013 (refs 16,17,23). The hydrograph for the lake level (http://nwis.waterdata.usgs.gov/tx/nwis/uv/?cb_00054=on&cb_00062=on&format=gif_default&period=&begin_date=2007-10-01&end_date=2014-02-26&site_no=08045000) shows that over the past 2 years the lake level has declined by 2.1 m from the Conservation Pool Elevation of 198 m (Supplementary Fig. 3). A falling lake level can sometimes strengthen the faults that are in hydrologic connection with the pool since lower water pressure results in a higher effective stress, increasing your mean stress and moving the stress state away from the failure envelope. The changing reservoir load could, however, encourage failure and can be modelled using the Boussinesq solution for a change in load on the surface of an elastic half-space (Supplementary Fig. 2)³⁵. The change in Coulomb stress created by the 2.1 m decline in lake level was computed on receiver faults corresponding to the main and antithetic faults imaged by the earthquake hypocenters at depths of 3 and 5 km (Supplementary Fig. 4). In the hypocentre zone, the Coulomb stress change is < 1 KPa and of about the same size as tidal stresses. Because the change is likely one to three orders of magnitude smaller than

the pore-pressure effect of injection on Coulomb stress we conclude that changes in the level of Eagle Mountain Lake can be ruled out as an important contributing factor to the Azle earthquake sequence.

Physical modelling of subsurface pressures. To determine the location and approximate magnitude of subsurface pressures generated by the injection and production wells, we develop a 3D pore-pressure model for the Ellenburger formation near the area of recent earthquake activity. The fault and surrounding formations above and below the Ellenburger are treated as low permeability (10^{-16} – 10^{-18} m²) zones. We apply both open and closed boundary conditions for an assortment of runs (see Table 1).

The model incorporates both brine injection and brine production from regional wells located nearest recent earthquake activity (Supplementary Fig. 5). Injection pressure is updated monthly in the model, production data is only updated annually at best due to the limited data available. Injection volumes for Well #1 and Well #2 discussed in the main text are shown in Supplementary Fig. 6. We describe in detail how we integrate subsurface pressure injection and production later in the Methods section.

We define the regional stratigraphy, 3D fault geometry, water injection and production rates using publicly available well logs, well log interpretations, and production/injection data provided by the TRC, regional published fault maps and discussions with oil and gas companies operating in the area^{20–22}. The match between earthquake epicentre locations and the fault maps generated from well logs ties suggests our proposed fault locations are accurate to within 1 km. The 1-km accuracy of the fault model is limited by uncertainty in the earthquake locations; uncertainty in depth interpolation between well logs used to constrain the fault location, and uncertainties that likely exist in some of the fault interpretations themselves that were supplied by other academic publications and industry researchers. Regional seismic and well log data indicate the Ellenburger is approximately flat-lying with an average thickness of $\sim 1,000$ m (refs 20–22).

We determine the effective permeability, k , for the Ellenburger at this site directly by using the Cooper–Jacob straight-line method that solves for permeability in a single well assuming non-equilibrium radial flow in a confined aquifer³⁶:

$$k = \frac{2.3Q\mu}{(4\pi\rho g(h_o - h))T} \quad (1)$$

Where k is permeability in m², Q is the pump rate in m³ per day, $(h_o - h)$ is the drawdown in head per log cycle of time in metres, ρ is the fluid density that we set at $1,031$ kg m⁻³, g is the gravitational acceleration constant, μ is the fluid viscosity, set at 1.1×10^{-3} Pa s, and T is the thickness of the Ellenburger where high permeability exist, which we vary between 300 and 1,000 m. Pump rates and drawdown in pressure for injector well #1 were provided by XTO Energy Inc. and are shown in Supplementary Fig. 8.

Using these data, we estimate the average effective permeability in the injection interval of the Ellenburger near injector well #1 ranges between 3×10^{-15} and 1×10^{-13} m². We assign a permeability of 1×10^{-18} m² to the overlying Barnett shale and underlying granite³⁷. Faults sometimes form seals in petroleum reservoirs and can in some instance act as strong barriers to cross fault flow^{24,28,32,38}. We therefore also assign a permeability that is 50% lower (1.5×10^{-15} – 0.5×10^{-13} m²) than the surrounding Ellenburger formation at the fault. Studies have demonstrated that the permeability of limestone faults is highly complex. Nonetheless, detailed permeability studies of normal faults in limestone host rock indicate a fault core with lower permeability surrounded by a higher permeability damage zone^{24,28}. This implies higher fluid flow immediately adjacent to the fault, but lower flow across the system.

The 3D model solves the groundwater-flow equation for pressure assuming single-phase flow and nearly flat-lying sedimentary layers, where

$$\frac{dP}{dt} = -\frac{1}{S} \nabla \cdot (-K \nabla P) - G \quad (2)$$

and $\frac{dP}{dt}$ is the change in pressure at a given location with time. S , the specific storage, we calculate assuming a mean Ellenburger porosity of $5 \pm 3\%$, a brine compressibility of $4.6 \times 10^{-10} \pm 0.3 \times 10^{-10}$ Pa⁻¹ and a mean rock matrix pore space compressibility for dolomitic limestone of $7 \times 10^{-10} \pm 6 \times 10^{-10}$ Pa⁻¹. The resulting end-member S values range from 1×10^{-6} m⁻¹ to 13×10^{-6} m⁻¹, with a mean value of 7.3×10^{-6} m⁻¹. K , the hydraulic conductivity, is based directly on previously derived permeability values. ∇P is the change in pressure with respect to space and G represents potential source (injection well) and sink (producer) terms at a given position and time. We recognize that significant variability in S likely exists, and this model therefore only represents a first-order estimate of subsurface pressure.

The 3D numerical model (a derivation of MODFLOW) uses a standard finite-difference forward-time, centre-space explicit approach to model pore pressure evolution with time²². The model consists of 194 cells in the north–south direction, 242 cells in the east–west direction and 40 cells in the vertical direction, with cell dimensions of $\sim 50 \times 50 \times 50$ m. We define the injection interval for injector well #1 and injector well #2 from 2,400 to 2,700 m and 2,200 to 2,850 m, respectively, consistent with reported injection intervals.

Since the shape, size and length of the well tubing and the injection volumes with time are known (made available through the TRC), we use the Darcy–Weisbach equation to calculate potential pressure loss due to friction in the pipe for each well, and from this, calculate the average bottom-hole pressure each month at the injection well site. The Darcy–Weisbach equation is the following:

$$P_f = f_d \rho_w \frac{L V^2}{D} \quad (3)$$

Where P_f is the pressure loss due to friction, $f_d = \sim 0.02$ is the Darcy friction coefficient that is calculated directly using the Colebrook approximation for smooth oilfield pipe tubing³⁹, $\rho_w = 1,031$ is the density of the injected fluid, L is the length of the pipe tubing to the packer, D is the internal diameter of the pipe and V is the average fluid velocity down the pipe. For injector well #1, $L = 2,427$ m, $D = 0.102$ m and V we estimate equals on average 2.3 m s^{-1} based on mean injector volumes with time and tubing surface area. As an example using this approach, we calculate that for an average wellhead pressure of 4 MPa at injector well #1 the pressure is reduced by ~ 1.25 MPa at the bottom of the well, so that the average bottom-hole pressure is 2.75 MPa. For injector well #2, $L = 2238$, $D = 0.076$ m and the average V is estimated equal to 1.5 m per s based on mean injection volumes with time and tubing surface area. From these parameters, we calculate that the average wellhead pressure at injector well #2 of 3.61 MPa is reduced by 0.69 MPa at the bottom of injector well #1, so that the average bottom-hole pressure is 2.92 MPa. We apply this technique to the monthly pressure/volume data provided for the well sites to estimate how bottom-hole pressure changes with time for each of the injectors.

Whether the bottom-hole pressure estimates using the Darcy–Weisbach equation are accurate is unclear, as no direct bottom-hole pressure measurements exist during pumping and solutions to the equation depend on several time-dependent factors such as flow and friction loss as well as uncertainties in pipe roughness changes. As an alternative approach for estimating bottom-hole pressure, we also estimate the subsurface pressure generated during injection using the Dupuit–Theim equation (the conical solution of Darcy's Law). This approach, unlike the Darcy–Weisbach equation that is primarily empirically based, estimates pressure by conserving mass and momentum, and has the following form:

$$P_b = P_o - \frac{\mu Q}{2\pi k H} \ln\left(\frac{R_b}{R_o}\right) \quad (4)$$

where, P_b is the pressure above hydrostatic at the base of the well, $P_o = 0$ is the pressure above hydrostatic at a distance of R_o , $\mu = 1.1 \times 10^{-3}$ Pa is the fluid viscosity, $k = 3 \times 10^{-15} \text{--} 1 \times 10^{-13} \text{ m}^2$ is the end-member mean effective permeability, Q is the average fluid flux out of the injector wells determined from monthly injection values provided by the TRC, $H = 1,000$ m is the approximate thickness of the reservoir (a maximum estimate for the pipe perforation zone and therefore minimum bottom-hole pressure estimate), $R_b = 0.1$ m is the radius of the production casing and $R_o = 1.5\text{--}150$ km is the radial distance where no elevated fluid pressure exists with the maximum value defined by the approximate radial distance of the Fort Worth Basin and the minimum value representing the nearest distance to the fault. On the basis of parameter uncertainties listed above and possible uncertainties in bottom-hole location of 50 m, we estimate end-member monthly injector well #1 bottom-hole pressures above *in situ* range from 0.53 to 20 MPa and end-member monthly injector well #2 bottom-hole pressures range from 0.17 to 8 MPa. Permeability plays an important role in the estimation of bottom-hole pressure using this method, and only in cases of low permeability ($\sim < 3 \times 10^{-13} \text{ m}^2$) do high injection pressures ($\sim > 8$ MPa) develop in the model. For our analysis, we only focus our results on more realistic, higher permeability values, where bottom-hole pressures are consistently below reported wellhead pressures (Table 1). As noted in Table 1, even in the conservative instance where bottom hole excess pressures are at a minimum 0.07–0.34 MPa, the pressure development along and near the fault is an order of magnitude greater than the stress change associated with lake level or groundwater change.

As noted previously, oil and gas production in the Fort Worth Basin involves not only the injection but the removal of brine, which we model as being entirely from the Ellenburger. Geophysicists working at production companies in the Fort Worth Basin indicate that brine is sometimes produced in the Ellenburger when an occasional frack-job fractures into a fault, or fractures through the Barnett into the Ellenburger formation, especially in regions where the Viola shale is absent below the Barnett shale^{20,37}—the case for the area were recent seismicity has occurred near Azle. To account for potential pressure reductions caused by Ellenburger production, the model incorporates pressure sinks generated by the production (and removal) of brine from the Ellenburger formation. For this analysis, we assume that potential production from the Ellenburger extends into fractures up to 500 m below the Barnett Shale, to a depth of $\sim 2,500$ m. This is an arbitrary depth estimate for fracture extension into the Ellenburger and in reality these fractures could be shallower or deeper. Currently, we do not know how continuous fractures are in the Ellenburger, although regional seismic images suggest natural fractures could extend through the entire Ellenburger and into the Barnett shale^{21,22}. Importantly, even if the water is produced only in the upper few metres of the Ellenburger, the change in pressure caused by water extraction will still impact other areas of the Ellenburger formation due to the nature of pore pressure diffusion. For brine production numbers, we use values for the region based on brine production reports made publicly available through the TRC from 70

regional wells near the NEFZ that have the largest water production in the region (Supplementary Table 5; Supplementary Fig. 5). Production data are provided in both G-1 and G-10 reports at the TRC. G-1 reports indicate the brine production during the first 48 h of production at a new well and therefore likely over-estimate long-term water production at a site since significant amounts of frack-water can be produced. G-10 reports represent a potentially more accurate estimate of brine production. Unfortunately, G-10 reports, like G-1 reports, are report as only 48-h pump test results that are conducted at most only on an annual basis. Thus, G-1 and G-10 reports represent only the gross estimates for regional brine production at each site. Although brine production often tracks with gas production, the lack of temporal resolution for brine production data makes it difficult to determine with high temporal resolution a clear time correlation between fluid production and seismicity at this site. For simplicity, we present only an average brine production value for each well in the region and typically discard G-1 reports, where anomalously high water production is observed. Future models will include more detailed brine production values if such data are made available.

For our analysis, we assume all brine produced from surrounding oil and gas wells near the NEFZ system derive from the Ellenburger formation. In reality, some of this brine could also derive from the Marble Falls formation, the release of interstitial formation brine from the Barnett or is water originally used for hydraulic fracturing. The estimated monthly water produced from individual production wells near the NEFZ yield volumes that are generally one to two orders of magnitude lower than wastewater injection well injection volumes. However, the sum of all water produced in surrounding wells during any given time could be as much as 35% of waste water injection volumes, assuming extrapolation of brine production estimates available at the TRC are accurate.

The model run time is for a 10-year period (from 2004 until the end of 2013). Model results demonstrate that end-member excess pressures of 0.008–0.2 MPa develop across the faults in areas where earthquake activity exists depending on model parameters. We find that higher pressures form along the fault for model runs where the Ellenburger contains laterally a continuous high-permeability zone bounded by lower permeability rock and a lower permeability fault. To test the role of the faults, we also ran the model with no faults. For this, we observe excess pressures in the earthquake region that are usually within 50–90% of values observed for model runs where faults exist (Supplementary Fig. 9). This implies the location and volume/pressures of injectors and producers are more important factors defining the subsurface pressure regime than the current fault permeability values prescribed in the model.

Modelling uncertainties. Compressibility and specific storage uncertainties.

Although we vary compressibility and reservoir-specific storage for different model runs, the compressibility/specific storage for each model run is held constant throughout. Variations in calculated specific storage may change by an order of magnitude, and we find that this uncertainty may result in a 10–15% change in pressure along the fault (Table 1). Future work should base compressibility/specific storage on actual measurements for porous Ellenburger from the region, if available.

Permeability uncertainties.

Although we vary the permeability of the Ellenburger by up to three orders of magnitude, each individual reservoir model assumes a mean effective permeability that is isotropic in different geological units except at the fault locations. In reality, it is likely that significant anisotropy may exist due to orientation of fractures in the subsurface. Future models should account for the orientation and magnitude of permeability anisotropy in the Ellenburger formation and surrounding faults/units once such data become available. Conversations with industry experts indicate that tremendous heterogeneity exists in the Ellenburger over short (< m) depth intervals. 3D seismic analysis of the Ellenburger indicates significant heterogeneity exists along polygonal fracture zones^{20,21}; fluid flow along higher permeability polygonal fractures could result in high pore-pressure development along the NEFZ relatively rapidly, since the flow would be channelled and more focused than the model suggests. Model runs where we supply a thinner zone (300 m or less) of high and more focused permeability material in the Ellenburger (which might represent a karst-like feature that exist in this formation) results in significant pressure changes at the fault, with pressures as much as a factor of 4 higher. Currently, the mean effective thickness of the flow zone in the Ellenburger is poorly constrained at this site, and as a conservative approach, we assume it is isotropic and thick, with uniform permeability throughout the entire 1,000 m Ellenburger formation. Tracer tests provide one valuable approach to constrain flow path, effective permeability and Ellenburger production rates at producer wells, and such tests should be considered in the future.

In addition, a less expensive, yet valuable approach for assessing effective permeability as well as the potential for induced seismicity due to oil and gas activities is through 24 h shut-in tests at injector wells. Such shut-in periods can be used both to estimate regional permeability near each injector well via the Cooper–Jacob Method and to determine if background *in situ* bottom-hole pressures are changing significantly with time. Annual 24-h shut-in tests or required pressure measurements during shut-in for maintenance would provide potentially critical insight into wastewater reservoir pressure changes with time that may lead to induced seismicity.

Brine production uncertainties. As previously noted, significant brine production uncertainty exists in the model. It is critical that future studies include high-resolution (ideally daily) brine production data for producing wells and better constraints on the source of brine production. Currently, all brine production data included in the model are based on extrapolations and averages of G-10 forms provided by the TRC, which are based only on 48-hour pump tests that are typically performed annually. Comparison of different annual G-10 reports for the same well indicates brine production can vary significantly from year to year, depending on the well. As a result, pressure changes associated with modelled brine production represent only a crude, first-order estimate. The depth/location of brine production is also limited to a resolution of a few hundred metres due to hydraulic fracturing zones extending sometimes over hundreds of metres. This uncertainty, however, is currently significantly less important than better constraints on brine production volumes with time and the brine source. Tracer tests or geochemical studies determining if the chlorinity content of the brine produced matches Ellenburger values would significantly help constrain brine source uncertainties.

Bottom-hole pressure uncertainties. Although we calculate bottom-hole pressures by incorporating pressure losses due to friction in the tubing and conservation of mass/momentum, it is unclear if these calculated pressure losses accurately reflect true bottom-hole pressures. More advanced pump tests including low-cost shut-in pressure measurements, and ideally, bottom-hole pressure measurement at injector wells and nearby sites can further elucidate pressure loss and true bottom-hole pressure. In addition, the model does not account for non-Darcy flow that likely occurs in the formation nearest production and injection well bores, and future models should consider the likely impact of such effects.

Regional structural geology uncertainties. Interpretations of region well logs made publically available by the TRC provide first-order insight into regional structural geology. Nonetheless, access to 3D seismic data and 3D structural interpretations based on high-resolution 3D seismic data are necessary to make the most accurate pore pressure model for the region. Although we note that two faults exist in the region, discussions with industry researchers indicate several large karst features also exist in this region. Some, but not all of these, features are observable in 3D seismic data and it is likely that these features represent zones of significant permeability changes. Seismic interpretations provided by industry researchers have been an invaluable tool for constrain regional structure. Access to 3D seismic data, or access to interpretations of such data, would therefore provide greater insight into the complex potential flow paths that exist in the subsurface.

Stress magnitude and orientation uncertainty. Improving the certainty of whether pressure changes associated with oil and gas activity are the primary cause of earthquakes requires a more detailed understanding of the subsurface stress regime that defines not only the orientation of the stress field, but also quantifies the stress changes necessary to cause failure. Detailed analysis of regional subsurface stress combined with longer-term regional stress studies will likely provide invaluable insight into the regional stress regime and the potential stresses required to induce failure on faults in this region.

References

1. Ellsworth, W. L. Injection-induced earthquakes. *Science* **341**, 1225942 (2013).
2. Carder, D. S. Seismic investigations in the Boulder Dam area, 1940-1944, and the influence of reservoir loading on local earthquake activity. *Bull. Seism. Soc. Am.* **35**, 175-192 (1945).
3. Amos, C. B. *et al.* Uplift and seismicity driven by groundwater depletion in central California. *Nature* **509**, 483-486 (2014).
4. National Research Council. *Induced Seismicity Potential in Energy Technologies* (National Academies Press, 2013).
5. Zoback, M. L. & Zoback, M. D. State of stress in the conterminous United States. *J. Geophys. Res.* **85**, 6113-6156 (1980).
6. Zoback, M. D. & Townend, J. Implications of hydrostatic pore pressures and high crustal strength for the deformation of intraplate lithosphere. *Tectonophysics* **336**, 19-30 (2001).
7. Barton, C. A., Zoback, M. D. & Moos, D. Fluid flow along potentially active faults in crystalline rock. *Geology* **23**, 683-686 (1995).
8. Terzaghi, K. *Theoretical Soil Mechanics* (John Wiley and Sons, 1943).
9. Reasenber, P. A. & Simpson, R. W. Response of regional seismicity to the static stress change produced by the Loma Prieta earthquake. *Science* **255**, 1687-1690 (1992).
10. Stein, R. S. The role of stress transfer in earthquake occurrence. *Nature* **402**, 605-609 (1999).
11. Hsieh, P. A. & Bredehoeft, J. D. A reservoir analysis of the Denver earthquakes: a case of induced seismicity. *J. Geophys. Res.* **86**, 903-920 (1981).
12. Horton, S. Disposal of hydrofracking waste fluid by injection into subsurface aquifers triggers earthquake swarm in central Arkansas with potential for damaging earthquake. *Seism. Res. Lett.* **83**, 250-260 (2012).

13. Keranen, K., Savage, H., Abers, G. & Cochran, E. Potentially induced earthquakes in Oklahoma, USA: links between wastewater injection and the 2011 Mw 5.7 earthquake sequence. *Geology* **41**, 699-702 (2013).
14. Kim, W.-Y. Induced seismicity associated with fluid injection into a deep well in Youngstown, Ohio. *J. Geophys. Res.-Solid Earth* **118**, 3506-3518 (2013).
15. Keranen, K., Weingarten, M., Abers, G. A., Bekins, B. A. & Ge, S. Sharp increase in central Oklahoma seismicity since 2008 induced by massive wastewater injection. *Science* **345**, 448-451 (2014).
16. Frohlich, C., Hayward, C., Stump, B. & Potter, E. The Dallas-Fort Worth earthquake sequence: October 2008 through May 2009. *Bull. Seism. Soc. Am.* **101**, 327-340 (2011).
17. Frohlich, C. Two-year survey comparing earthquake activity and injection-well locations in the Barnett Shale, Texas. *Proc. Natl Acad. Sci. USA* **109**, 13934-13938 (2012).
18. Justinic, A. H., Stump, B., Hayward, C. & Frohlich, C. Analysis of the Cleburne, Texas, earthquake sequence from June 2009 to June 2010. *Bull. Seism. Soc. Am.* **103**, 3083-3093 (2013).
19. Frohlich, C. *et al.* The 17 May 2012 M4.8 earthquake near Timpson, East Texas: an event possibly triggered by fluid injection. *J. Geophys. Res.-Solid Earth* **119**, 581-593 (2014).
20. Pollastro, R. M., Jarvie, D. M., Hill, R. J. & Adams, C. W. Geologic framework of the Mississippian Barnett Shale, Barnett-Paleozoic total petroleum system, Bend arch Fort Worth Basin, Texas. *AAPG Bull.* **91**, 405-436 (2007).
21. Sullivan, E. C., Marfurt, K. J., Lacazette, A. & Ammerman, M. Application of new seismic attributes to collapse chimneys in the Fort Worth Basin. *Geophysics* **71**, B111-B119 (2006).
22. McDonnell, A., Loucks, R. G. & Dooley, T. Quantifying the origin and geometry of circular sag structures in northern Fort Worth Basin, Texas: paleocave collapse, pull-apart fault systems, or hydrothermal alteration? *Am. Assoc. Pet. Geol. Bull.* **91**, 1295-1318 (2007).
23. Frohlich, C. & Davis, S. D. *Texas Earthquakes* (University of Texas Press, 2002).
24. do Nascimento, A. F., Lunn, R. J. & Cowie, P. A. Modeling the heterogeneous hydraulic properties of faults using constraints from reservoir induced seismicity. *J. Geophys. Res.* **110**, B09201 (2005).
25. Haar, L. C., Fletcher, J. B. & Mueller, C. S. The 1982 Enola, Arkansas, swarm and scaling of ground motion in the eastern United States. *Bull. Seis. Soc. Am.* **74**, 2463-2482 (1984).
26. Hanks, T. C. Small earthquakes, tectonic forces. *Science* **256**, 1430-1432 (1992).
27. McDonald, M. G. & Harbaugh, A. W. *A modular three-dimensional finite-difference ground-water flow model: USGS Open File Report 83-875* (1984).
28. Agosta, F., Prasad, M. & Aydin, A. Physical properties of carbonate fault rocks, fucino basin (Central Italy): implications for fault seal in platform carbonates. *Geofluids* **7**, 19-32 (2007).
29. Segall, P. Earthquake triggered by fluid extraction. *Geology* **17**, 942-946 (1989).
30. Pratt, W. E. & Johnson, D. W. Local subsidence of the Goose Creek Oil Field. *J. Geol.* **34**, 577-590 (1924).
31. Segall, P. & Fitzgerald, S. D. A note on induced stress changes in hydrocarbon and geothermal reservoirs. *Tectonophysics* **289**, 117-128 (1998).
32. Caine, J. S., Evans, J. P. & Forster, C. B. Fault zone architecture and permeability structure. *Geology* **24**, 1025-1028 (1996).
33. Van Everdingen, A. F. in *Subsurface Disposal in Geologic Basins: A Study Of Reservoir Strata* (ed. Galley, J. E.) 32-42 (American Assoc. Petroleum Geologists Memoir 10, 1968).
34. Pavlis, G. L., Vernon, F., Harvey, D. & Quinlan, D. The generalized earthquake-location (GENLOC) package: an earthquake-location library. *Comput. Geosci.* **30**, 1079-1091 (2004).
35. Fund, Y. C. *Foundations of Solid Mechanics* (Prentice-Hall, 1965).
36. Cooper, Jr H. H. & Jacob, C. E. A generalized graphical method for evaluating formation constants and summarizing well-field history. *Eos Trans. AGU* **27**, 526-534 (1946).
37. Loucks, R. G., Reed, R. M., Ruppel, S. C. & Jarvie, D. M. Morphology, genesis, and distribution of nanometer-scale pores in siliceous mudstones of the Mississippian Barnett Shale. *J. Sed. Res.* **79**, 848-861 (2009).
38. Faulkner, D. R. *et al.* A review of recent developments concerning the structure, mechanics and fluid flow properties of fault zones. *J. Struct. Geol.* **32**, 1557-1575 (2010).
39. Colebrook, C. F. & White, C. M. Experiments with fluid-friction in roughened pipes. *Proc. R. Soc. Lond. Series A* **161**, 367-381 (1937).
40. Wessel, P. & Smith, W. H. New, improved version of Generic Mapping Tools released. *Eos, Trans. AGU* **79**, 579-579 (1998).

Acknowledgements

All seismic waveform data are publically available at the IRIS Data Management Center. Wastewater injection, brine production and surface injection pressure data are publically available at the TRC. We thank Craig Pearson at the TRC, Bob Patterson from the Upper Trinity Groundwater Conservation District; scientists at XTO Energy, ExxonMobil, MorningStar Partners and EnerVest for valuable discussions; Robert Simpson for assistance with the Boussinesq modelling. We thank Barbara Bekins, Art McGarr and

Ruth Harris for initial reviews. The SMU University Research Council and the Institute for the Study of Earth and Man provided partial support. Some figures were prepared using Generic Mapping Tools⁴⁰.

Author contributions

M.J.H., W.L.E., C.F., J.E.O. and C.B. developed/refined pore pressure and stress models. H.R.D., H.R.O., C.H., W.L.E., B.W.S., M.B.M. and J.H.L. developed/deployed the seismic experiment and processed/interpreted all seismic data. All authors shared in the writing of this manuscript.

Additional information

Supplementary Information accompanies this paper at <http://www.nature.com/naturecommunications>

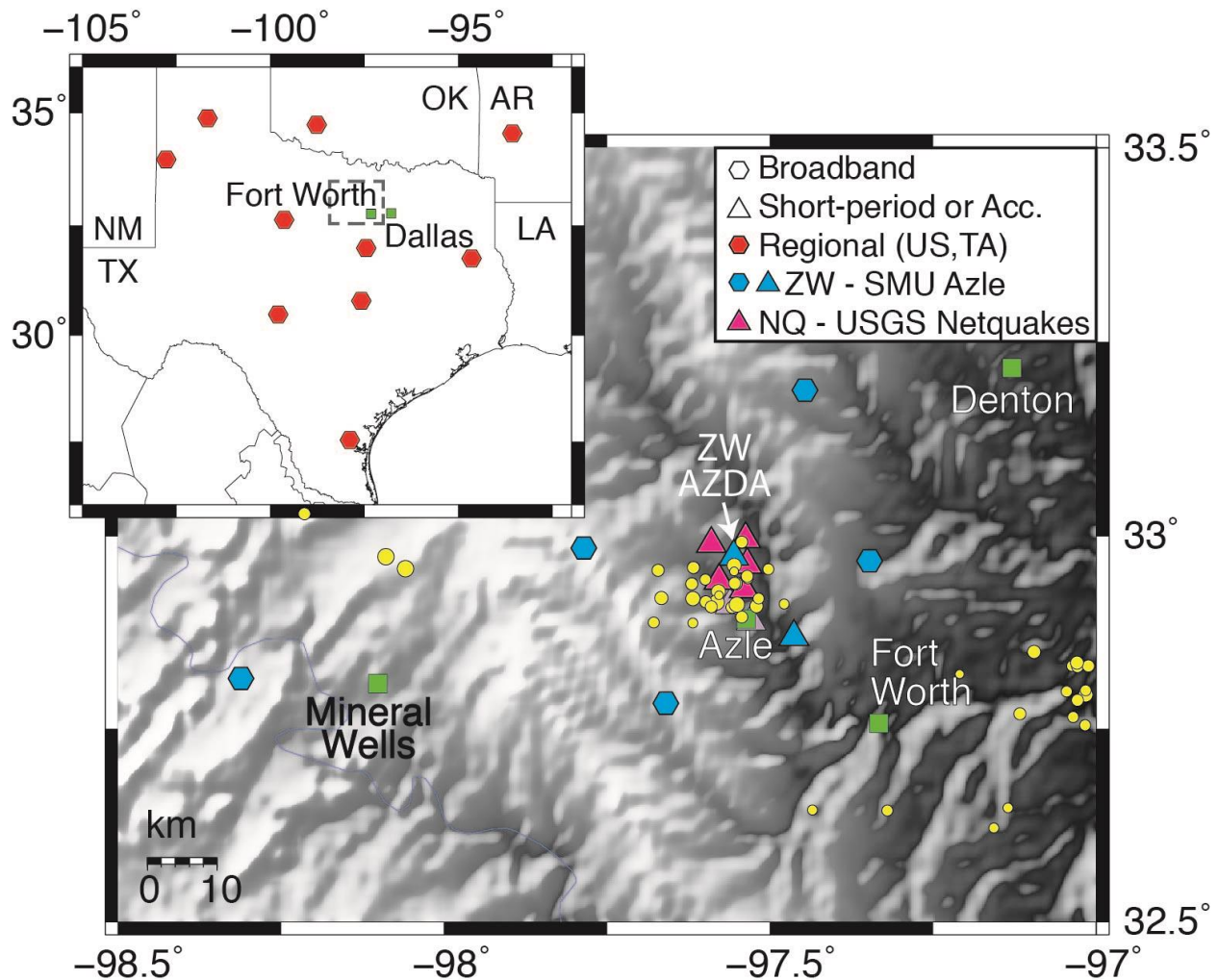
Competing financial interests: The authors declare no competing financial interests.

Reprints and permission information is available online at <http://npg.nature.com/reprintsandpermissions/>

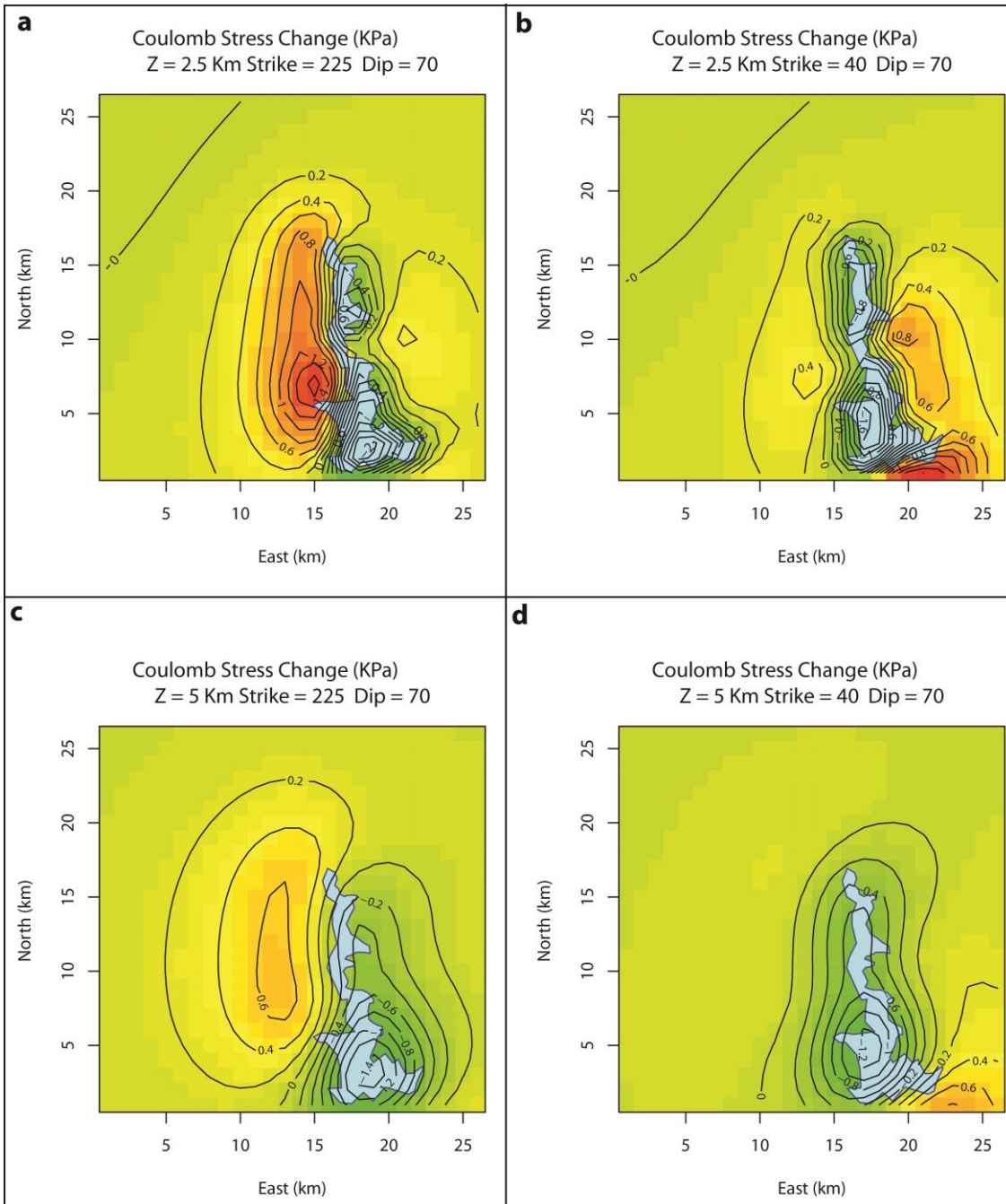
How to cite this article: Hornbach, M. J. *et al.* Causal factors for seismicity near Azle, Texas. *Nat. Commun.* 6:6728 doi: 10.1038/ncomms7728 (2015).



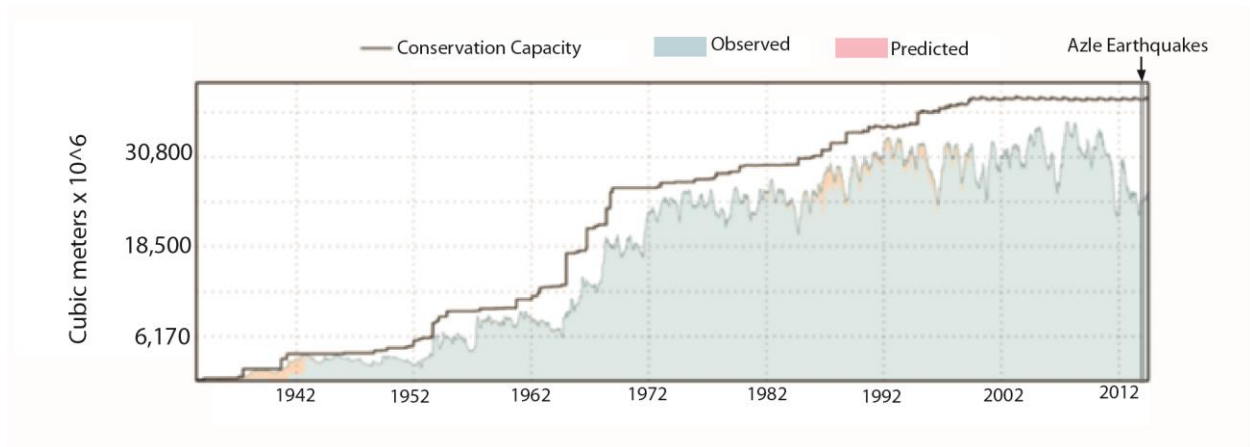
This work is licensed under a Creative Commons Attribution 4.0 International License. The images or other third party material in this article are included in the article's Creative Commons license, unless indicated otherwise in the credit line; if the material is not included under the Creative Commons license, users will need to obtain permission from the license holder to reproduce the material. To view a copy of this license, visit <http://creativecommons.org/licenses/by/4.0/>



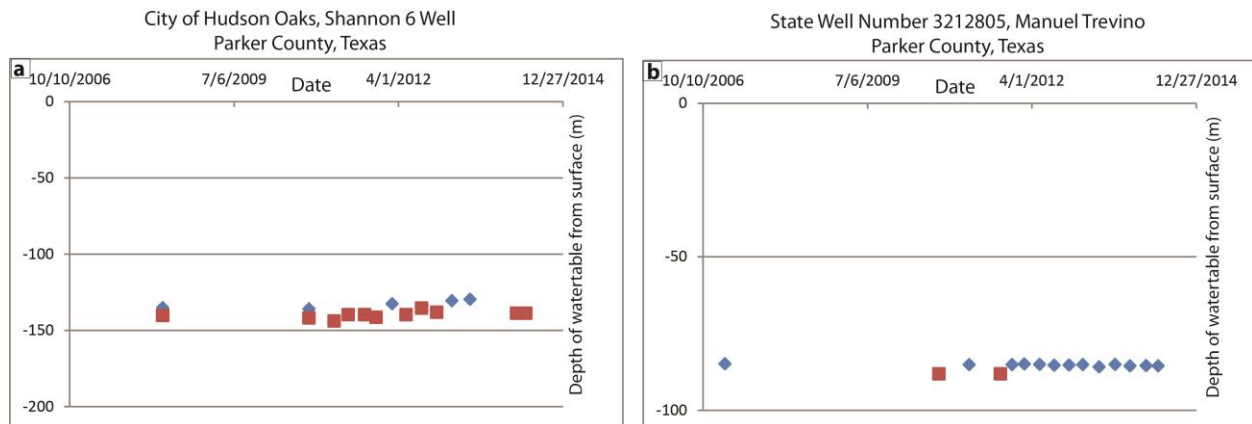
Supplementary Figure 1. USGS NEIC catalogue locations 2008-present (yellow circles) and seismograph stations for North Texas. The Azle earthquake sequence consists of the 27 felt events located to the north and west of Azle, TX (shown here) and seismicity recorded by the temporary network (see Figure 1). Additionally, two M3.7 earthquakes near Mineral Wells occurred in November 2013. NEIC locations are determined using the regional broadband stations (red hexagons) shown in the inset. The temporary Azle network (ZW and 5 NQ stations) was deployed starting on 15 December 2013 and completed to 12 stations by mid-January 2014.



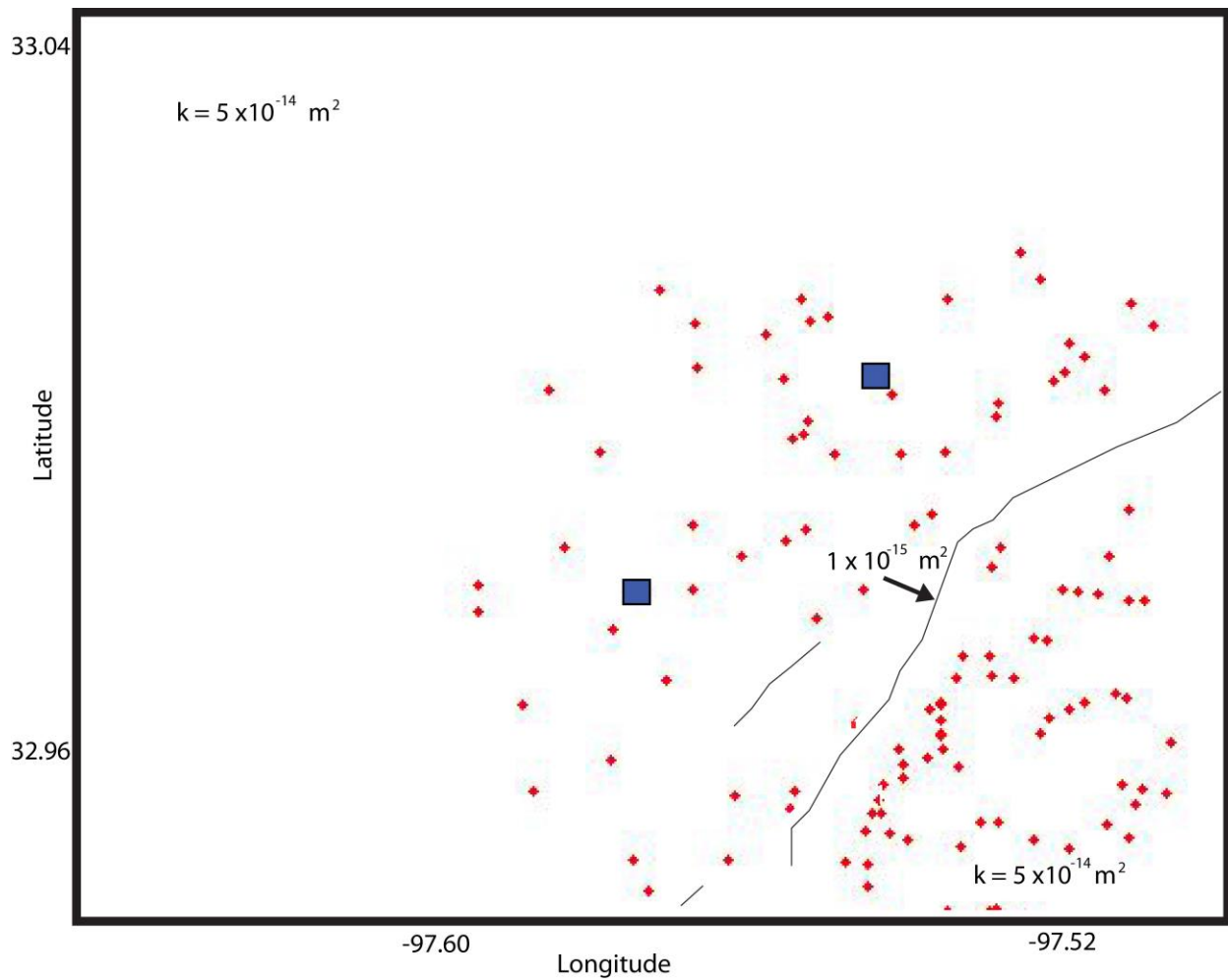
Supplementary Figure 2. Change in Coulomb stress at 2.5 km (**a**, **b**) and 5 km (**c**, **d**) depth for normal faulting caused by the 2.1 m drop in water level in Eagle Mountain Lake between April 2012 and November 2013, computed using the Boussinesq solution for a change in surface load on an elastic half-space³⁷. Warm colours indicate increased failure potential; cool colours indicate decreased failure potential. **a** and **c** correspond to orientation of the main fault defined by earthquake hypocentres. **b** and **d** correspond to antithetic normal fault orientation.



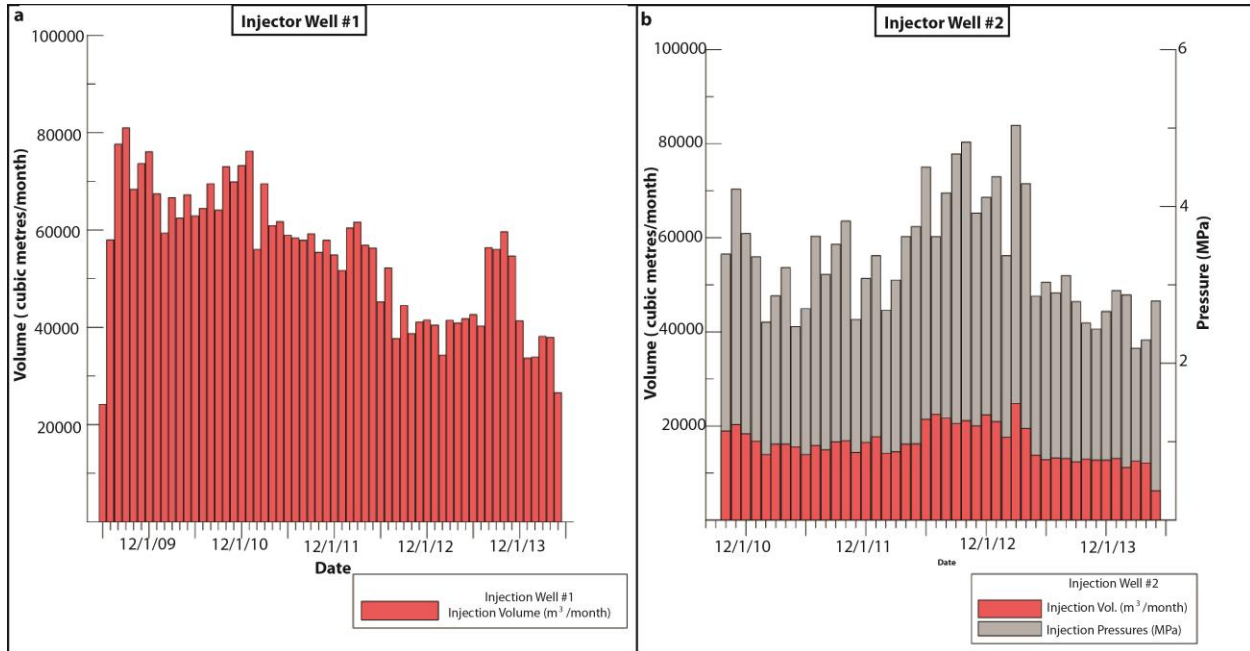
Supplementary Figure 3. Water volume stored in Eagle Mountain Lake since dam construction in 1932 (<http://www.waterdatafortexas.org/reservoirs/statewide>). During the period of earthquake activity, lake volumes have not been at record high or record low values.



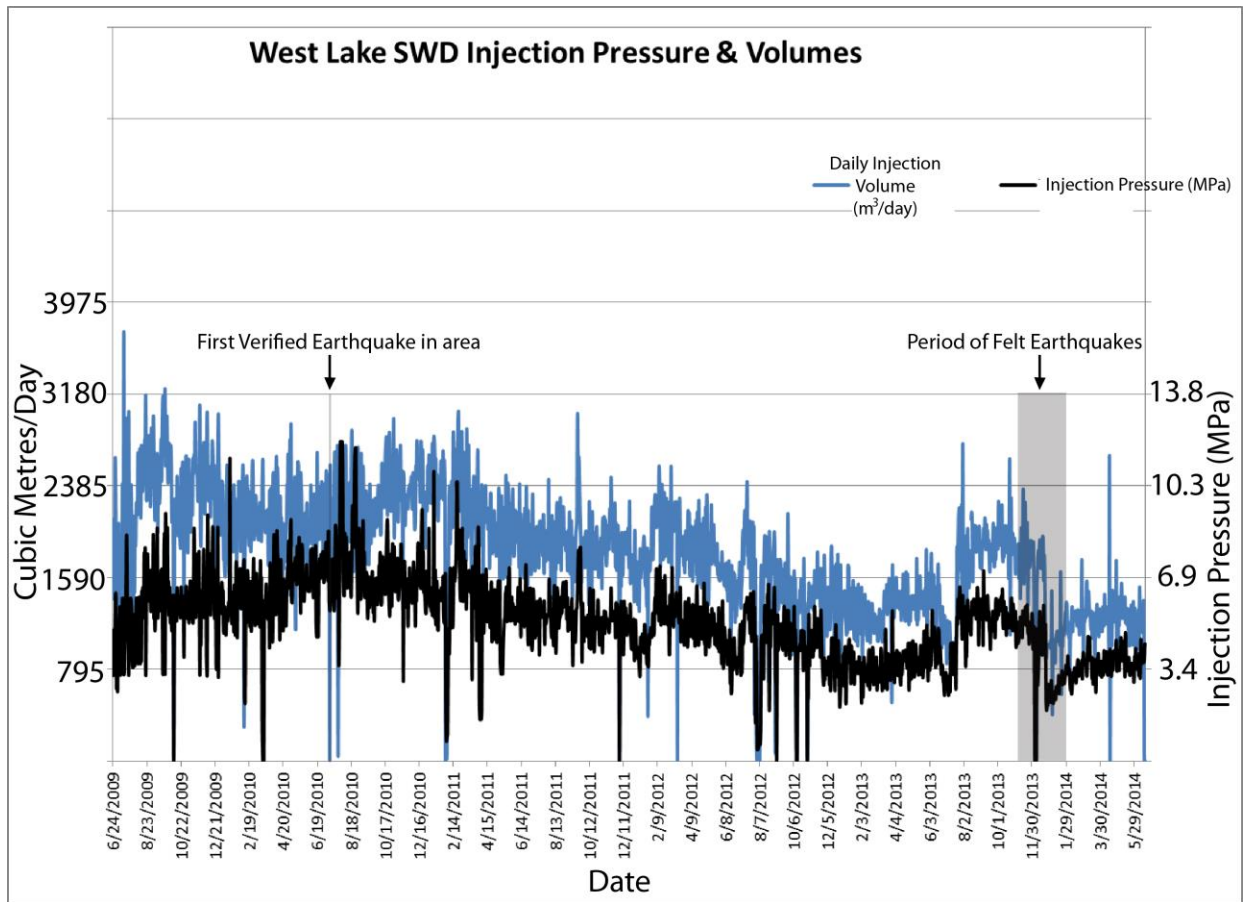
Supplementary Figure 4. Depth from the surface to the top of the unconfined Trinity Aquifer at two wells near Azle, Texas, in metres, monitored and provided by the Upper Trinity Groundwater Conservation District. Unfortunately, no Trinity Aquifer monitoring wells exist directly over the earthquake area. The Shannon #6 Well (**a**) is located at 32.7479 N, -97.7032 W, and appears to be the closest Trinity Aquifer Monitoring Well to the earthquakes. The Manuel Trevino Well (**b**), located 32.783 N, -97.573 W, provides another example of water levels in the Trinity Aquifer in Parker County. Blue diamonds are static water levels; red squares are pumping water levels. Water levels of the Trinity aquifer appear to fluctuate vertically by a few metres on an annual basis, and therefore likely have a similar negligible impact on the subsurface stress regime as lake level change at Eagle Lake Reservoir.



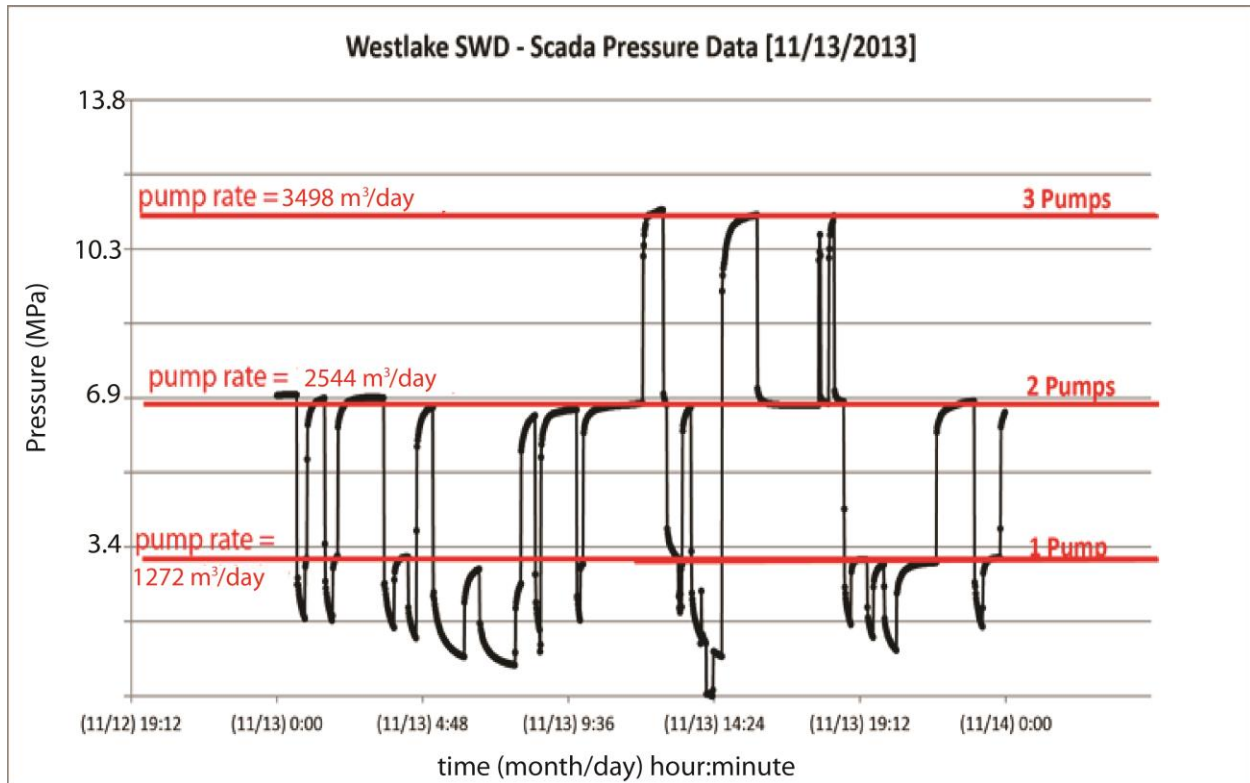
Supplementary Figure 5. Map view of model space at a depth of 2500 m showing the location of the two injector wells (blue), the 70 largest brine producer wells in the region (red), and an example of assigned mean effective permeability values for the Ellenburger formation versus fault permeability for an example model run. Black lines indicate the fault location at the top of the Ellenburger formation.



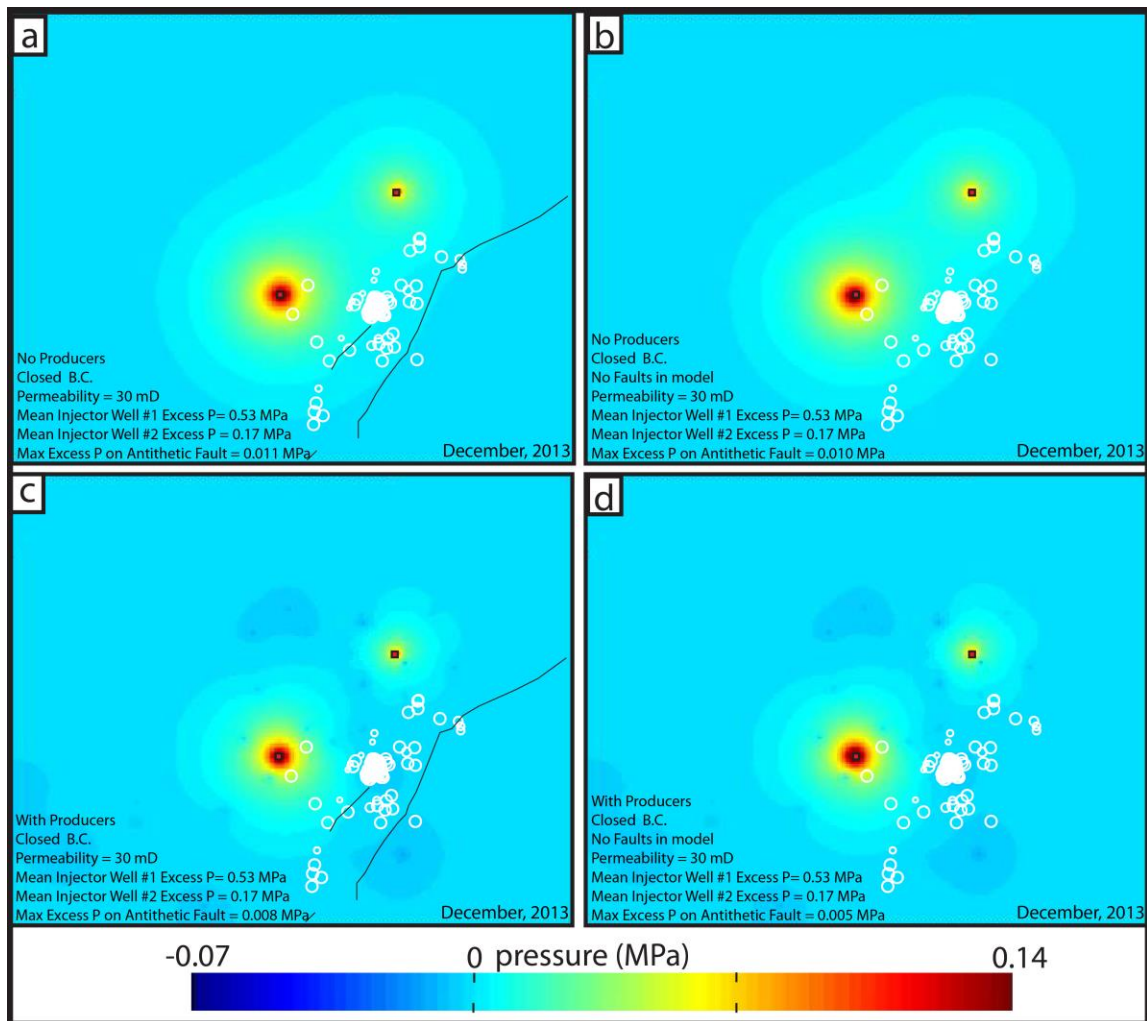
Supplementary Figure 6. Monthly Injection volumes up to September, 2013 for Injector Well #1 (a) and Injector Well #2 (b) based on TRC public data. See also Supplementary Tables 3 and 4. Grey bars indicate the average monthly wellhead pressure reported for Injector Well #2. Note that average pressure values generally increase and decrease with increasing and decreasing injection volumes. Nonetheless, during the period of earthquake activity (~12/1/13), the injection pressure increases without a clear increase in injection volume implying decreasing compressibility in the injection reservoir during the period of earthquake activity. Injector Well #1 owners provide average daily injection pressures and volumes below (Supplementary Figure 7).



Supplementary Figure 7. Average daily injection pressures for Injector Well #1 since the start of injection provided by XTO Energy Inc. and now available through the TRC. Although a pressure increase occurs in late 2013, three months before felt earthquake activity begins, it is also clear that injection well pressures and volumes were significantly higher during the 2009-2011 period when only one recorded earthquake was reported by a temporary seismic network was placed in the region from November 2009 to September 2011¹⁷. Data provided courtesy of XTO Energy Inc.



Supplementary Figure 8. Measured wellhead pressures at Injector Well #1 for time periods where different pump rates and periods of no pumping occurred. We use these data to place constraints on permeability in the Ellenburger near Injector Well #1. During periods when all injection pumps are off, wellhead pressure exponentially decays. Industry researchers indicate that during periods of sustained shutdown (several days) well head pressures converge to ~0.5 MPa. Data provided courtesy of XTO Energy Inc.



Supplementary Figure 9. Estimate for excess pressure in the Ellenburger, December 2013, based on model results assuming average pressures of 0.57 MPa and 0.17 MPa exist at Injector Well #1 and Injector Well #2, respectively. These injection pressures are low end-member estimates. For all models, the Ellenburger is 1000 m thick. **(a)** only brine injection occurs; **(b)** only brine injection occurs and no subsurface faults exist; **(c)** brine injection and water production occur, and **(d)** brine injection and water production occur and no faults exist. The existence of faults and no production wells results in the largest pressure development at earthquake locations. The scenario with no faults and brine production results in the lowest pressure development in the area of earthquake locations. Even for the lowest pressure case, model-predicted pressure is still ~1 order of magnitude higher than the expected pressure changes caused by lake level and ground water changes near the surface.

Supplementary Table 1:

Seismic Station information

Station	Network	Ondate*	Offdate*	Latitude	Longitude	Elevation (km)	Instrument	Sample Rate (samples per second)
AZCT	NQ	201334 8	201400 7	32.910 3	- 97.5617	0.223	GeoSIG GMS-IA18 NetQuakes	200
AZEP	NQ	201400 7	-	32.963 4	- 97.5354	0.224	GeoSIG GMS-IA18 NetQuakes	200
AZFS	NQ	201334 6	201335 8	32.889 1	- 97.5291	0.135	GeoSIG GMS-IA18 NetQuakes	200
AZHS	NQ	201334 8	-	32.929 7	- 97.5397	0.219	GeoSIG GMS-IA18 NetQuakes	200
AZNH	NQ	201335 8	-	32.989 32.989	- 97.5904	0.273	GeoSIG GMS-IA18 NetQuakes	200
AZCF	ZW	201403 0	-	33.184 1	- 97.4463	0.381	Guralp CMG3T_120sec/Guralp DM24 Datalogger	100
AZDA	ZW	201400 8	-	32.972 8	- 97.5553	0.238	Mark Products L28/Reftek 130 Datalogger	100
AZDA	ZW	201400 8	-	32.972 8	- 97.5553	0.238	Chapparral 2.5 microphone/Reftek 130 Datalogger	40/200
AZDA	ZW	201400 8	-	32.972 8	- 97.5553	0.238	Mark Products L4C/Reftek 130 Datalogger	100/200
AZHL	ZW	201401 1	-	32.965 6	- 97.3483	0.222	Guralp CMG3T_120sec/Guralp DM24 Datalogger	100
AZLE	ZW	201401 1	-	32.982 4	- 97.7862	0.381	Guralp CMG3T_120sec/Guralp DM24 Datalogger	100
AZWP	ZW	201401 5	-	32.779 5	-97.66	0.381	Guralp CMG3T_120sec/Guralp DM24 Datalogger	100
AZWR	ZW	201402 8	-	32.811 5	-98.312	0.381	Guralp CMG3T_120sec/Guralp DM24 Datalogger	100
BRRD	NQ	201335 4	-	32.994 8	- 97.5379	0.223	GeoSIG GMS-IA18 NetQuakes	200
EML1	ZW	201334 8	-	32.873 5	- 97.4603	0.211	Sprengnether S6000/Reftek 130 Datalogger	100
RESD	NQ	201334 8	-	32.941 9	- 97.5786	0.223	GeoSIG GMS-IA18 NetQuakes	200

*Ondate and Offdate in YearJulianDay

Supplementary Table 2:

Local P-wave (VP) and S-wave (VS) Velocity Model Used to Relocate Earthquakes Near Azle, Texas.

Depth BSL (km)*	Depth Surface (km)	VP (km s ⁻¹)	VS (km s ⁻¹)	VP/VS
-0.235	0.000	2.75	1.53	1.8
0.135	0.370	3.70	2.05	1.8
0.565	0.800	4.00	2.22	1.8
1.465	1.700	4.35	2.44	1.8
1.865	2.100	6.00	3.37	1.8

Supplementary Table 3:

Monthly Injection Rates for Injection Well #1

Time (month-year)	m ³ per month
Jun-09	18135
Jul-09	43451
Aug-09	58222
Sep-09	60730
Oct-09	51254
Nov-09	55239
Dec-09	57047
Jan-10	50566
Feb-10	44490
Mar-10	49979
Apr-10	46830
May-10	50399
Jun-10	47146
Jul-10	48299
Aug-10	52117
Sep-10	48041
Oct-10	54769
Nov-10	52380
Dec-10	54903
Jan-11	57145
Feb-11	41982
Mar-11	52118
Apr-11	45664
May-11	46272
Jun-11	44180
Jul-11	43758
Aug-11	43391
Sep-11	44397

Oct-11	41548
Nov-11	43401
Dec-11	41127
Jan-12	38728
Feb-12	45290
Mar-12	46196
Apr-12	42636
May-12	42186
Jun-12	33910
Jul-12	39147
Aug-12	28259
Sep-12	33347
Oct-12	29015
Nov-12	30802
Dec-12	31106
Jan-13	30343
Feb-13	25720
Mar-13	31080
Apr-13	30640
May-13	31295
Jun-13	31927
Jul-13	30170
Aug-13	42264
Sep-13	41987
Total	2225028
Mean	43628

Supplementary Table 4:**Monthly injection rates and average wellhead pressure rates for Injector Well #2.**

Time (month-year)	Av. Monthly Pressure (MPa)	Volume (m ³ per month)
Oct-10	3.4	14194
Nov-10	4.2	15207
Dec-10	3.7	13746
Jan-11	3.4	12580
Feb-11	2.5	10419
Mar-11	2.9	12123
Apr-11	3.2	12136
May-11	2.5	11658
Jun-11	2.7	10427
Jul-11	3.6	11888
Aug-11	3.1	11223
Sep-11	3.5	12488
Oct-11	3.8	12647
Nov-11	2.6	10778
Dec-11	3.1	12378
Jan-12	3.4	13294
Feb-12	2.7	10649
Mar-12	3.1	10870
Apr-12	3.6	12116
May-12	3.7	12153
Jun-12	4.5	16055
Jul-12	3.6	16875
Aug-12	4.2	16264
Sep-12	4.7	15381

Oct-12	4.8	15843
Nov-12	3.9	15010
Dec-12	4.1	16784
Jan-13	4.4	15710
Feb-13	3.4	13220
Mar-13	5.0	18584
Apr-13	4.3	14582
May-13	2.9	10342
Jun-13	3.0	9603
Jul-13	2.9	9918
Aug-13	3.1	9792
Sep-13	2.8	9275
Total		466213

Supplementary Table 5:

Production well number (American Petroleum Institute “API” number), location, and start date for the 70 largest brine-producing production wells in the earthquake area based on G-10 TRC reports. All G-10 data can be found through the TRC.

API	Latitude	Longitude	Mean Monthly brine production (m ³ per month)	Start Date
43932613	32.97092	-97.5304	2770	Oct. 2008
36735205	32.9562	-97.5898	1297	Jan. 2012
43932605	32.97099	-97.534	1161	Oct. 2008
43935738	32.94141	-97.5267	1116	Sept. 2011
36733989	32.985277	-97.54019	980	Oct. 2006
36734139	32.96381	-97.5476	683	Nov. 2006
49736104	33.00734	-97.5091	539	Nov. 2006
43935807	32.94141	-97.5267	533	Aug. 2011
36734349	32.95557	-97.5635	522	May, 2007
43934469	32.94124	-97.5285	467	Mar. 2010
36733762	32.95958	-97.5795	448	June, 2006
43931502	32.98667	-97.5378	446	Aug. 2006
43935733	32.94322	-97.5296	417	July, 2011
36733709	32.956184	-97.55569	385	Sept. 2005
36734045	32.97524	-97.5528	370	Oct. 2006
43935846	32.9418	-97.5257	368	Aug. 2011
43931850	32.96596	-97.5179	337	Aug. 2007
36734070	32.984983	-97.55416	329	Sept. 2006
49736435	33.00393	-97.518	306	July, 2008
36735272	32.97873	-97.5967	304	Aug. 2012
43934619	32.97791	-97.5163	295	April, 2010
36735271	32.97589	-97.5969	290	Jan, 2013
49736433	33.00537	-97.52	290	July, 2008
36734715	32.96238	-97.5367	284	Nov. 2008
36733868	32.9659	-97.5367	281	Mar. 2006
43932449	32.95082	-97.5247	279	Oct. 2007
43936094	32.96507	-97.5201	279	Feb. 2012

43931961	32.98087	-97.53	265	Aug. 2007
49736119	33.00978	-97.512	240	Jan. 2007
43931868	32.95649	-97.5107	235	Dec. 2007
43935732	32.94303	-97.5304	214	Sept. 2011
43933173	32.98303	-97.529	200	June, 2008
36734395	32.965689	-97.5912	195	July, 2007
43931370	32.93891	-97.5272	188	Mar. 2006
36733927	32.96827	-97.5723	180	July, 2006
36734714	32.96513	-97.538	175	Nov. 2008
49736184	33.01524	-97.5265	162	Feb. 2007
43934202	32.94977	-97.5199	162	Dec. 2009
49736702	33.00213	-97.5206	154	Jan. 2009
43931807	32.96871	-97.53	152	Sept. 2007
43934611	32.99339	-97.536	149	Aug. 2010
43931809	32.96862	-97.5346	140	April, 2007
43934088	32.95259	-97.515	137	Dec. 2009
43934486	32.97809	-97.5189	137	June, 2010
43936082	32.96678	-97.5139	129	Mar. 2012
36733734	32.99323	-97.5419	128	Nov. 2005
36735139	32.96571	-97.5367	125	Sept. 2011
36734972	32.956926	-97.54423	119	Sept. 2009
49735655	33.00013	-97.5153	116	Jan. 2005
36734249	32.982997	-97.58554	118	Feb.2008
43936073	32.97837	-97.5208	109	Feb. 2012
36733979	32.94865	-97.5766	104	July, 2006
36735138	32.96393	-97.5368	94	Sept. 2011
43931700	32.95886	-97.5344	94	April, 2007
43931357	32.95098	-97.5124	92	Feb.2006
49736415	32.99882	-97.5291	91	Feb.2008
36733925	32.93989	-97.5461	91	Sept. 2006
49737176	33.00028	-97.5877	91	July, 2011
43934499	32.95176	-97.5464	76	June, 2010
36734628	32.95899	-97.5415	75	Dec. 2008

43934368	32.96245	-97.5239	75	Mar. 2012
36733879	32.95753	-97.5416	73	Sept. 2006
36734744	32.97401	-97.5794	72	Nov. 2008
43933657	32.97287	-97.5246	71	Dec. 2008
49736416	33.00748	-97.5685	71	April, 2008
43936121	32.96645	-97.5125	71	Mar. 2012
36734471	32.95423	-97.5564	69	Nov. 2007
36735080	32.95368	-97.5456	65	Dec. 2010
43936232	32.94811	-97.5462	63	April, 2012
49736003	32.99729	-97.5296	63	July, 2006